AGARD-AG-335

AGARD

ADVISORY GROUP FOR AEROSPACE RESEARCH & DEVELOPMENT

7 RUE ANCELLE, 92200 NEUILLY-SUR-SEINE, FRANCE

AGARDOGRAPH 335

Turbulent Boundary Layers in Subsonic and Supersonic Flow

(les Couches limites turbulentes dans les écoulements subsoniques et supersoniques)

This AGARDograph has been produced at the request of the Fluid Dynamics Panel of AGARD.
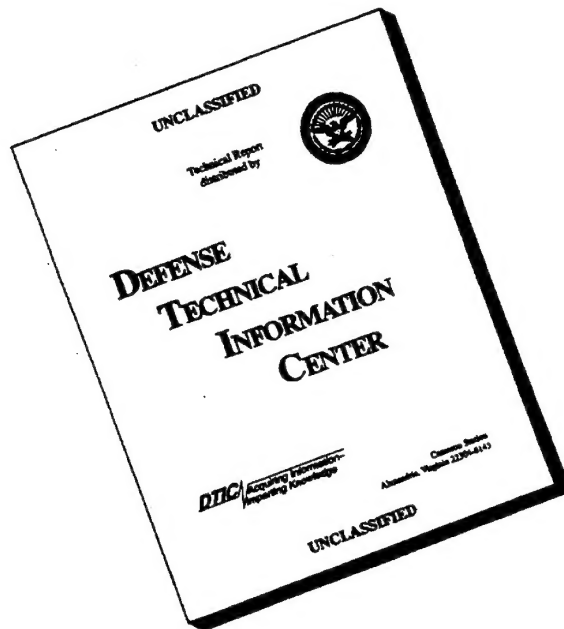
NORTH ATLANTIC TREATY ORGANIZATION

19960815 062

Published July 1996

Distribution and Availability on Back Cover

DISCLAIMER NOTICE

THIS DOCUMENT IS BEST QUALITY AVAILABLE. THE COPY FURNISHED TO DTIC CONTAINED A SIGNIFICANT NUMBER OF PAGES WHICH DO NOT REPRODUCE LEGIBLY.

AGARD-AG-335

AGARD

ADVISORY GROUP FOR AEROSPACE RESEARCH & DEVELOPMENT

7 RUE ANCELLE, 92200 NEUILLY-SUR-SEINE, FRANCE

AGARDOGRAPH 335

Turbulent Boundary Layers in Subsonic and Supersonic Flow

(les Couches limites turbulentes dans les écoulements subsoniques et supersoniques)

by

J.P. Dussauge
Institut de Recherche sur
  les Phénomènes Hors d'Equilibre
12, avenue Général Leclerc
13003 Marseille
France

H. Fernholz
Herman Föttinger Institut
  für Thermo-und-Fluiddynamik
Technische Universität Berlin
D-1000 Berlin 12
Strasse des 17 Juni 135
Germany

R.W. Smith
Experimental Sciences Group
Applied Research Laboratories
Austin, Texas 78713-8029
United States
United States

P.J. Finley
Aeronautics Department
Imperial College of
  Science and Technology
Prince Consort Road
London, SW7 2 BY
Great Britain

A.J. Smits
Gas Dynamics Laboratory
Department of Mechanical and
  Aerospace Engineering
Princeton University
Princeton, New Jersey 08554-0710

Eric F. Spina
Mechanical and Aerospace
  Engineering Department
Syracuse University
Syracuse, New York 13244
United States

Edited by

Professor William S. Saric
Mechanical and Aerospace Engineering
Arizona State University
Tempe, Arizona 85287-610
United States

This AGARDograph has been produced at the request of the Fluid Dynamics Panel of AGARD.

North Atlantic Treaty Organization
Organisation du Traité de l'Atlantique Nord

The Mission of AGARD

According to its Charter, the mission of AGARD is to bring together the leading personalities of the NATO nations in the fields of science and technology relating to aerospace for the following purposes:

— Recommending effective ways for the member nations to use their research and development capabilities for the common benefit of the NATO community;

— Providing scientific and technical advice and assistance to the Military Committee in the field of aerospace research and development (with particular regard to its military application);

— Continuously stimulating advances in the aerospace sciences relevant to strengthening the common defence posture;

— Improving the co-operation among member nations in aerospace research and development;

— Exchange of scientific and technical information;

— Providing assistance to member nations for the purpose of increasing their scientific and technical potential;

— Rendering scientific and technical assistance, as requested, to other NATO bodies and to member nations in connection with research and development problems in the aerospace field.

The highest authority within AGARD is the National Delegates Board consisting of officially appointed senior representatives from each member nation. The mission of AGARD is carried out through the Panels which are composed of experts appointed by the National Delegates, the Consultant and Exchange Programme and the Aerospace Applications Studies Programme. The results of AGARD work are reported to the member nations and the NATO Authorities through the AGARD series of publications of which this is one.

Participation in AGARD activities is by invitation only and is normally limited to citizens of the NATO nations.

Turbulent Boundary Layers
in Subsonic and Supersonic Flow
(AGARD AG-335)

Executive Summary

The aim of this work is to determine the state of the art of experimental knowledge in this field, by gathering and analysing the most recent data on subsonic and supersonic turbulent boundary layers and focussing on scaling laws with respect to Reynolds number and Mach number effects. Hypersonic flows are not considered in depth, mainly because of the lack of comprehensive data. A major drawback of the current knowledge of Reynolds number and Mach number effects is that the data have been collected from many different sources, using different data acquisition and analysis procedures. These differences have resulted in large variations among the published results. Nevertheless, some definite conclusions are made. Given the diversity of the data, participation was called for from research workers in 4 different NATO nations. This report provides the latest developments in this field to the scientific and technical community.

The most important parameter in the description of incompressible turbulent boundary layer behavior is, of course, the Reynolds number. Engineering applications cover an extremely wide range and values based on the streamwise distance can vary from 10^5 to 10^9. Most laboratory experiments are performed at the lower end of this range, and to be able to predict the behavior at very high Reynolds numbers, as found in the flows over aircraft and ships, it is therefore important to understand how turbulent boundary layers scale with Reynolds number. For compressible flows, the Mach number becomes an additional scaling parameter.

What is more, we know that friction and heat transfer are directly related to the structure of these layers. In particular, in the case of turbulent boundary layers, the various transfers are mainly governed by large scale eddies (or "organised structures"), whose size is of the order of the thickness of the layer. Knowledge of the properties of these eddies is crucial to the control and manipulation of turbulence; in particular it conditions drag reduction, which in turn enables a reduction in specific fuel consumption.

For subsonic flows, Reynolds number can have a significant effect on the level of the maximum turbulence stresses, and the location of that maximum in the boundary layer. The properties of the organised structures are dependent on the Reynolds number. In particular, in the outer part of the layers, the space scale which characterises the size of structures in the longitudinal direction is especially sensitive to this, and increases with the Reynolds number. For supersonic flows at moderate Mach numbers, it appears that the direct effects of compressibility on wall turbulence are rather small. It is noted that certain characteristics cannot be collapsed by simple density scaling, and that the existing data indicates that longitudinal space scales fall sharply with Mach number. There appears to be an urgent requirement for detailed experimental data on turbulence with more pronounced compressibility effects, these effects being produced either by increasing the Mach number with Reynolds number constant, or by increasing the Mach number and decreasing the Reynolds number.

Les couches limites turbulentes
dans les écoulements subsoniques et supersoniques
(AGARD AG-335)

Synthèse

L'objectif de ce travail est de faire le point sur l'état des connaissances expérimentales dans ce domaine, en rassemblant et analysant les données les plus récentes sur les couches limites turbulentes subsoniques et supersoniques et en mettant l'accent sur les effets d'échelle en ce qui concerne les lois de similitude par rapport au nombre de Reynolds et au nombre de Mach. Les écoulements hypersoniques ne sont pas traités en détail, principalement à cause du manque d'un ensemble complet de données. L'un des points faibles des connaissances actuelles des effets du nombre de Reynolds et du nombre de Mach résulte du fait que les données obtenues proviennent de sources multiples, issues de procédures d'acquisition et d'analyse de données différentes. Ces différences expliquent les écarts importants dans les résultats publiés. Certaines conclusions précises en sont néanmoins tirées. Compte tenu de la diversité des données, il a nécessité la participation de chercheurs de quatre pays de l'OTAN. Ce rapport met à la disposition de la communauté scientifique et technique les derniers développements des connaissances dans ce domaine.

Le paramètre le plus important pour la description du comportement de la couche limite turbulente incompressible est, bien entendu, le nombre de Reynolds. Les applications techniques sont extrêmement diverses et les valeurs, basées sur la distance le long de l'écoulement, varient entre 10^5 et 10^9. La plupart des expériences réalisées en laboratoire concernent la partie inférieure de cette gamme. Pour être capable de prédire le comportement de l'environnement à des nombres de Reynolds très élevés tels qu'ils existent dans les écoulements autour des navires et des aéronefs, il est très important de comprendre comment les couches limites turbulentes évoluent avec le nombre de Reynolds. Dans le cas des écoulements compressibles, l'influence du nombre de Mach devient un paramètre additionnel important.

On sait de plus que le frottement et le transfert de chaleur dépendent directement de la structure de ces couches. En particulier, pour les couches limites turbulentes, ces différents transferts sont gouvernés principalement par les tourbillons à grande échelle (ou "structures organisées"), dont la taille est de l'ordre de l'épaisseur de la couche. La connaissance des propriétés de ces tourbillons est très importante pour le contrôle et la manipulation de la turbulence; cela conditionne notamment la réduction de la traînée, dont on peut attendre une réduction de la consommation spécifique des avions.

Pour ce qui concerne les écoulements subsoniques, le nombre de Reynolds peut avoir un effet significatif sur le niveau de contrainte de turbulence maximale, ainsi que sur la localisation de ce maximum dans la couche limite. Les structures organisées ont des propriétés qui dépendent du nombre de Reynolds. En particulier, dans la partie externe des couches, l'échelle d'espace caractérisant la taille des structures dans la direction longitudinale y est particulièrement sensible, et est une fonction croissante du nombre de Reynolds.

Pour les écoulements supersoniques aux nombres de Reynolds modérés, il semblerait que les effets directs de la compressibilité sur la turbulence de paroi soient assez faibles. Il est à noter que certaines caractéristiques ne peuvent pas être éliminées par un simple calcul de densité et que les données existantes indiquent que les échelles spatiales longitudinales diminuent fortement avec le nombre de Mach. Il apparaît qu'il existe un besoin urgent de disposer de données expérimentales détaillées sur la turbulence avec des effets de compressibilité plus élevés, ces effets pouvant être produits soit en augmentant le nombre de Mach à nombre de Reynolds constant, soit en augmentant le nombre de Mach et en diminuant le nombre de Reynolds.

Contents

Recent Publications of
the Fluid Dynamics Panel

AGARDOGRAPHS (AG)

Computational Aerodynamics Based on the Euler Equations
AGARD AG-325, September 1994

Scale Effects on Aircraft and Weapon Aerodynamics
AGARD AG-323, July 1994

Design and Testing of High-Performance Parachutes
AGARD AG-319, November 1991

Experimental Techniques in the Field of Low Density Aerodynamics
AGARD AG-318 (E), April 1991

Techniques Expérimentales Liées à l'Aérodynamique à Basse Densité
AGARD AG-318 (FR), April 1990

A Survey of Measurements and Measuring Techniques in Rapidly Distorted Compressible Turbulent Boundary Layers
AGARD AG-315, May 1989

Reynolds Number Effects in Transonic Flows
AGARD AG-303, December 1988

REPORTS (R)

Hypersonic Experimental and Computational Capability, Improvement and Validation
AGARD AR-319, Vol. I, Report of WG-18, May 1996

Parallel Computing in CFD
AGARD R-807, Special Course Notes, October 1995

Optimum Design Methods for Aerodynamics
AGARD R-803, Special Course Notes, November 1994

Missile Aerodynamics
AGARD R-804, Special Course Notes, May 1994

Progress in Transition Modelling
AGARD R-793, Special Course Notes, April 1994

Shock-Wave/Boundary-Layer Interactions in Supersonic and Hypersonic Flows
AGARD R-792, Special Course Notes, August 1993

Unstructured Grid Methods for Advection Dominated Flows
AGARD R-787, Special Course Notes, May 1992

Skin Friction Drag Reduction
AGARD R-786, Special Course Notes, March 1992

Engineering Methods in Aerodynamic Analysis and Design of Aircraft
AGARD R-783, Special Course Notes, January 1992

Aircraft Dynamics at High Angles of Attack: Experiments and Modelling
AGARD R-776, Special Course Notes, March 1991

ADVISORY REPORTS (AR)

Aerodynamics of 3-D Aircraft Afterbodies
AGARD AR-318, Report of WG17, September 1995

A Selection of Experimental Test Cases for the Validation of CFD Codes
AGARD AR-303, Vols. I and II, Report of WG-14, August 1994

Quality Assessment for Wind Tunnel Testing
AGARD AR-304, Report of WG-15, July 1994

Air Intakes of High Speed Vehicles
AGARD AR-270, Report of WG13, September 1991

Appraisal of the Suitability of Turbulence Models in Flow Calculations
AGARD AR-291, Technical Status Review, July 1991

Rotary-Balance Testing for Aircraft Dynamics
AGARD AR-265, Report of WG11, December 1990

Calculation of 3D Separated Turbulent Flows in Boundary Layer Limit
AGARD AR-255, Report of WG10, May 1990

Adaptive Wind Tunnel Walls: Technology and Applications
AGARD AR-269, Report of WG12, April 1990

CONFERENCE PROCEEDINGS (CP)

Progress and Challenges in CFD Methods and Algorithms
AGARD CP-578, April 1996

Aerodynamics of Store Integration and Separation
AGARD CP-570, February 1996

Aerodynamics and Aeroacoustics of Rotorcraft
AGARD CP-552, August 1995

Application of Direct and Large Eddy Simulation to Transition and Turbulence
AGARD CP-551, December 1994

Wall Interference, Support Interference, and Flow Field Measurements
AGARD CP-535, July 1994

Computational and Experimental Assessment of Jets in Cross Flow
AGARD CP-534, November 1993

High-Lift System Aerodynamics
AGARD CP-515, September 1993

Theoretical and Experimental Methods in Hypersonic Flows
AGARD CP-514, April 1993

Aerodynamic Engine/Airframe Integration for High Performance Aircraft and Missiles
AGARD CP-498, September 1992

Effects of Adverse Weather on Aerodynamics
AGARD CP-496, December 1991

Manoeuvring Aerodynamics
AGARD CP-497, November 1991

Vortex Flow Aerodynamics
AGARD CP-494, July 1991

Missile Aerodynamics
AGARD CP-493, October 1990

Aerodynamics of Combat Aircraft Controls and of Ground Effects
AGARD CP-465, April 1990

Computational Methods for Aerodynamic Design (Inverse) and Optimization
AGARD CP-463, March 1990

Applications of Mesh Generation to Complex 3-D Configurations
AGARD CP-464, March 1990

Fluid Dynamics of Three-Dimensional Turbulent Shear Flows and Transition
AGARD CP-438, April 1989

Validation of Computational Fluid Dynamics
AGARD CP-437, December 1988

Aerodynamic Data Accuracy and Quality: Requirements and Capabilities in Wind Tunnel Testing
AGARD CP-429, July 1988

Aerodynamics of Hypersonic Lifting Vehicles
AGARD CP-428, November 1987

Aerodynamic and Related Hydrodynamic Studies Using Water Facilities
AGARD CP-413, June 1987

Applications of Computational Fluid Dynamics in Aeronautics
AGARD CP-412, November 1986

Turbulent Boundary Layers
in Subsonic and Supersonic Flow

1 Introduction

The most important parameter in the description of incompressible turbulent boundary layer behavior is, of course, the Reynolds number. Engineering applications cover an extremely wide range and values based on the streamwise distance can vary from 10^5 to 10^9. Most laboratory experiments are performed at the lower end of this range, and to be able to predict the behavior at very high Reynolds numbers, as found in the flow over aircraft and ships, it is therefore important to understand how turbulent boundary layers scale with Reynolds number.

For compressible flows, the Mach number becomes an additional scaling parameter. Because of the no-slip condition, however, a subsonic region persists near the wall, although the sonic line is located very close to the wall at high Mach number. Furthermore, a significant temperature gradient develops across the boundary layer at supersonic speeds due to the high levels of viscous dissipation near the wall. In fact, the static-temperature variation can be very large even in an adiabatic flow, resulting in a low-density, high-viscosity region near the wall. In turn, this leads to a skewed mass-flux profile, a thicker boundary layer, and a region in which viscous effects are somewhat more important than at an equivalent Reynolds number in subsonic flow.

Figure 1 shows two sets of air boundary layer profiles at about the same Reynolds number, one set measured on an adiabatic wall, the other measured on an isothermal wall. The momentum thickness Reynolds number R_θ is approximately 2200 when based on the freestream velocity u_e, and the kinematic viscosity evaluated at the freestream temperature ν_e, in accord with usual practice. That is, $R_\theta = \theta u_e / \nu_e$. The temperature of the air increases near the wall, even for the adiabatic wall case, since the dissipation of kinetic energy by friction is an important source of heat in supersonic shear layers. Somewhat surprisingly, the velocity, temperature and mass-flux profiles for these two flows appear very much the same, even though the boundary conditions, Mach numbers and heat transfer parameters differ considerably. The velocity profiles in the outer region, in fact, follow a 1/7th power law distribution quite well, just as a subsonic velocity profile would at this Reynolds number. With increasing Mach number, however, the elevated temperature near the the wall means that the bulk of the mass flux is increasingly found toward the outer edge of the boundary layer. This effect is strongly evident in the boundary-layer profiles shown in figure 2, where the freestream Mach number was 10 for a helium flow on an adiabatic wall. For this case, the temperature ratio between the wall and the boundary layer edge was about 30.

If the total temperature T_o was constant across the layer, then from the definition of the total temperature, $T_o = T + U^2/2C_p$, we see that there is a very simple relationship between the temperature T and the velocity u. Since there is never an exact balance between frictional heating and conduction (unless the Prandtl number equals one), the total temperature is not quite constant, even in an adiabatic flow, and the wall temperature depends on the recovery factor r. Hence:

$$\frac{T_w}{T_e} = 1 + r\frac{\gamma - 1}{2}M_e^2$$

where M is the Mach number, the subscript w denotes conditions at the wall, and the subscript e denotes conditions at the edge of the boundary layer, that is, in the local freestream. Since $r \approx 0.9$ for a turbulent boundary layer, the temperature at the wall in an adiabatic flow is nearly equal to the freestream total temperature. For example, at a freestream Mach number of 3, the ratio $T_w/T_0 = 0.93$.

As a result of these large variations of temperature through the layer, the fluid properties are far from constant. To the boundary layer approximation, the static pressure variation across the layer is constant, as in subsonic flow, and therefore for the examples shown in figure 1 the density varies by about a factor of 5. The viscosity varies by somewhat less than that: if we assume some form of Sutherland's law to express the temperature dependence of viscosity, for instance $(\mu/\mu_e) = (T/T_e)^\omega$ where $\omega = 0.765$, then the viscosity varies by a factor of 3.4. Since the density increases and the viscosity decreases with distance from the wall, the kinematic viscosity decreases by a factor of about 17 across the layer. It is therefore difficult to assign a single Reynolds number to describe the state of the boundary layer. Of course, even in a subsonic boundary layer the Reynolds number varies through the layer since the length scale depends (in a general sense) on the distance from the wall. But here the variation is more complex in that the non-dimensionalizing fluid properties also change with wall distance. One consequence is that the relative thickness of the viscous sublayer depends not only on the Reynolds number, but also on the Mach number and heat transfer rate since these will influence the distribution of the fluid properties. At very high Mach numbers, most of the layer may become viscous-dominated. Now the boundary layers at the lower Mach numbers shown in figure 1 are certainly turbulent, but the Mach 10 boundary layer shown in figure 2 may well be transitional. For that case, the Reynolds number based on freestream fluid properties (for example, $R_\theta = \rho_e U_e \theta / \mu_e$ suggests a fully turbulent flow, but when the Reynolds number is based on fluid properties evaluated at the wall temperature ($R_{\delta 2} = \rho_e U_e \theta / \mu_w$) it suggests a laminar flow. The difference between Re_θ and $R_{\delta 2}$ increases steadily with Mach number and heat
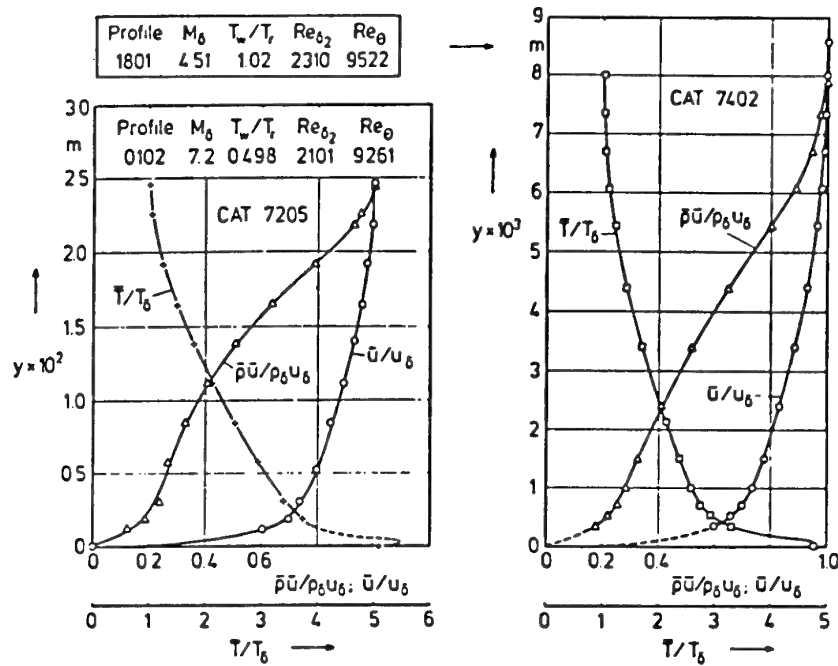
Figure 1: Turbulent boundary layer profiles in air ($T_\delta = T_e$). From Fernholz & Finley (1980), where catalog numbers are referenced.
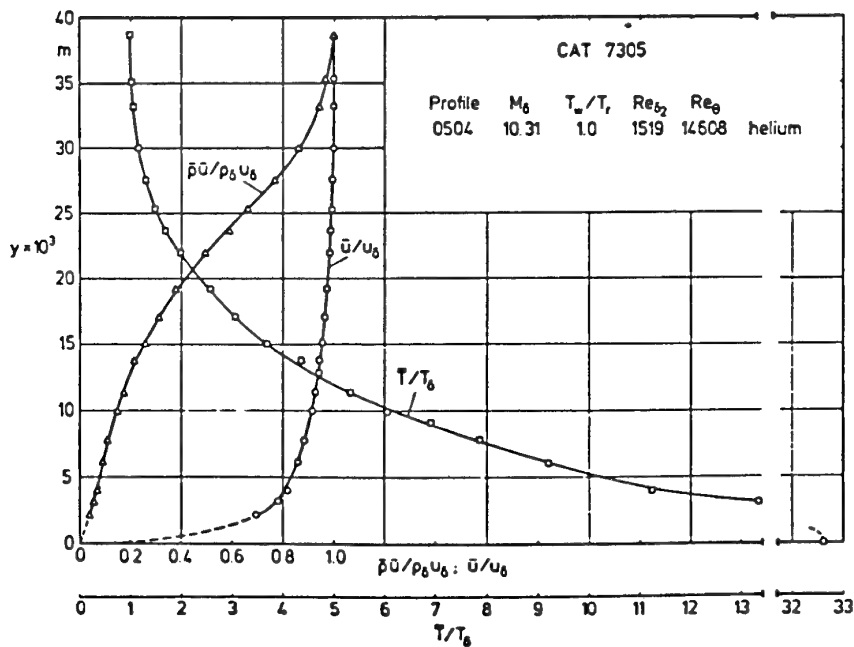

Figure 2: Turbulent boundary layer profiles in helium ($T_\delta = T_e$). Figure from Fernholz & Finley (1980), where catalog numbers are referenced. Original data from Watson *et al.* (1973).

transfer, and can become very significant at high Mach number (for a full discussion, see Fernholz & Finley, 1976).

We can see that any comparisons we try to make between subsonic and supersonic boundary layers must take into account the variations in fluid properties, which may be strong enough to lead to unexpected physical phenomena, as well as the gradients in Mach number. Intuitively, one would expect to see significant dynamical differences between subsonic and supersonic boundary layers. However, it appears that many of these differences can be explained by simply accounting for the fluid-property variations that accompany the temperature variation, as would be the case in a heated incompressible boundary layer. This suggests a rather passive role for the density differences in these flows, most clearly expressed by Morkovin's hypothesis (Morkovin, 1962): the dynamics of a compressible boundary layer follow the incompressible pattern closely, as long as the Mach number associated with the fluctuations remains small. That is, the fluctuating Mach number, M', must remain small, where M' is the r.m.s. perturbation of the instantaneous Mach number from its mean value, taking into account the variations in velocity and sound speed with time. If M' approaches unity at any point, we would expect direct compressibility effects such as local "shocklets" and pressure fluctuations to become important. If we take $M' = 0.3$ as the point where compressibility effects become important for the turbulence behavior, we find that for zero-pressure-gradient adiabatic boundary layers at moderately high Reynolds numbers this point will be reached with a freestream Mach number of about 4 or 5 (see figure 3).

Recently, some measurements in moderately supersonic boundary layers ($M_\infty < 5$) have indicated subtle differences in the instantaneous behavior of certain quantities and parameters as compared to subsonic flow. These differences do not seem to be due simply to fluid-property variations. In particular, differences in turbulence length and velocity scales, the intermittency of the outer layer, and the structure of the large-scale shear-stress containing motions may indicate that the turbulence dynamics are affected at a lower fluctuating Mach number than previously believed. It is also possible that some of these changes in the turbulence structure are due to Reynolds number effects. As pointed out earlier, the characteristic Reynolds numbers encountered in high-speed flow can cover a very large range, extending well beyond values of the Reynolds number typically found in the laboratory. Furthermore, the temperature gradients which are found in the boundary layer in supersonic flow lead to variations in Reynolds number across the layer which must be considered along with the usual variations in the streamwise direction.

We begin this report by reviewing the boundary layer equations in Section 2. In Section 3, we discuss the behavior of boundary layers in subsonic flow, and in Section 4 we consider their behavior in supersonic flow. A summary is given in the final section, Section 5. We will focus on scaling laws with respect to Reynolds number and Mach number effects. Hypersonic flows will not be considered in depth, mainly because of the lack of comprehensive data. Similarly, we do not consider transonic flows, so that the term "subsonic" will be taken to be equivalent to "incompressible." The preparation of this AGARDo-
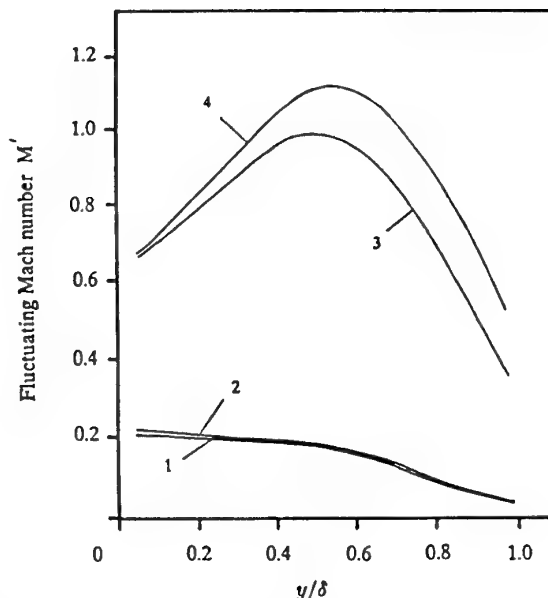

Figure 3: Fluctuating Mach number distributions. Flow 1: $M_e = 2.32$, $Re_\theta = 4,700$, adiabatic wall (Eléna & Lacharme, 1988); Flow 2: $M_e = 2.87$, $Re_\theta = 80,000$, adiabatic wall (Spina & Smits, 1987); Flow 3: $M_e = 7.2$, $Re_\theta = 7,100$, $T_w/T_r = 0.2$ (Owen & Horstman, 1972); Flow 4: $M_e = 9.4$, $Re_\theta = 40,000$, $T_w/T_r = 0.4$ (Laderman & Demetriades, 1974). Figure from Spina et al. (1994).

graph was greatly helped by the availability of the recent reviews and commentaries on subsonic boundary layers by Smith (1994), Gad-el-Hak & Bandyopadhyay (1994) and Fernholz & Finley (1995), and the reviews of supersonic boundary layers by Smits et al. (1989), Spina et al. (1994), as well as the catalogs of supersonic turbulence data compiled by Fernholz & Finley (1976), Fernholz & Finley (1980), Fernholz & Finley (1981), Fernholz et al. (1989)), and by Settles & Dodson (1991).

2 Boundary-Layer Equations

Derivations of the incompressible boundary layer equations can be found in many places, and they will not be repeated here. In any case, since we will need both the compressible and incompressible forms, it is expedient to concentrate on the former, and treat the latter as a special case.

Detailed derivations of the equations for compressible turbulent boundary layers have been provided in kinematic variables by van Driest (1951), Schubauer & Tchen (1959), Cebeci & Smith (1974) and Fernholz & Finley (1980). While it is well-known that the inclusion of density as an instantaneous variable is to add terms other than $-\overline{\rho u'v'}$ to the Reynolds-averaged boundary layer equations, the interpretation of these terms and their significance is not universally agreed upon. One of the reasons is that these terms do not appear in the mass-

4

averaged (Favre-averaged) equations, as shown by, for example, Morkovin (1962), Favre (1965), and Rubesin & Rose (1973). A critical review of the equations of compressible turbulent flow and a discussion of the relative merits of the mass-averaged form is given by Lele (1994).

2.1 Continuity

The Reynolds-averaged, stationary, two-dimensional continuity equation for compressible flow is:

$$\frac{\partial}{\partial x}(\overline{\rho}U) + \frac{\partial}{\partial y}(\overline{\rho}V) + \frac{\partial}{\partial y}(\overline{\rho'v'}) + \frac{\partial}{\partial y}(\overline{\rho'u'}) = 0. \quad (1)$$

The additional terms in this equation, $\frac{\partial}{\partial y}(\overline{\rho'v'})$ and $\frac{\partial}{\partial y}(\overline{\rho'u'})$, act as apparent sources/sinks to the mean flow (Schubauer & Tchen, 1959). To the boundary-layer approximation, $\frac{\partial}{\partial y}(\overline{\rho'u'})$ is negligible, and a simple mixing-length argument indicates that $\overline{\rho'v'}$ is negative. The absolute magnitudes of ρ' and v' increase with y near the wall before decreasing with y in the outer part of the boundary layer, and therefore $\frac{\partial}{\partial y}(\overline{\rho'v'})$ acts as a mass-flux source in the inner layer and as a sink in the outer region of the boundary layer. The presence of a source term in the continuity equation may indicate that the physics of the flowfield are not well represented.

An alternative approach uses "Favre-averaging", where the instantaneous variable is decomposed into the sum of a mass-weighted average, $\tilde{\alpha}$, and a fluctuation, α'' (Favre, 1965). The use of mass-averaged variables leaves the continuity equation devoid of turbulent mass transport terms:

$$\frac{\partial}{\partial x}(\overline{\rho}\tilde{u}) + \frac{\partial}{\partial y}(\overline{\rho}\tilde{v}) = 0. \quad (2)$$

2.2 Momentum

For two-dimensional compressible flow, the y-component (wall-normal) momentum equation contains many terms associated with density and velocity fluctuations. For zero-pressure-gradient boundary layers in a steady supersonic flow, however, the usual order-of-magnitude arguments show that the pressure across the layer can be taken as constant, as for subsonic flows. The pressure is then a function only of streamwise distance, so that $\partial \overline{p}/\partial x$ may be replaced by $d\overline{p}/dx$ in the x-momentum equation. Hence, the mean pressure is considered to be "imposed" on the boundary layer in that it appears as a boundary condition rather than as an independent variable.

If the continuity equation is multiplied by the streamwise velocity, added to the boundary-layer approximation of the x-momentum equation, and the resulting equation Reynolds-averaged, we obtain:

$$\frac{\partial}{\partial x}(\overline{\rho}U^2) + \frac{\partial}{\partial y}(\overline{\rho}UV) = \frac{-d\overline{p}}{dx} + \frac{\partial}{\partial y}(\mu\frac{\partial U}{\partial y} - \overline{\rho}\overline{u'v'}$$
$$- U\overline{\rho'v'} - V\overline{\rho'u'} - \overline{\rho'u'v'}). \quad (3)$$

Equation 3 is the most general form of the compressible boundary layer equation. The triple-product term may be neglected since it is one order of magnitude smaller than the other terms, and $V\overline{\rho'u'}$ can be neglected since

it is smaller than $U\overline{\rho'v'}$ ($\overline{\rho'u'}$ and $\overline{\rho'v'}$ are assumed to be the same order and $V << U$). The resulting equation is:

$$\frac{\partial}{\partial x}(\overline{\rho}U^2) + \frac{\partial}{\partial y}(\overline{\rho}UV) = \frac{-d\overline{p}}{dx} + \frac{\partial}{\partial y}(\mu\frac{\partial U}{\partial y} - \overline{\rho}\overline{u'v'} - U\overline{\rho'v'}). \quad (4)$$

Alternatively, the boundary-layer form of the compressible x-momentum equation can be written:

$$\overline{\rho u}\frac{\partial}{\partial x}U + \overline{\rho v}\frac{\partial}{\partial y}U = \frac{-d\overline{p}}{dx} + \frac{\partial}{\partial y}(\mu\frac{\partial U}{\partial y} - \overline{\rho}\overline{u'v'}), \quad (5)$$

where $\overline{\rho u} = \overline{\rho}U + \overline{\rho'u'}$ and $\overline{\rho v} = \overline{\rho}V + \overline{\rho'v'}$, and $\overline{\rho'u'}$ can usually be neglected. When the Favre-averaged form of the x-momentum equation is considered, that is,

$$\frac{\partial}{\partial x}(\overline{\rho}\tilde{u}^2) + \frac{\partial}{\partial y}(\overline{\rho}\tilde{u}\tilde{v}) = \frac{-d\overline{p}}{dx} + \frac{\partial}{\partial y}(\overline{\tau}_{yx} - \overline{\rho u''v''}), \quad (6)$$

it is clear that three different forms of the equation exist, and some physical insight regarding the differences is necessary.

In Equation 4 the traditional Reynolds stress and another "apparent" stress, $-U\overline{\rho'v'}$, comprise the turbulent shear stress. Now, $U\overline{\rho'v'}$ is not a "true" Reynolds stress, but simply a consequence of the type of averaging used. Nevertheless, its contribution to the total stress cannot be discounted. The correlations $\overline{\rho}\overline{u'v'}$ and $U\overline{\rho'v'}$ are both negative (as evident from a mixing-length argument), and thus $U\overline{\rho'v'}$ acts in addition to the "incompressible" Reynolds shear stress. Assuming small pressure fluctuations and using the Strong Reynolds Analogy (SRA) (Morkovin, 1962) (see Section 2.3), it is a simple matter to express the ratio of $U\overline{\rho'v'}$ to $\overline{\rho}\overline{u'v'}$ as $(\gamma - 1)M^2$ ((see, for example, Spina et al. , 1991a). Of course, this expression is subject to the inaccuracies inherent in the SRA (see below), but it is a good approximation to at least $M = 5$, and provides an order-of-magnitude comparison even at higher Mach numbers. This relation indicates how quickly $U\overline{\rho'v'}$ becomes important in the boundary layer. For a Mach 3 adiabatic-wallboundary layer with $Re_\theta = 80,000$, $(\gamma - 1)M^2$ rises to a value of 1.0 at approximately 0.05δ ($\sim 500y^+$), and asymptotes to a value of 3.5 at the boundary layer edge (Spina, 1988). Since the Mach number is small across much of the constant-stress layer, Schubauer & Tchen (1959) neglected the "second-order term" when developing a skin-friction theory, but this should not be considered a general result.

The correlation $U\overline{\rho'v'}$ also appears in the turbulent kinetic energy (TKE) equation for a compressible boundary layer. This equation is much more complex than the incompressible TKE equation, with eight production terms, including one due to the Reynolds shear stress, $-\overline{\rho}\overline{u'v'}\frac{\partial U}{\partial y}$, and one due to the "fictitious" stress, $-U\overline{\rho'v'}\frac{\partial V}{\partial x}$. A comparison between these two terms indicates that the production of turbulent kinetic energy due to the Reynolds shear stress is two orders-of-magnitude greater than that due to the term in question (in fact, there are three other terms that are an order-of-magnitude larger than $-U\overline{\rho'v'}\frac{\partial V}{\partial x}$). This indicates that $U\overline{\rho'v'}$ is less important than the other terms in determining the energy flow in a compressible boundary layer because it interacts with a considerably smaller mean strain.

If the convective terms are written as the product of the average instantaneous mass flux and a strain (as in

Equation 5), the only additional term (in addition to those found in laminar flow) is the traditional Reynolds stress, $\overline{\rho u'v'}$. This form of the equation was advocated by Morkovin (1962) to isolate the turbulent momentum transport, and the new parts of the convective terms represent the fact that there is no mean mass transfer between mean streamlines. Since $U\overline{\rho'v'}$ may be thought of as a turbulent mass-transport term, it is not surprising that this form of the equation is free from this term, and the interpretation of the equation is physically and intuitively attractive.

The major drawback to writing the x-momentum equation in Favre-averaged variables (Equation 6) is that $\overline{\tau}_{yx}$ is more complex than for incompressible boundary layers (Rubesin & Rose, 1973). Expressing the instantaneous stress tensor in mass-weighted variables, expanding, and time-averaging results in:

$$\overline{\tau}_{ij} = \tilde{\mu}\tilde{S}_{ij} + \tilde{\mu}\overline{S''}_{ij}$$

where $S_{ij} = [(u_{i,j} + u_{j,i}) - \frac{2}{3}\delta_{ij}u_{k,k}]$. This expression contains additional terms that are not amenable to a simple physical interpretation, but the similarity of the Favre-averaged representation of the compressible momentum equation to that of the incompressible equation makes its use nevertheless attractive, especially in computations.

2.3 Energy and the Strong Reynolds Analogy

The mean energy equation was developed in terms of the stagnation enthalpy by Young (1951) (see Howarth, 1953, Gaviglio, 1987) in the forms corresponding to the Reynolds-averaged and Favre-averaged variables, respectively. In Reynolds-averaged variables, the boundary-layer approximation for the equation is:

$$\overline{\rho u}\frac{\partial \overline{H}}{\partial x} + \overline{\rho v}\frac{\partial \overline{H}}{\partial y} = \frac{\partial}{\partial y}\left[\frac{k}{c_p}\frac{\partial \overline{H}}{\partial y}\right.$$

$$\left. + \mu\left(1 - \frac{1}{Pr}\right)\frac{\partial}{\partial y}\left(\frac{U^2}{2}\right) - \overline{\rho v'H'}\right], \quad (7)$$

where, neglecting higher-order terms, $\overline{H} = \overline{h} + \frac{1}{2}U^2$, and $H' = h' + Uu'$. As in the development of the mean x-momentum equation (Equation 5), there are no additional terms beyond those found in incompressible flow, although the convective terms are slightly altered, as noted by Morkovin.

A useful relation for the reduction of experimental data and the comparison of compressible to incompressible results is the Strong Reynolds Analogy [first identified as such by Morkovin (1962), but primarily due to Young (1951)]. This analogy, leading to simplified solutions of the energy equation, is based upon the similarity between Equations 5 and 7 when $Pr = 1$ (or when molecular effects are negligible compared to turbulent processes) and the similarity of the boundary conditions for $\overline{T_0}$ and U, and T_0' and u'. For zero-pressure-gradient flow of a perfect gas with heat transfer, the equations admit the solutions:

$$c_p(\overline{T}_0 - T_w) = \frac{\overline{q}_w}{\overline{\tau}_w}U, \quad (8)$$

$$c_p T_0' = \frac{\overline{q}_w}{\overline{\tau}_w}u', \quad (9)$$

where the heat-transfer rate and shear stress at the wall enter through the boundary conditions. For adiabatic flows, it follows that

$$T_0' = 0, \quad (10)$$

$$\frac{T'}{\overline{T}} = -(\gamma - 1)M^2\frac{u'}{U}, \quad (11)$$

$$\text{and} \quad R_{uT} = -1. \quad (12)$$

The solution given by $\overline{T}_0 = T_w$ and Equation 10 satisfies the energy equation independently, and therefore may be applied for any pressure gradient (Gaviglio, 1987).

Gaviglio notes that these relations (Equations 8 - 12) are so strict (that is, they apply in an instantaneous sense) that they cannot be expected to hold exactly. Morkovin (1962) gives a "milder" form of the SRA that relates the r.m.s. of the static temperature fluctuations to that of the velocity fluctuations (also see Spina *et al.*, 1991a)). Morkovin (1962) and Gaviglio (1987) tested the time-averaged form of the SRA and found that R_{uT} is not -1.0 but is closer to -0.8 or -0.9. Still, this high correlation level indicates that large-scale eddies moving away from the wall in a supersonic flow almost always contain warmer, lower-speed fluid than the average values found at that distance from the wall. As for the instantaneous form of the SRA (Equation 10), Morkovin & Phinney (1958), Kistler (1959), Dussauge & Gaviglio (1987), and Smith & Smits (1993a) have shown that T_0' is not negligible, but that the results derived from such an assumption still represent very good approximations. The instantaneous form of the SRA has been validated to a freestream Mach number of 3 (Smith & Smits, 1993a), but the only limit to its first-order approximation at higher Mach number may be the increasing importance of low-Reynolds-number effects near the wall at higher hypersonic Mach numbers (Morkovin, 1962). There is also the fact that $T'/\bar{T}$ is bounded, which means there exists an upper Mach number limit on the SRA unless $u'/\bar{U}$ approaches very small values at the same time.

3 Subsonic Flows

We will now consider the behavior of turbulent boundary layers in subsonic flows, starting with the mean flow. Unless otherwise indicated this discussion follows Smith (1994) closely.

3.1 Mean flow behavior

The boundary-layer equations for subsonic flows may be derived from the general equations given in Section 2 in a straightforward manner. The mean continuity and x-momentum equations are, respectively:

$$\frac{\partial U}{\partial x} + \frac{\partial V}{\partial y} = 0 \quad (13)$$

$$\rho U\frac{\partial U}{\partial x} + \rho V\frac{\partial U}{\partial y} = -\frac{d\bar{p}}{dx} + \frac{\partial}{\partial y}\left(\mu\frac{\partial U}{\partial y} - \overline{\rho u'v'}\right). \quad (14)$$

The energy equation is now redundant, as long as the flow is adiabatic and fluid properties are constant.

The turbulent boundary-layer equations differ from the laminar equations only in the additional turbulent shear stress term $-\rho\overline{u'v'}$. One immediate result is that a turbulent boundary layer has *two* characteristic length scales, rather than one. A measure of the boundary layer thickness, such as δ, is the appropriate length scale in the outer part of the layer, away from the wall, and is thus termed the *outer* length scale. The viscous length, ν/u_τ (u_τ is defined in Equation 17), is the appropriate length scale near the wall, and is termed the *inner* length scale. In contrast, a laminar boundary layer in zero pressure gradient is characterized by a single length scale, $\sqrt{\nu L/U_\infty}$. This is why it is possible to obtain full similarity solutions for laminar boundary layers, but not for turbulent boundary layers. For turbulent boundary layers, separate similarity laws for the inner and outer flows must be sought. The ratio of the outer and inner length scales, δ^+ ($= \delta u_\tau/\nu$), increases with increasing Reynolds number and therefore the shape of the mean velocity profile must also be Reynolds-number dependent.

3.1.1 The viscous sublayer

For the flow very near the wall, the "no-slip" condition at the wall requires that $\overline{U}$, $\overline{V}$, u' and v' must approach zero as the wall is approached. Thus, for a zero-pressure-gradient flow, for the region very near the wall, Equation 14 reduces to

$$\mu\frac{\partial^2\overline{U}}{\partial y^2} = 0. \tag{15}$$

Equation 15 may be integrated to give:

$$\frac{\overline{U}}{u_\tau} = \frac{yu_\tau}{\nu}, \tag{16}$$

where u_τ is the friction velocity and is defined as

$$u_\tau = \sqrt{\frac{\tau_w}{\rho}} = U_e\sqrt{\frac{C_f}{2}}, \tag{17}$$

where C_f is the skin friction coefficient defined as

$$C_f = \frac{\tau_w}{\frac{1}{2}\rho U_e^2}. \tag{18}$$

Equation 16 may also be written as $u^+ = y^+$, where the superscript ($^+$) denotes normalization with inner variables (u_τ for velocity, and ν/u_τ for length). That is, very near the wall, the velocity varies linearly with distance from the wall.

3.1.2 The law-of-the-wall and the defect-law

For the inner, near-wall flow (including the linear part of the sublayer), Prandtl (1933) argued that the viscosity and wall shear stress are the important parameters, and thus the velocity must have the following functional dependence:

$$\overline{U} = f(y, \tau_w, \rho, \mu). \tag{19}$$

In the outer layer, viscosity is less important, but the presence of the wall is still felt through the magnitude of the wall shear stress. Thus, von Kármán (1930) suggested
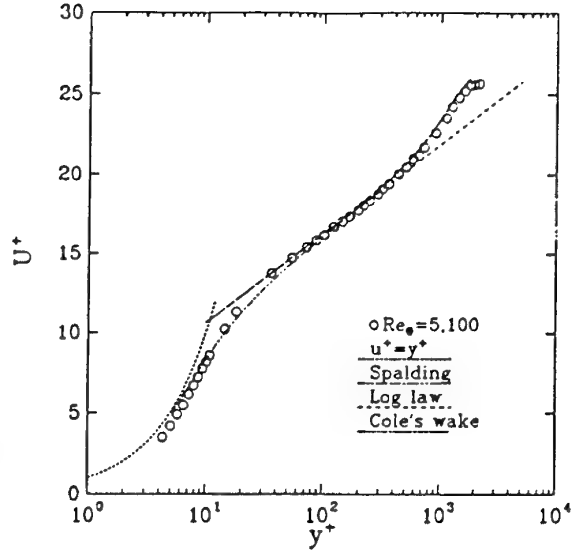

Figure 4: Example of a measured mean velocity profile at $Re_\theta = 5,100$ from Purtell *et al.* (1981) scaled on inner variables, and compared to theoretical and empirical scaling-laws: ○ data; ···················· the linear sublayer; ------------ the buffer region according to Spalding (1961); - - - - - - - - the logarithmic overlap region (equation 24); ---·---·--- Coles' law-of-the-wake (equation 27). Figure from Smith (1994).

that the velocity defect, $U_e - \overline{U}$, should have the following functional dependence

$$U_e - \overline{U} = g(y, \delta, \tau_w, \rho). \tag{20}$$

Dimensional analysis of Equations 19 and 20 leads to

$$\frac{\overline{U}}{u_\tau} = f\left(\frac{yu_\tau}{\nu}\right), \tag{21}$$

and

$$\frac{U_e - \overline{U}}{u_\tau} = g\left(\frac{y}{\delta}\right). \tag{22}$$

Equation 21 is known as the *law-of-the-wall*, and is valid only in the inner layer. Equation 22 is known as the *defect-law*, and is valid only in the outer layer. Rotta (1950), Rotta (1962) suggested that the defect law should be written as:

$$\frac{U_e - \overline{U}}{u_\tau} = g\left(\frac{y}{\delta}, \frac{u_\tau}{U_e}\right). \tag{23}$$

where u_τ/U_e indicates a weak or vanishing Reynolds number dependence. Millikan (1938) proposed that at large enough Reynolds numbers (where the u_τ/U_e dependence is assumed to vanish), in a region where $\nu/u_\tau \ll y \ll \delta$, there may be a region of overlap where both the inner and outer similarity laws are simultaneously valid. Matching the velocity, and velocity gradients, given by Equations 21 and 22 yields the following forms for the law-of-the-wall and the defect-law in the overlap region:

$$\frac{\overline{U}}{u_\tau} = \frac{1}{\kappa}\ln\left(\frac{yu_\tau}{\nu}\right) + C, \tag{24}$$
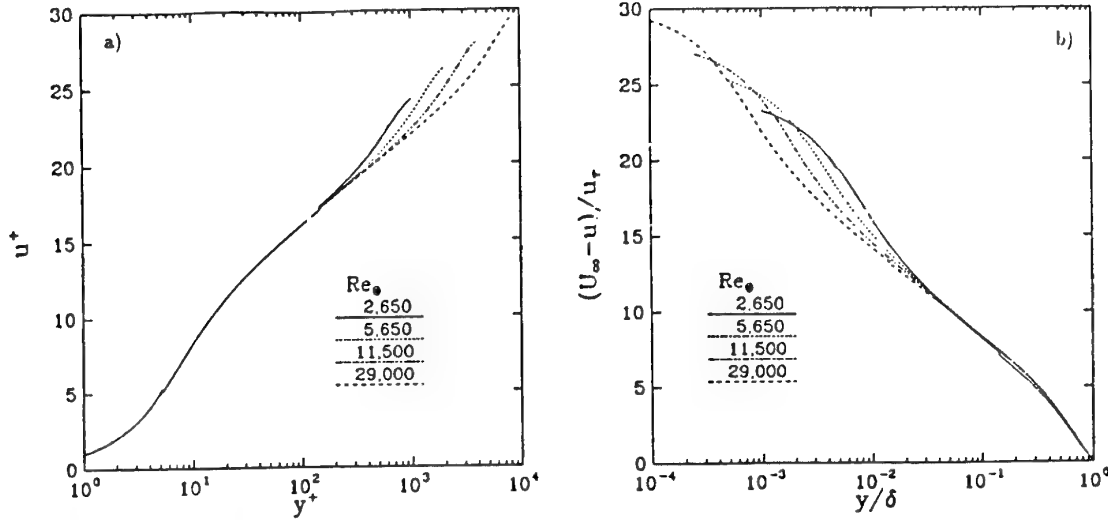
Figure 5: Mean velocity profiles for four different Reynolds numbers using a) inner scaling, illustrating the Reynolds-number dependence of the outer region, and b) outer scaling, illustrating the Reynolds-number dependence of the inner region. $Re_\theta = 2,650$ ——————; 5,650 ----------------; 11,500 -------------; 29,000 - - - - - - - - . Figure from Smith (1994).

and

$$\frac{U_e - \overline{U}}{u_\tau} = -\frac{1}{\kappa} \ln \left(\frac{y}{\delta}\right) + C', \qquad (25)$$

where C, C', and κ (called von Kármán's constant) may or may not be Reynolds-number dependent. Thus, the velocity profile in the overlap region is logarithmic, and the overlap region is often referred to as the *logarithmic region*.

The preceding discussion has outlined the "orthodox" view of mean-flow scaling. An alternative scheme, proposed by George *et al.* (1992) is discussed in Section 3.1.4. Also, the "physical" boundary layer thickness, δ, is experimentally ill-defined [this is especially true in supersonic flows — see Fernholz & Finley (1980) and Section 4], and it ought to be replaced by a well-defined integral thickness, such as the Clauser or Rotta (Rotta, 1950) thickness:

$$\Delta = \int_0^\infty \frac{U_e - \bar{U}}{u_\tau} dy = \delta^* \sqrt{\frac{2}{C_f}} \qquad (26)$$

where δ^* is the usual (incompressible) displacement thickness.

It should be pointed out that the similarity scaling of the mean incompressible boundary layer velocity profile is most usefully expressed in terms of the scaling for the mean velocity gradient $\partial U/\partial y$. That is, $\partial U/\partial y$ in the near-wall region scales with a length scale ν/u_τ and in the outer region the length scale is δ. In the overlap region, the length scale becomes the wall-normal distance, y. The velocity scale for the inner and outer regions of the boundary layer is the same, and it is, of course, u_τ.

3.1.3 The law-of-the-wake

Coles (1956) compiled and analysed all of the data available at that time for velocity profiles in turbulent boundary layers and proposed a scaling law to include the outer layer as well as the overlap region. He found that the portion of the velocity profile which deviated from the logarithmic formula in all cases shared a similar form that resembled the velocity profile in a wake. Coles thus expressed the departure as a *wake function* and added it to Equation 24 obtaining

$$\frac{\overline{U}}{u_\tau} = \frac{1}{\kappa} \ln \left(\frac{yu_\tau}{\nu}\right) + C + \frac{\Pi}{\kappa} w \left(\frac{y}{\delta}\right). \qquad (27)$$

Here, Π is equivalent to the maximum deviation of the velocity profile from the log-law of Equation 24 and it indicates the strength of the wake; $w(y/\delta)$ is Coles's wake function $(= 2\sin^2(\frac{\pi}{2}\frac{y}{\delta})$ such that $\int_0^1 (y/\delta)dw = 1$ and $w(1) = 2)$. This combined law-of-the-wall and law-of-the-wake describes the velocity profile from the inner edge of the log region all the way to the edge of the boundary layer. Figure 4 shows a typical velocity profile scaled with inner variables. The figure also shows the theoretical linear profile deep in the viscous sublayer, a line corresponding to the logarithmic overlap region, and Coles's wake function w. The curve which is used to interpolate the velocity profile between the sublayer and the log region was derived by Spalding (1961), and this region is called the buffer layer. Figure 5 shows how these semi-empirical expressions for the mean velocity profile change with Reynolds number. In figure 5a, the profiles are plotted using inner scaling, and figure 5b shows the same profiles plotted using outer scaling. When using inner scaling, only the wake component (the outer layer) is Reynolds-number dependent. When using outer scaling, only the inner layer is Reynolds-number dependent. This is the expected behavior. However, what may be unexpected is that the logarithmic overlap region, when scaled with outer variables, is also weakly Reynolds number dependent, at least for the lowest-Reynolds-number profile. This point is discussed further below.

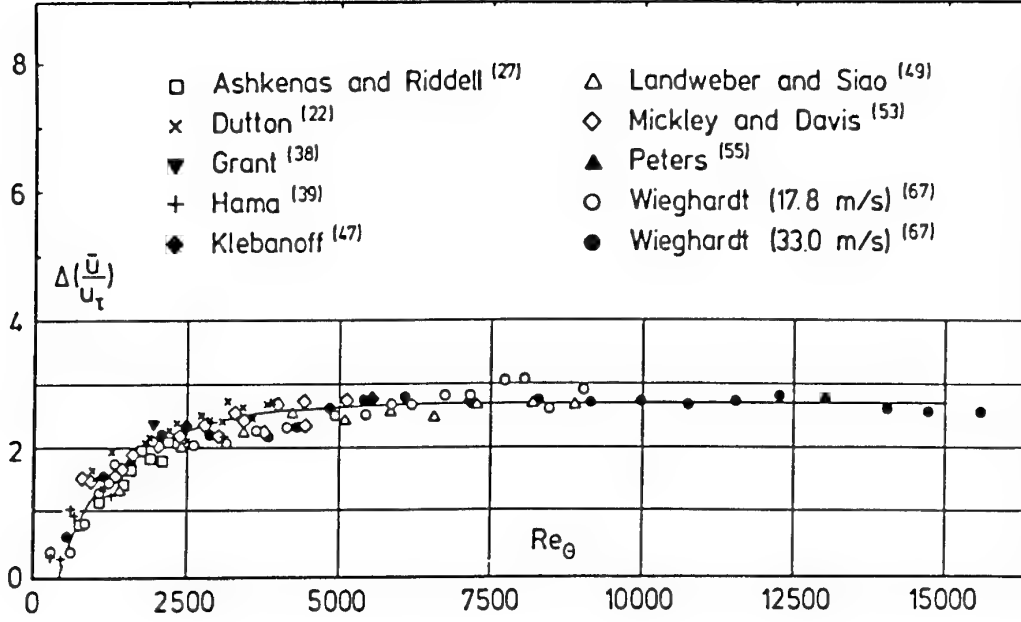A local friction law is obtained from Equation 27 by using

Figure 6: Strength of the wake component in zero pressure-gradient equilibrium subsonic turbulent flow. Here, $\Delta\left(\overline{U}/u_\tau\right) = 2\Pi/\kappa$. From Coles (1962).

the boundary condition $\overline{U} = U_e$ at $y = \delta$, giving

$$\sqrt{\frac{2}{C_f}} = \frac{1}{\kappa}\ln\left(Re_\delta\sqrt{\frac{C_f}{2}}\right) + C + \frac{2\Pi}{\kappa}, \qquad (28)$$

where $Re_\delta = \delta U_e/\nu$. Equation 28 provides an implicit expression for determining C_f, if Re_δ, Π, and C are all known.

In 1962, Coles again surveyed the available data. He assumed that κ and C were constant, independent of Reynolds number. By fitting measured velocity profiles to the logarithmic overlap region, he determined u_τ for each profile, and then determined Π by measuring the maximum deviation from the log-law. He found that, for $Re_\theta < 6,000$, Π is a strong function of Reynolds number, as shown in figure 6.

In 1968, Coles further re-analysed the data. This time, he fit the data to the logarithmic overlap region and part of the wake to determine u_τ and δ simultaneously. He again assumed that $\kappa = 0.41$ and $C = 5.0$. In this new analysis, Coles found the asymptotic value of Π to be about 0.6 (Erm et al. , 1985), as opposed to 0.55 in the earlier study, although the difference may be due to the different fitting process used to determine u_τ.

3.1.4 An alternative outer-flow scaling

So far, we have only considered the law-of-the-wall and the defect-law in the forms of Equations 21 and 22, which give rise to a logarithmic overlap region. These similarity laws are generally accepted by most researchers. Recently, however, George et al. (1992) have raised serious objections to the form of the defect-law given in Equation 22. Based on the asymptotic behavior of the logarithmic laws (see below), George et al. argue that u_τ is not the correct

velocity scale for the outer flow. Instead, they favor using U_e. Thus the defect-law takes the new form

$$\frac{U_e - \overline{U}}{U_e} = g\left(\frac{y}{\delta}\right). \qquad (29)$$

Matching this to the law-of-the-wall in Equation 21 results in an overlap region having a power-law form, and the law-of-the-wall and the defect-law take the following forms, respectively, in the overlap region:

$$\frac{\overline{U}}{u_\tau} = C_i\left(\frac{yu_\tau}{\nu}\right)^\gamma + B_i, \qquad (30)$$

and

$$\frac{U_e - \overline{U}}{U_e} = 1 - C_o\left(\frac{y}{\delta}\right)^\gamma - B_o, \qquad (31)$$

where C_i, C_o, and γ are all Reynolds number dependent. The functional forms for C_i, C_o, γ must all be found empirically from data. It is also not possible to determine u_τ by fitting the data to some predetermined curve because of the Reynolds number dependence of Equations 30 and 31. Instead, u_τ must be measured by some independent means. George et al. analysed several data sets for which the values of u_τ were known, and empirically found the corresponding values for C_i, C_o, and γ. They argue that the power-law similarity laws collapse the data better than the logarithmic similarity laws. As evidence, figure 7 shows one of Purtell et al. (1981) velocity profiles plotted using George et al. 's inner scaling compared with Equation 30. One drawback of the power-law similarity laws is that they have not yet been extended to account for the wake. However, George et al. derive a local friction law by matching the mean velocity given by Equations 30 and 31, which are simultaneously valid in the overlap region.

A power-law overlap region provides significant theoretical and practical advantages over the traditional logarithmic form. George et al. (1992) discuss the fact that
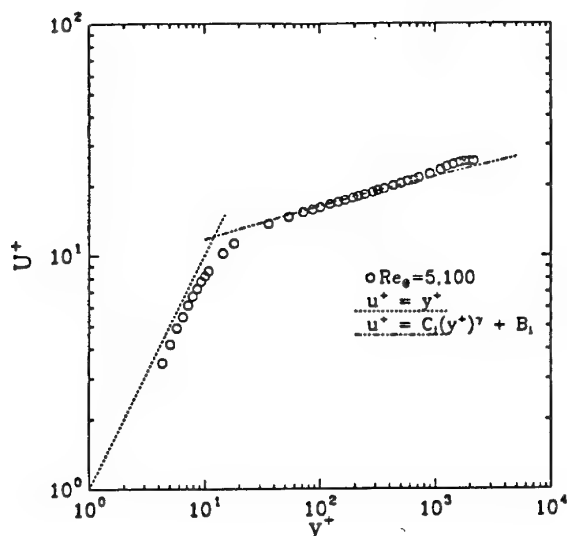
Figure 7: Example of a measured mean velocity profile at $Re_\theta = 5,100$ (from Purtell *et al.*, 1981) compared to the scaling laws proposed by George *et al.* (1992), George & Castillo (1993): ---------------the linear sublayer; -------------------the power-law overlap region (Equation 30). Figure from Smith (1994).

the log-law form indicates that, in the limit of infinite Reynolds number, 1) the velocity profile essentially disappears (that is, $\overline{U}/U_e \to 1$); 2) the ratio of δ to either of the integral scales, δ^* or θ, asymptotes to infinity, and 3) the shape factor, H, asymptotes to a value of 1. The first point poses a theoretical problem, in that if the Reynolds number is increased towards infinity by simply moving downstream on an infinitely long surface, there should always exist a boundary layer. In addition, velocity profile data collapse equally well using either δ^* or θ, as a length scale, as with using δ, which conflicts with the second point. Finally, shape factors below 1.25 have never been measured in zero-pressure-gradient turbulent boundary layers (see, for example, figure 18), which conflicts with the third point. In contrast, the power-law forms predict that 1) a velocity profile will always exist, even in the limit of infinite Reynolds number, 2) the ratios δ/δ^* and δ/θ asymptote to finite values, and 3) the asymptotic value of the shape factor is greater than unity.

It is difficult to judge whether the traditional logarithmic forms or the power-law forms are correct. In practice, the two forms are not very different. This can be seen by comparing figures 4 and 7, which show the same data plotted using both types of scaling.

However, the difference may be important when extrapolating results to very high Reynolds numbers, and the issue needs to be resolved. As shown by Smith (1994), a full similarity analysis supports the use of U_e as the outer-layer velocity scale. His mean-flow measurements in the range $4,600 \leq Re_\theta \leq 13,200$ also appear to support the view that the outer region scales using the freestream velocity as the velocity scale. Although these results tend to give some confidence in power-law similarity laws, the log-law is well-entrenched and unlikely to be replaced by

alternative scalings unless the practical consequences become compelling. Certainly the data presented in this report (see section 3.1.5) is consistent with the traditional log-law over a very wide Reynolds number range, and suggests that the log-law will continue to be widely used.

In contrast to the case for boundary-layer flows, George *et al.* (1992) concluded that for fully-developed pipe and channel flows u_τ is indeed the correct velocity scale throughout the flow. The wall shear stress and the pressure drop are intimately connected through the equations of motion for these flows, and thus u_τ influences the entire flow. This connection is absent in boundary-layer flows. Since there are fundamental differences between developing boundary-layer flows and fully-developed internal flows, it may not be appropriate to compare results from internal flows with results from boundary-layer flows.

3.1.5 The data

Table 1 gives an over-view of the principal sources of data discussed in this section. The discussion follows Fernholz & Finley (1995) closely, and further details may be found there. The table indicates the symbols used for plotting the data in later sections for overall comparison purposes, the range of Reynolds number based on momentum defect thickness and the shape factor, the experimental techniques and the measurements made, the experimental situation and potentially important secondary factors such as tripping devices, freestream turbulence and pressure history. The survey not only shows that relevant data exist in a Reynolds number range $3 \times 10^2 \leq Re_\theta \leq 2.2 \times 10^5$, but indicates several gaps, especially in the case of turbulence data in the medium-to-high range. The recently published measurements by Saddoughi & Veeravalli (1994) reach a peak Reynolds number of 3.2×10^5, but were obtained on a rough wall.

The turbulence data shown in Table 1 were obtained largely by using hot-wire probes, which can give rise to problems with spatial resolution, especially at high Reynolds numbers. This problem will be discussed in Section 3.2.1 below. The only laser Doppler anemometer data listed in Table 1 are those of Petrie *et al.* (1990) although there are two further investigations (Table 2) at low Reynolds numbers (≤ 2100) (Karlsson & Johansson, 1988, Bisset & Antonia, 1991, Djenidi & Antonia, 1993).

We begin the discussion of Reynolds number effects by considering the value of the minimum Reynolds number for a fully-developed turbulent layer. At low Reynolds numbers, the transition trip, the upstream history, or boundary conditions such as freestream turbulence, can all influence the development of the boundary layer, and therefore the Reynolds number alone is thus not sufficient to determine whether a zero presure gradient boundary layer fulfills all the conditions for a "fully developed" state. The shape parameter H, skin friction coefficient C_f and the strength of the wake component Π should also be used as criteria, as well as the Reynolds stress maxima and the shape of the spectra.

Preston (1958) compared measurements made on a flat plate by Dutton (1955) with a reworking of Nikuradse's (Nikuradse, 1932, Nikuradse, 1933) pipe flow measurements, and "the rather limited experimental information"

1 Symbol	2 Author	3 Date	11 Reynolds No. R[H]2; EX-3	14 Shape Factor H12	6 Wall Shear Measurement	7 Mean Velocity Probe (Profiles)	8 Fluctuation Measurements	12 Turbulence Data	9 Probe 1/d	10 Wall Scaling 1+ = 1 utau/nu	16 Stations	4 Free stream Turbulence	5 Tripping Device	15 Upstream History	13 Model
⊠	Winter & Gaudet	1973	22 - 212	1.30 - 1.24	Balance	Pitot Tube 16	-	-	10	10	11	Not Given	Natural	Unknown	Tunnel Side-Wall
△	Collins et al. and (Dimotakis et al.)	1978	5.9 - 7.9	1.39 - 1.34	Coles Fit / Preston Tube	Flattened Pitot Rake (6)	- (LDV)	-	-	-	6	Not Given	Transition Strip	Unknown	Flat Plate
▲	Karlsson	1978	1.6 - 11.7	1.40 - 1.34	Coles Fit	Hot wire (5)	Hot Wire	u'	250	22 - 100	1	0.20%	Trip-Wire	Nozzle Flow	Tunnel Wall
		1980	0.8 - 16.3	1.48 - 1.30	Preston Tube	Pitot Rake (24)									
○	Purtell et al.	1981	0.46 - 5.1	1.60 - 1.35	Log-Law / MV Balance	Hot Wire 11	Hot Wire / LDA	u'	400	8 - 30	7	≤ 0.05%	No.4 Floor Sand Paper	None	Aluminium Plate
▶	Head & Bandyopadyay	1981	0.61 - 17.4	1.53 - 1.35	Preston Tube	Rake (5) Pitot Tube	-	-	-	-	Probably 2	Not Given	Trip, not Described	Unknown	Tunnel Wall
+	(Spalart)	1988	0.3 - 1.4	1.66 - 1.40	(Numerical)	(Numerical)	(Numerical)	(Numerical) (All)	-	-	4	0	(Natural)	None	Flat place
⊗	Erm & Joubert	1988 1991	0.5 - 2.8	1.55' - 1.40	Preston Tube (1 mm)	Hot Wire (N) (28) Pitot-Static	Hot Wires N & X	u', v', w', u'v' u'^2v, v'^2u'	60 - 180	21 - 30	15	≤ 0.32%	Trip Wire, Grit, Pins	Unknown	Tunnel Wall
⬤	Roach & Brierley	1989	0.4 - 1.1	1.57 - 1.46	Preston Tube	Hot Wire (8)	Hot Wire N & X	u', v', w', u'v'	200	- 8	8	≤ 3%	Natural	None	Perspex
◖			0.4 - 2.1	1.51 - 1.38	MV Balance	Hot Wire (9)		u', v', w', u'v'	200	- 16	9	≤ 6%	Natural	None	Plate
■	Bruns et al.	1992	2.6 - 16.1	1.37 - 1.28	Preston Tube, Wall Pulsed, Wall Hot Wire	Hot Wire 4	Hot Wire N & X	u', v', w', u'v' u'^2v, v'^2u' Higher Moments	200	9 - 32	2	≤ 0.1%	V-Dymotape Velcro-tape	None	Aluminum Plate
×	DNW	1994	29 - 60	1.29 - 1.26	Preston Tube HRF (1971)	Hot Wire 3	Hot Wire N, X & Triple	u', v', w', u'v' u'^2v, v'^2u' Higher Moments	200	24 - 70	2	≤ 0.01%	Natural	Unknown Nozzle Flow	Tunnel Wall
▽	Smith & Smits	1994	4.6 - 13.1	1.39 - 1.31	Preston Tube Clauser Chart *	Flattened Pitot 10 + 2	Hot Wire N & X	u', v', w', u'v' u'^2v' Higher Moments	160	- 60	10	Not Given	Trip Wire	Unknown	Tunnel Wall
▢	Murlisa et al.	1982	0.8 - 4.8	1.49 - 1.43	Preston Tube Stanton Tube	Pitot Tube (11) 10 Tabulated	Hot Wire N & X	u', v', u'v' u'^2v, v'^2u' u'^3, v'^3	200	- 30	11	≤ 0.1%	Trip wire 0.76 mm	None	Tunnel Floor BL Removed
	Perry & Li Li	1990 1989	2.8 - 11.1	?	Preston Tube Clauser Chart	Hot Wire 9	Hot Wire N & X	u'v'w'u'v'	200	?	9	Not Given	Trip wire	?	Tunnel Wall
⬤	Andropoulos et al.	1984	3.6 - 15.4	1.31 - 1.28	Slope du/dy Preston Tube	Pitot tube Hot Wire	Hot Wire N & X	u',v',w',u'v' Higher Moments	200	17 - 66	?	6.06%	Not given	None	Flat Plate
	Durst et al.	1987			Clauser plot Preston Tube							6.05%	Not given		
⌀	Willmarth & Tu	1967	38	1.30	Stanton Tube	Pitot Tube Hot wire	Hot Wire	?	233	56	1	Not Given	Natural	Unknown	Tunnel Wall
	Lu & Willmarth	1973	4.8	1.32	Clauser Plot	Pitot Tube Hot wire	Hot Wire	?	233	13.5	1	Not Given	Natural	Unknown	Tunnel Wall

Table 1: Sources for subsonic mean flow and turbulence data. Table from Fernholz & Finley (1995).

Author	Date	Minimum RED2	H12	CF.EX3	Δu/utau	FST %	Transition Promoter	Wall Shear Measurement	Log Law Present
1	2	3	4	5	6	7	8	9	10
Purtell et al. (1)	1981	498	1.55	5.4	0.85	0.05	Distributed	Momentum	Yes
		458 <					Roughness	Equation	
Murlis et al. (2)	1982	780	1.49	4.55	≈ 1.2	< 0.1	Trip Wire	Preston Tube	Yes
								Stanton tube	
Smits et al. (3)	1983	354	1.64	≈ 5.5	≈ 1.0	0.4		Preston Tube	Yes
							Pin Type		
Roach & Brierley (4)	1989	502	1.51	5.41	0.1	4.33	FST	Momentum	Yes
		361 <						Equation	
		731	1.45	4.86	1	1.45	FST	Momentum	Yes
		613 <						Equation	
Erm & Joubert (5)	1991	581	. –	–	≈ 0.53	0.32	Trip Wire	Preston Tube	Yes
		537	Unusual form of wake			0.32	Grit	Preston Tube	Yes
		509	Unusual form of wake			0.32	Trip Wire	Preston Tube	Yes
Spalart (6)	1988	670	1.5	4.84	≈ 1.5	≈ 0	None	Calculated	Yes
		300	1.66	5.78	≈ 1.4	≈ 0	None	Calculated	Uncertain
Djenidi & Antonia	1993	≈ 560	–	–	–	–	Pebbles as	Slope du/dy	Yes
		500 <					3D Trip	of Profile	

Table 2: Additional sources for subsonic mean flow and turbulence data. Table from Fernholz & Finley (1995).

available at the time led him to place the lower limit at $Re_\theta \approx 320$ for a boundary layer tripped by a transition wire. Table 2 lists some more recent investigations, together with relevant characteristic information, and it would appear that a logarithmic profile can be identified down to Re_θ values of the order of 350.

Murlis *et al.* (1982) suggested "that the main changes in mean velocity profiles at low Reynolds number arise because of a reduction in the wake component and not through a failure of the inner logarithmic law". This is clearly seen in figure 8 where a range of fully turbulent low Reynolds number profiles are shown. The appearance of a log-law with a greater slope is also noted by White (1981) in the range $400 < Re_\theta < 600$.

Figure 9 shows some skin-friction data compared to a laminar correlation due to Walz (1966) and a turbulent correlation, extended to low Reynolds number, due to Fernholz (1971). The dependence of the transition process on the freestream turbulence level is clearly demonstrated, and the shear stress level reached after transition is closely related to the turbulent correlation, which agrees well with the data of Purtell *et al.* (1981) and Smits *et al.* (1983b). In contrast, it is possible for strong tripping devices to over-stimulate the boundary layer and cause an over-shoot, with C_f values above the turbulent C_f curve (see Dhawan & Narasimha, 1958).

As indicated earlier, the development of a low Reynolds number boundary layer is also indicated by the strength of the wake component (see figure 6). Figure 10 shows data for more recent data, as listed in Tables 1 and 2, including some very high Reynolds number results. There is some question regarding the trend to zero strength wake at $Re_\theta = 500$, as suggested by Coles (see also Smits *et al.* , 1983b). In figure 10, the trend at low values of Re_θ is principally given by the data affected by high levels of freestream turbulence. Coles proposed that "except possibly at very low Reynolds number the effect of increased

stream turbulence is to decrease the strength of the wake component and that the skin-friction value is higher than for comparable experimental data." The data indicate that the wake factor may decrease with freestream turbulence level even at very low Reynolds number, whereas the skin-friction coefficient does not show any particular trend (see figure 9). At high Reynolds numbers, the data also suggest that the value of the wake strength may lie below that suggested by Coles.

In preparing figure 10, the strength of the wake component was found using the constants $\kappa = 0.40$ and $C = 5.10$ in the log law. As Smith (1994) and Fernholz & Finley (1995) indicate, choosing different values can have a significant effect, since the strength of the wake component is always found as the difference between two relatively large quantities. Spalart (1988), in evaluating his own low Reynolds number computational data, found "intolerably large discrepancies between wake-strength values consequent upon small variations in the log-law constants", and concluded that "very accurate measurements or simulations over a wide Re_θ range, as well as a strong consensus on the value of κ (at least two significant digits) will be needed before definitive results can be obtained for $\Delta (U/u_\tau)$". At very high Reynolds numbers, where U/u_τ near the edge of the layer takes large values, this problem becomes even more serious, so a high-Reynolds-number asymptotic value (if one exists) is very difficult to establish.

Velocity profiles for a wide range of Reynolds numbers are shown in inner-layer scaling in figures 11 – 13. Over the entire Reynolds-number range, the agreement with Equation 24 is excellent. Small departures are evident but appear to relate more to differences between investigators than to variation with Reynolds number. The data in figure 12 were measured using the same hot-wire probes and electronic equipment in two different wind-tunnels (HFI at TU Berlin and the DNW in Holland). The measurements by Winter & Gaudet (1973) cover the
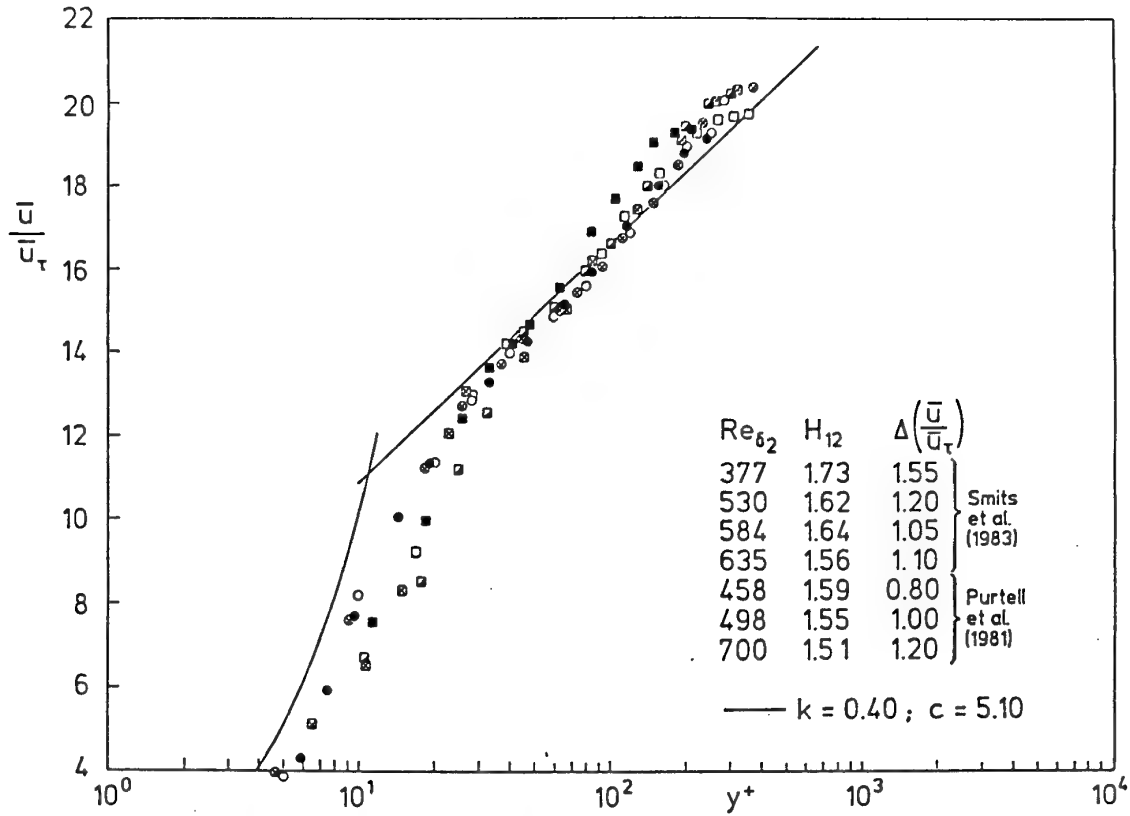
Figure 8: Development of the mean velocity in inner-law scaling in a zero pressure gradient low-Reynolds-number incompressible boundary layer. Figure from Fernholz & Finley (1995).
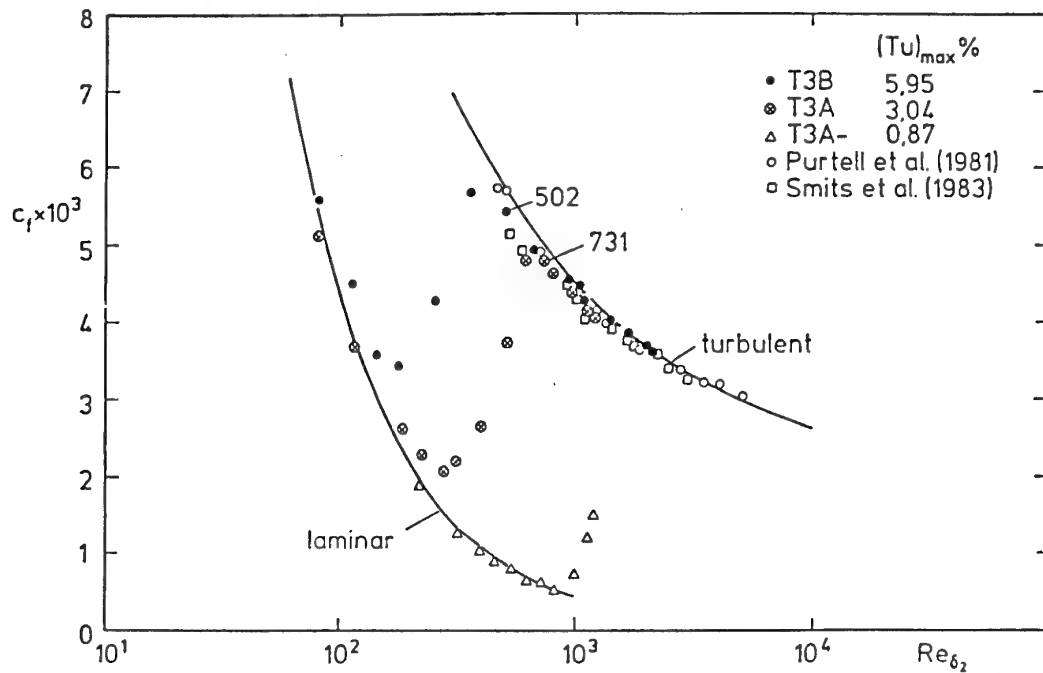
Figure 9: Comparison of measured skin-friction coefficients with skin-friction relationships from Walz (1966) and Fernholz (1971). Data from Roach & Brierley (1989). Wall stress from Preston tube or momentum balance in a laminar-transitional-turbulent boundary layer. Figure from Fernholz & Finley (1995).
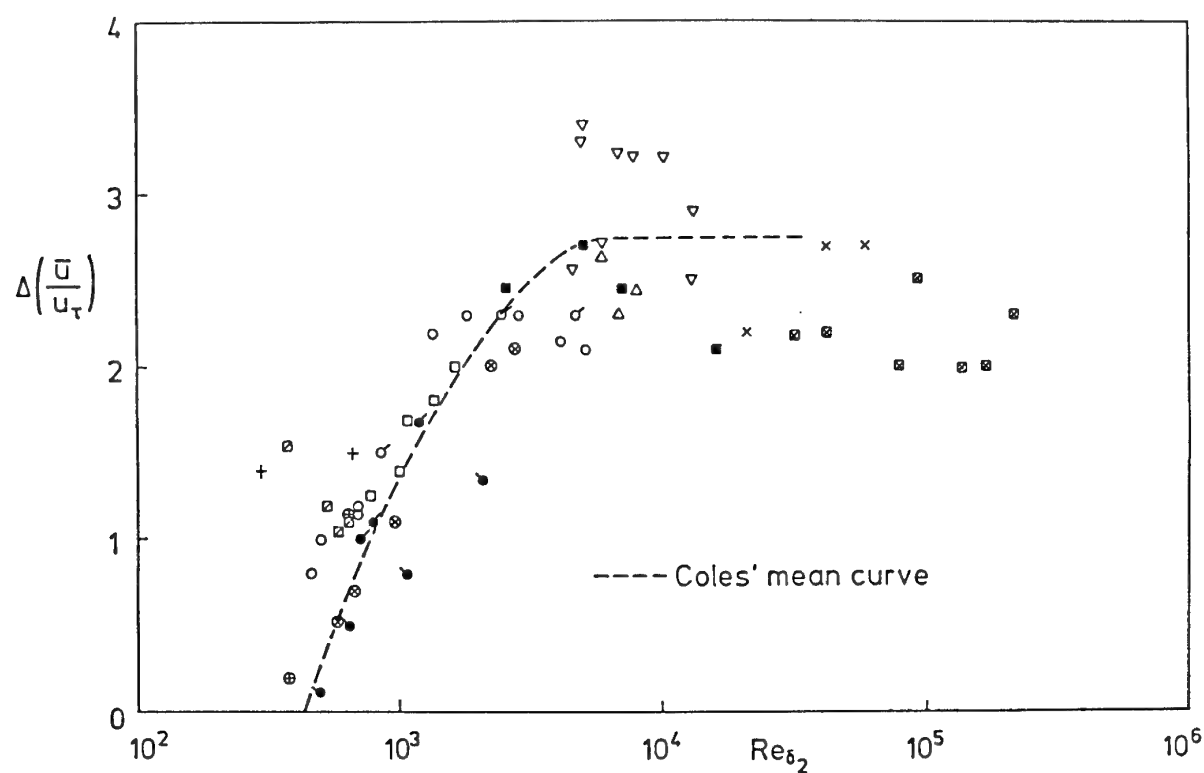
Figure 10: More recent data on the Reynolds-number dependence of the wake strength in subsonic boundary layers (for symbols see Table 1). Figure from Fernholz & Finley (1995).

Figure 11: Development of the mean velocity in inner-layer scaling at low to medium Reynolds numbers. The line is equation 24 with $\kappa = 0.40$ and $C = 5.1$. Figure from Fernholz & Finley (1995).

Figure 12: Development of the mean velocity in inner-layer scaling for medium Reynolds numbers. Data from Bruns *et al.* (1992) and Nockemann *et al.* (1994). The line is equation 24 with $\kappa = 0.40$ and $C = 5.1$. Figure from Fernholz & Finley (1995).

Figure 13: Mean velocity profiles in inner-layer scaling at high Reynolds numbers. Data from Winter & Gaudet (1973) ($M_e = 0.20$). The line is equation 24 with $\kappa = 0.40$ and $C = 5.1$. Figure from Fernholz & Finley (1995).

widest Reynolds number range, and the skin friction was measured using a large floating element balance.

The data are displayed using outer-layer scaling in figures 14 – 16, using the Rotta thickness as the outer-layer length scale. The data collapse is impressive throughout. Over nearly two decades (for $Re_\theta \geq 2,500$), Reynolds-number effects are not detectable within the scatter of the data. Further support for the "universal" outer region similarity is provided by, for instance, Rotta (1962), Coles (1962), and by the agreement with transformed supersonic boundary-layer profiles found in Fernholz & Finley (1980), where similar low-Reynolds-number behavior was also observed.

The skin friction coefficients are shown as a funtions of Re_θ in figure 17. Agreement with the semi-empirical relations developed by Coles (1962) and Fernholz (1971) is within 5% for the range $600 \leq Re_\theta \leq 220,000$, though with a general tendency for the data to lie systematically low at the lower end of the range (see also Smits *et al.* , 1983b).

Figure 18 shows the experimental values of H as derived from the data in Table 1. Agreement with Coles is in general terms good, with the Roach & Brierley data, with high freestream turbulence, lying systematically low.

3.1.6 Discussion of Reynolds-number effects

Despite the fact that the experimental data exhibit considerable scatter, they generally agree with Coles' results, at least in trend. The law-of-the-wall and the law-of-the-wake seem to describe the data reasonably well. As shown in figures 6, 10 and 18, the Reynolds number dependence of Π, C_f, and H is strong at low Reynolds numbers, that is, $Re_\theta < 5,000$. At higher Reynolds numbers, these parameters change only very slowly.

Smith (1994) suggested that the behavior of C_f, Π and H might be explained partially as follows. The inner layer occupies an increasingly smaller fraction of the total boundary-layer thickness as the Reynolds number increases. That is, the ratio $\delta^+ = \delta u_\tau / \nu$ increases with Reynolds number. In the early stages of a boundary layer's development, the Reynolds number is low, δ^+ is relatively small, and the inner and outer layers are likely to interact very strongly. Once an overlap region has been established further downstream, the inner layer may act to set a lower boundary condition for the outer layer. The time scales in the outer layer (one measure is δ/U_e) become much larger than in the inner layer (one measure is ν/u_τ^2), and thus it may take some time (*i.e.* Reynolds number range) for the outer layer to adjust to the boundary condition dictated by the inner layer. Once the Reynolds number is high enough, the inner and outer layers will have become essentially independent. The outer layer will become more like a wake, with the velocity defect scaling with the inner boundary condition set by the local value of u_τ, and the mean-flow properties will have reached their asymptotic values. The fact that C_f, δ and δ^+ continue to vary, and do not reach strictly constant values, implies that the above argument neglects some of the physics.

In all of his studies, Coles assumed that κ and C are constant (using $\kappa = 0.41$ and $C = 5.0$). Purtell *et al.* (1981) also found that κ and C are constant. However, Tennekes & Lumley (1972) claimed that κ is Reynolds number dependent but that C and C' are not. In contrast, Huffman & Bradshaw (1972) provided strong support for a constant κ (they used $\kappa = 0.41$). They found that C is only very weakly Reynolds-number dependent, and then only at very low Reynolds number. As to the actual values of κ and C, Brederode & Bradshaw (1974) analysed several data sets and suggested that $\kappa = 0.41$ and $C = 5.2$ provided the best overall fit to the data. For a large data set of compressible boundary layers, Fernholz & Finley (1980) found that $\kappa = 0.40$ and $C = 5.1$ represented a very good fit to the data. In practice, these differences among values of the constants are not too important, except perhaps for finding the wake function precisely. For example, using either de Brederode & Bradshaw's values, or those recommended by Fernholz $ Finley results in only 1.2% difference in U/u_τ over the range $100 \leq yu_\tau/\nu \leq 10,000$. Finally, the matching procedure used to obtain Equations 24 and 25 requires an integration with respect to y. The constants of integration, C and C', depend on the inner limit of the integration. Duncan *et al.* (1970) point out that this inner limit is Reynolds-number dependent, and therefore C and C' must also be Reynolds-number dependent. Smith (1994) demonstrated that the traditional inner and outer scaling laws cannot both be Reynolds-number independent. If C is assumed to be Reynolds number-independent, then C' must be a function of Reynolds number.

The above discussion has focused on the law-of-the-wall, and most of the published data are presented in this form, as opposed to using the defect-law. Now, if κ and C are taken as constants in Equation 24, and if Π is assumed to be Reynolds-number dependent, then this implies a Reynolds-number dependence of the defect-law, Equation 22. Following both Simpson (1970) and Purtell *et al.* (1981), Equation 27 may be rewritten, using the conditions that at $y = \delta$, $\overline{U} = U_\infty$ and $w(1) = 2$, as

$$\frac{U_e - \overline{U}}{u_\tau} = -\frac{1}{\kappa}\ln\left(\frac{y}{\delta}\right) - \frac{\Pi}{\kappa}w\left(\frac{y}{\delta}\right) + \frac{2\Pi}{\kappa}. \qquad (32)$$

Alternatively, Equation 24 may be substituted into Equation 25, since both are valid in the logarithmic overlap region, to yield (after using Equation 17)

$$C' = -C + \sqrt{\frac{2}{C_f}} - \frac{1}{\kappa}\ln\left(\frac{\delta u_\tau}{\nu}\right). \qquad (33)$$

(Smith, 1994). Because both C_f and δ^+ are Reynolds number dependent, C' must be a function of Reynolds number. If both C and C' are assumed to be constant, this requires that C_f and δ^+ have a very specific relationship, namely that $\sqrt{2/C_f} - (1/\kappa)\ln(\delta^+) = $ constant. Coles's (1968) correlations for C_f and δ^+ do not support this relationship. It is clear that if C is a constant, C' is not. Consequently, if the log-law given by Equation 24 is universal, then the log-law given by Equation 25 is not. Smith (1994) suggested that this may explain the slight Reynolds-number dependence of the logarithmic region when using outer scaling, as was shown in figure 5b.
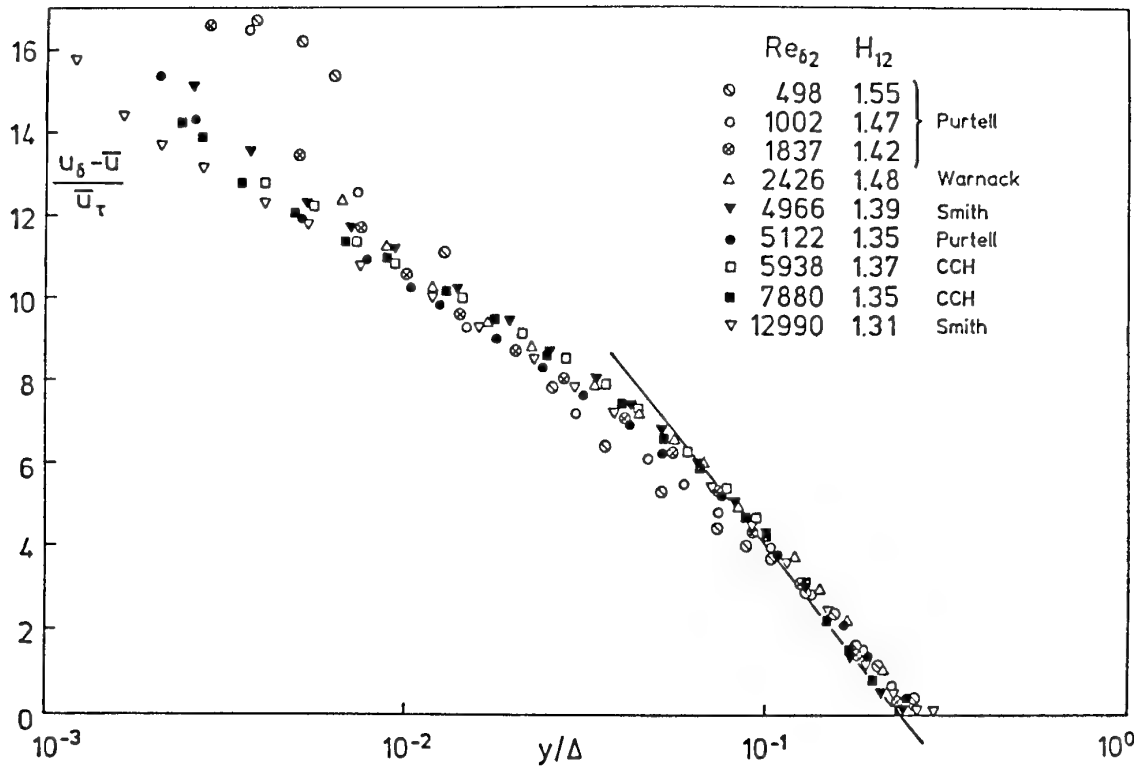
Figure 14: Development of the mean velocity in outer-layer scaling at low to medium Reynolds numbers. The line is equation 69. Figure from Fernholz & Finley (1995).
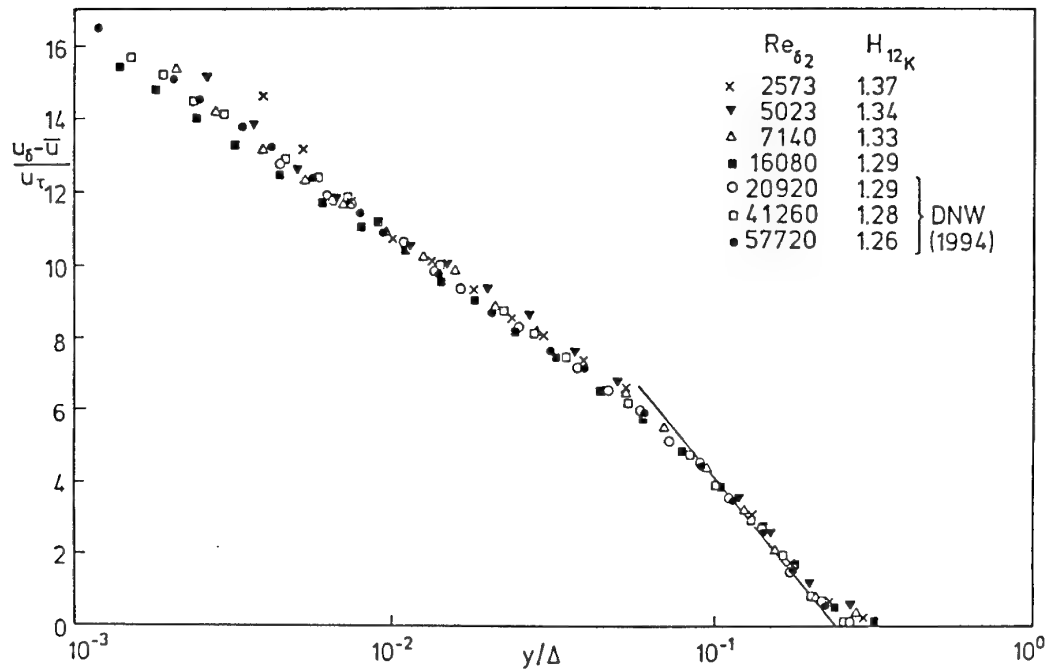
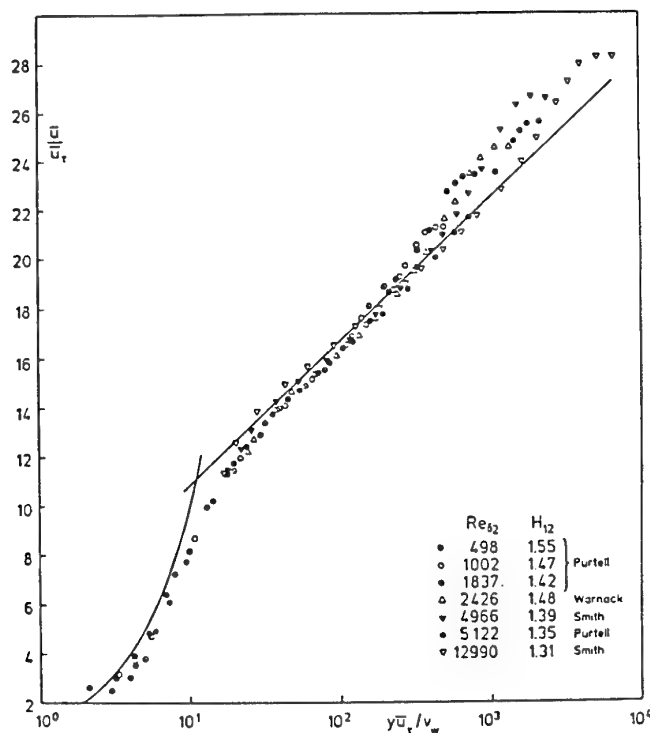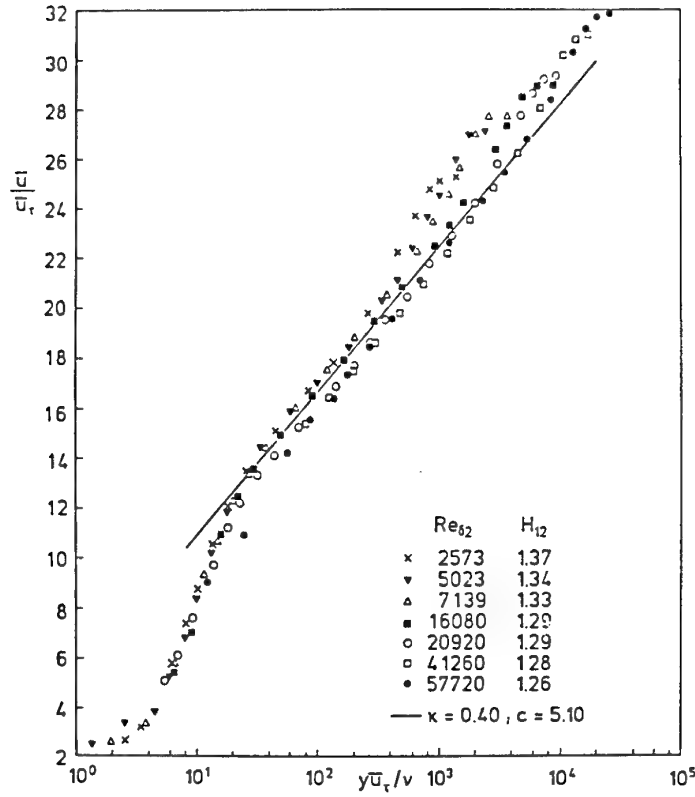Figure 15: Mean velocity profiles in outer-layer scaling for medium Reynolds numbers. Data from Bruns et al. (1992) and Nockemann et al. (1994). The line is equation 69. Figure from Fernholz & Finley (1995).

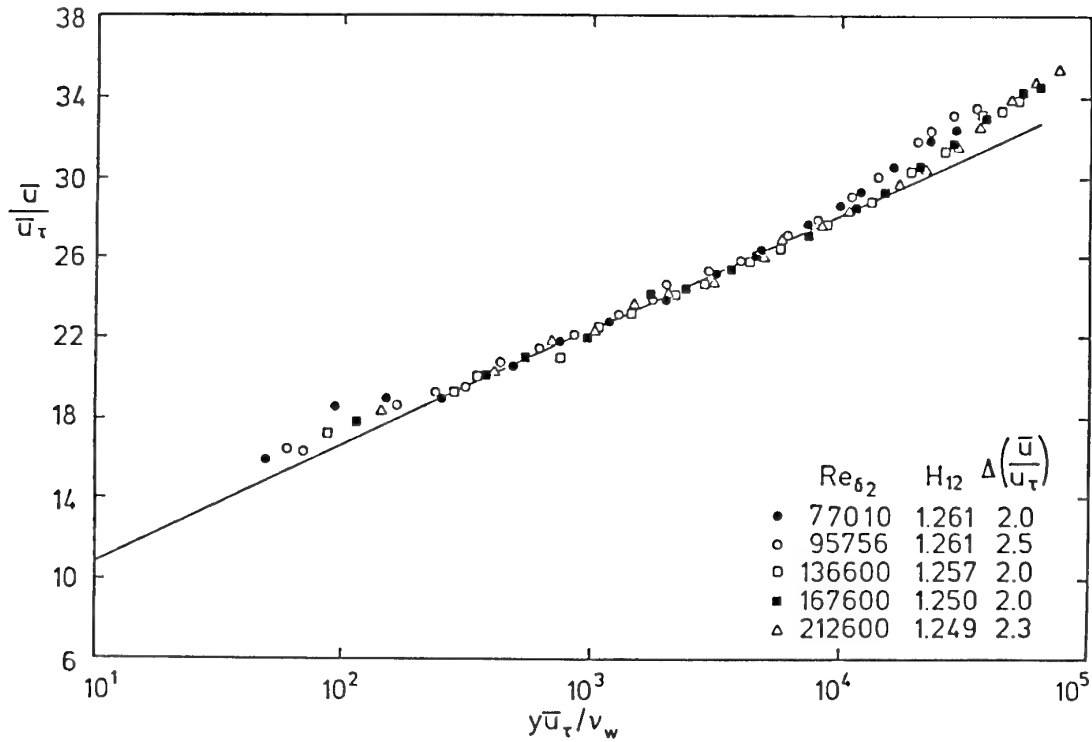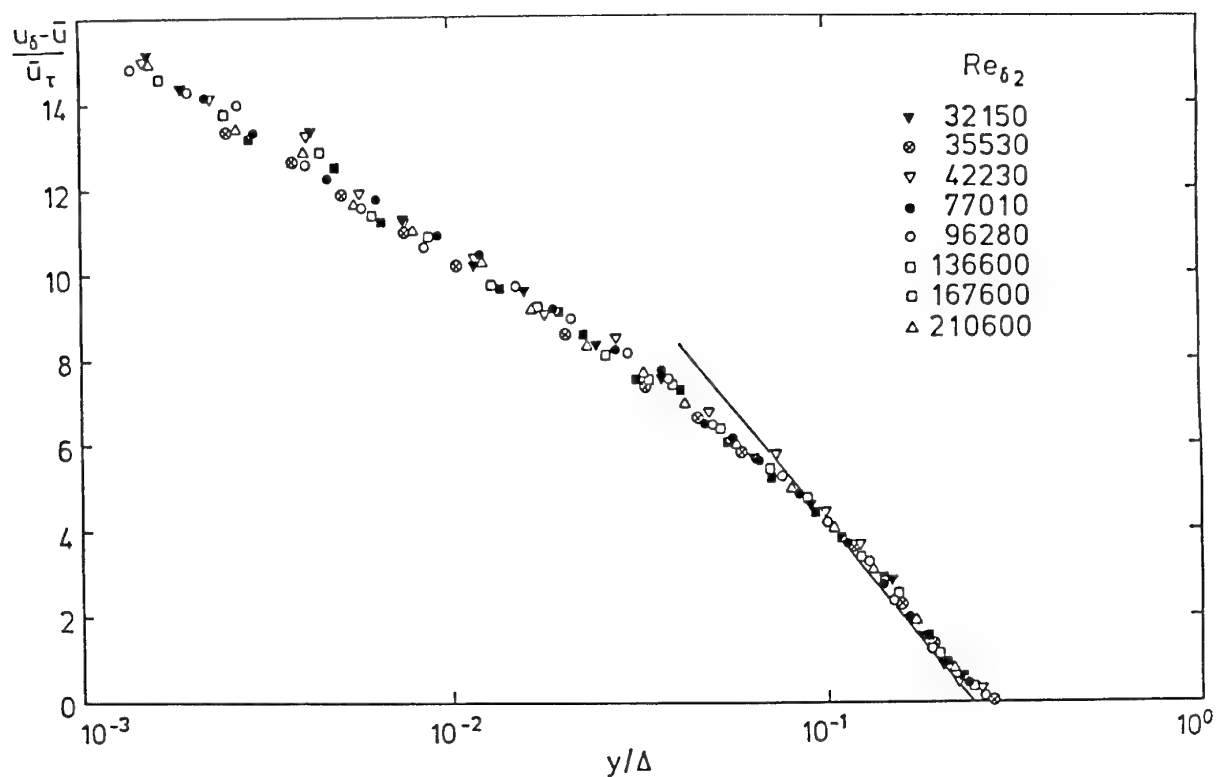Figure 16: Development of the mean velocity in outer-layer scaling at high Reynolds numbers. Data from Winter & Gaudet (1973) ($M_e = 0.20$). The line is equation 69. Figure from Fernholz & Finley (1995).
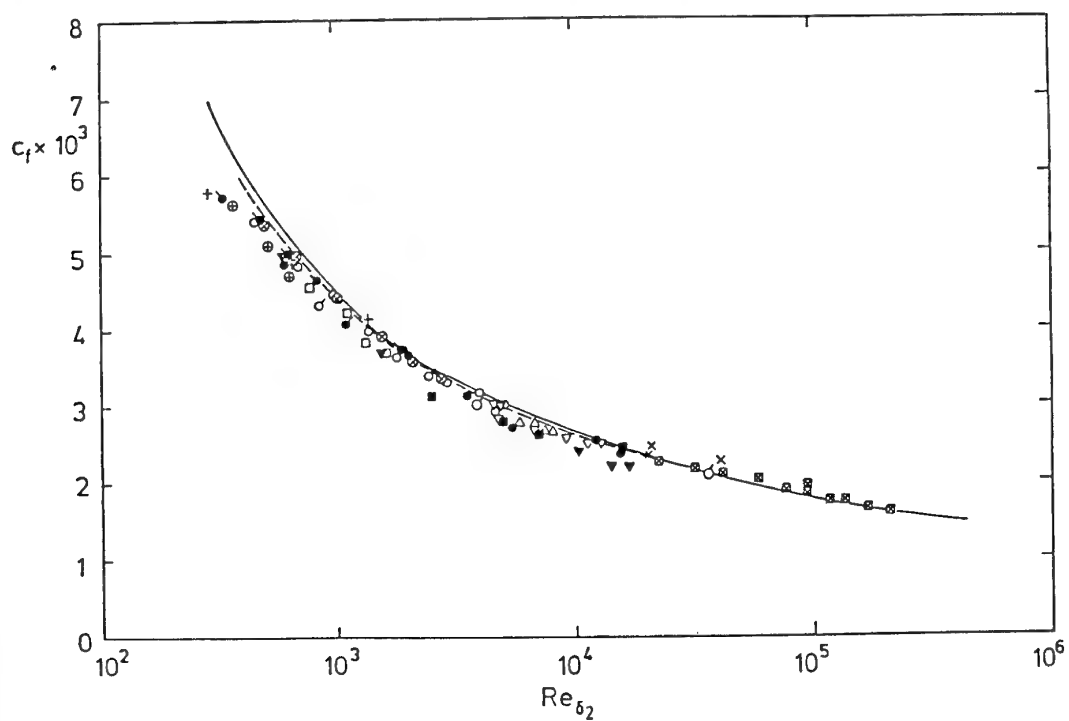
Figure 17: Skin-friction coefficient variation with Reynolds number. $--------$, Coles (1962); ———————, Fernholz (1971) (for symbols see Table 1). Figure from Fernholz & Finley (1995).
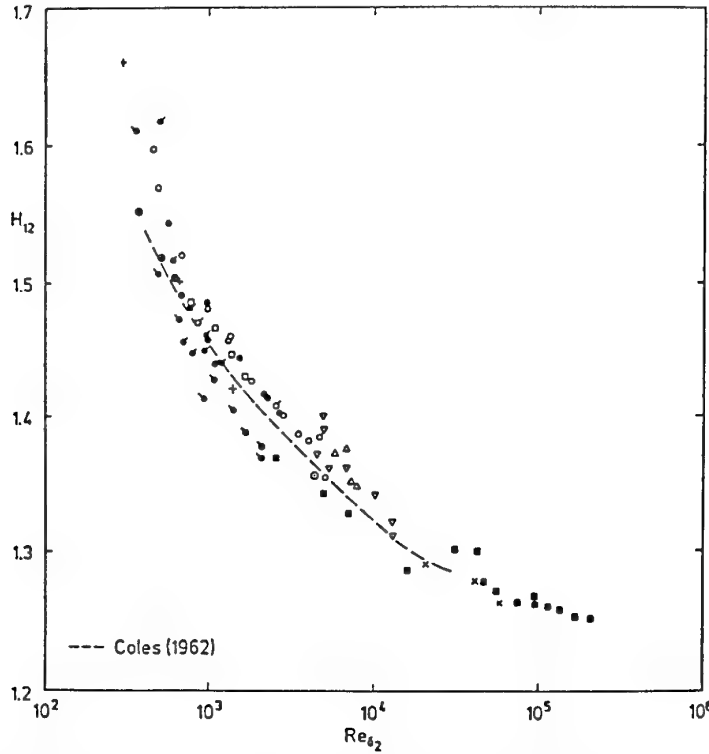
Figure 18: Variation of shape parameter H with Reynolds number (for symbols see Table 1). Figure from Fernholz & Finley (1995).

3.2 Turbulence statistics

Despite the discussion given above, the mean flow inner/outer scaling scheme as expressed by Equations 21 and 22 (or better in terms of the velocity gradient $\partial U/\partial y$ appears to be very successful in practice. A similar inner/outer scaling is therefore expected to apply to the time-averaged turbulence statistics. That is, for the inner region,

$$\frac{\overline{u'^2}}{u_\tau^2} = f\left(\frac{yu_\tau}{\nu}\right), \tag{34}$$

and for the outer region,

$$\frac{\overline{u'^2}}{u_\tau^2} = g\left(\frac{y}{\delta}\right). \tag{35}$$

(these statements imply that the mean velocity and turbulence intensities scale with the same set of velocity and length scales: more precisely, they imply that the velocity gradient and the turbulence intensities scale similarly). However, matching the turbulence intensity in the overlap region leads to the conclusion that $\overline{u'^2}/u_\tau^2$ is constant in the log-law region (see, for example, Townsend, 1976). This is not observed (see figures 29 and 30. One explanation of this (Bradshaw, 1967, Bradshaw, 1994)) is that the "true" or "active" turbulent motion is overlaid by an irrotational "inactive" motion imposed by the pressure field of the large eddies in the outer part of the layer. Motions of this nature have large wavelengths, of order δ, and so are large as compared to the scale of motions in the inner layer. However, as the wall is approached the v' component of the inactive motion must become small due to the

wall constraint (the "splat" effect) so that its influence on the shear stress is minor, and the mean velocity log-law is preserved. The question remains as to what extent the turbulence profiles are similar in the sense that they collapse onto a Reynolds-independent curve.

Unfortunately, the methods available for measuring turbulence quantities are less accurate than the relatively simple methods used to measure the mean flow. Willmarth (1975) states that in 1960 he attempted to collect all the available data for turbulence intensity profiles and show them on a single plot. The data did not agree to within ±50%. Willmarth attributed the large scatter to freestream disturbances and differences in tripping devices among the various investigations considered. Difficulties and uncertainties associated with hot-wire anemometry, such as differences in calibration methods, calibration drift, and spatial averaging and attenuation due to finite probe size also contributed to the uncertainty. It is important to take these measurement difficulties into account, before we conclude that the turbulence statistics are Reynolds-number dependent.

3.2.1 Spatial resolution effects

Before analyzing the existing turbulence data, we present the following discussion by Smith (1994) on the effects of spatial averaging on turbulence measurements. The velocity measured by a probe such as a hot wire is a spatial average along the sensor length, and, according to Johansson & Alfredsson (1983) a weighted average ow-

ing to the effects of non-uniform temperature distribution along the wire. If the velocity variation along the sensor is large, the averaging is also likely to be influenced by the non-linearity of the probe calibration. Thus eddies which have scales smaller than the length of the wire will not be accurately resolved. Not all components of the three-dimensional spectrum are filtered equally: for example, the attenuation of the turbulence intensity as measured by a single-wire probe is determined by the relative magnitude of the wave-number parallel to the probe. The spatial filtering of the wire is applied to the three-dimensional spectrum, and it will not remove all the disturbances with a wavelength smaller than the wire length (see Blackwelder & Haritonidis, 1983, Ewing et al. , 1995).

Uberoi & Kovasznay (1953) first developed a technique for calculating the effect of spatial averaging on measured energy spectra. Wyngaard (1968), Wyngaard (1969) extended this work and developed a framework for correcting measured energy spectra to account for the attenuation at high frequencies (or high wavenumbers) due to spatial averaging. Wyngaard showed that when using normal wire probes, measurements of the energy spectra begin to show significant attenuation at wavenumbers $k_1 l > 1$ for wires of length $l/\eta = 1$ (l is the wire length, k_1 is the longitudinal wavenumber, and η is the Kolmogorov length scale defined in Equation 39). For longer wires, the effects are more severe and begin at lower wavenumbers. For crossed-wires, the issue is even more complicated, because the spacing of the two wires and the cross-talk between them are further sources of error. Wyngaard's correction method assumes that the small scales are isotropic and that Pao's (Pao, 1965) formulation for the three-dimensional energy spectrum is correct.

Ligrani & Bradshaw (1987) studied wire-length effects on turbulence measurements in the near-wall region ($y^+ \approx 17$) of turbulent boundary layers. They found that adequate resolution ($\pm 4\%$) of turbulence statistics (mean squared values and higher-order moments) requires probe dimensions of $l/d > 200$, and $l^+ = l u_\tau / \nu < 20$. They also found that adequate resolution of the high wavenumber end of the energy spectra appears to require $l^+ < 5$ (in their study, $\eta^+ = 2$ at $y^+ = 17$). Browne et al. (1988) proposed much more stringent criteria: they suggested that for accurate measurements ($\pm 4\%$) of turbulence statistics, crossed-wire probes should have dimensions $l/\eta < 5$ and $d_w/\eta < 3$ (d_w is the distance between the two wires of the crossed-wire probe). These criteria are difficult to meet in a typical laboratory experiment: such small probes are very difficult to manufacture, and with such small distances between wires, cross-talk will be a major problem.

Perry et al. (1986) found that probe dimensions can dramatically affect measured energy spectra and turbulence statistics and thereby alter the apparent scaling behavior of the data. Klewicki & Falco (1990) compiled data from several investigations in boundary layers and channel flows, along with their own measurements in a boundary layer. Although they do not give any specific recommendations for the probe dimensions, they show that wire length effects can easily obscure Reynolds-number effects, leading to incorrect conclusions about the scaling behavior of the turbulence. They also studied the effect of wire spacing on measurements of velocity derivatives (both spatial and temporal) and suggest that wires should be spaced only a few Kolmogorov lengths apart at most.

For high-Reynolds-number laboratory flows, η is very small, and these restrictions are extremely difficult to meet in a laboratory flow, particularly when it is necessary to maintain $l/d > 200$ to minimize end-conduction effects, as discussed by Perry et al. (1979) and Hinze (1975). Fernholz & Finley (1995) point out that high Reynolds number experiments using hot wires therefore need to be made in large wind tunnels where the Reynolds number is a consequence of large physical scale and development length rather than high velocity, so as to take advantage of the smallest wires available, with minimum diameters of about $0.6 \mu m$. This requirement argues for the development of new techniques to study small-scale turbulence. For example, cryogenic tunnels achieve high Reynolds numbers with very small viscosities. In such cases the physical length scales are even smaller than that of the equivalent flight environment, and hot-wire anemometry is only of limited use.

To illustrate the effects of spatial filtering on turbulence levels, figure 19 is reproduced from Fernholz & Finley (1995). Here, the maximum value of $\overline{u'^2}/u_\tau^2$ is clearly seen to decrease as the dimensionless wire length l^+ increases. This trend is shown even more clearly by the results of Ligrani & Bradshaw (1987) (see figure 20), where the maximum value of $\overline{u'^2}/u_\tau^2$ increases from 2 to 2.8 as l^+ decrease from 60 to 3. (These results are discussed further in Section 3.2.3.)

Westphal (1990) presented a method for estimating spatial resolution errors in which the error is assumed to depend on the ratio of probe dimension to the Taylor microscale. Westphal's analysis is an extension of work by Frenkiel (1954) and includes corrections for normal wires, crossed-wire probes, and dual wire V-configuration probes. Nakayama & Westphal (1986) studied the effects of sensor length and spacing on turbulence statistics measured using a crossed-wire probe in a turbulent boundary layer ($Re_\theta = 8,300$). Their results showed that the Reynolds normal stresses suffer more severe errors than the Reynolds shear stress. However, the shear correlation coefficient, $-\overline{u'v'}/u'_{rms} v'_{rms}$, was quite insensitive to probe dimensions, because increased sensor spacing acted to overestimate $\overline{v'^2}$ but underestimate $\overline{u'^2}$. Overall, $\overline{u'^2}$ showed the greatest sensitivity to sensor length, while $\overline{v'^2}$ was most influenced by sensor spacing.

The effect of sensor-wire separation of one viscous length on the synthetic response of an X-wire probe was investigated by Moin & Spalart (1987). They found that even this small separation led to an overestimation of the $\sqrt{\overline{v'^2}}$ component of more than 10% near the wall. Park & Wallace (1993) have computed the influence on an X-array, and found that for $L^+ = 9$ at $y^+ = 30$ the $\sqrt{\overline{v'^2}}$ value was about 40% high, while $\overline{u'v'}$ was about 3% low. With $L^+ = 2.3$ the corresponding values were 3% and 5%. These calculations do not provide the final answer, but indicate that we can expect the error in $\sqrt{\overline{v'^2}}$ will be larger than the error in $\overline{u'v'}$ and will increase with L^+.
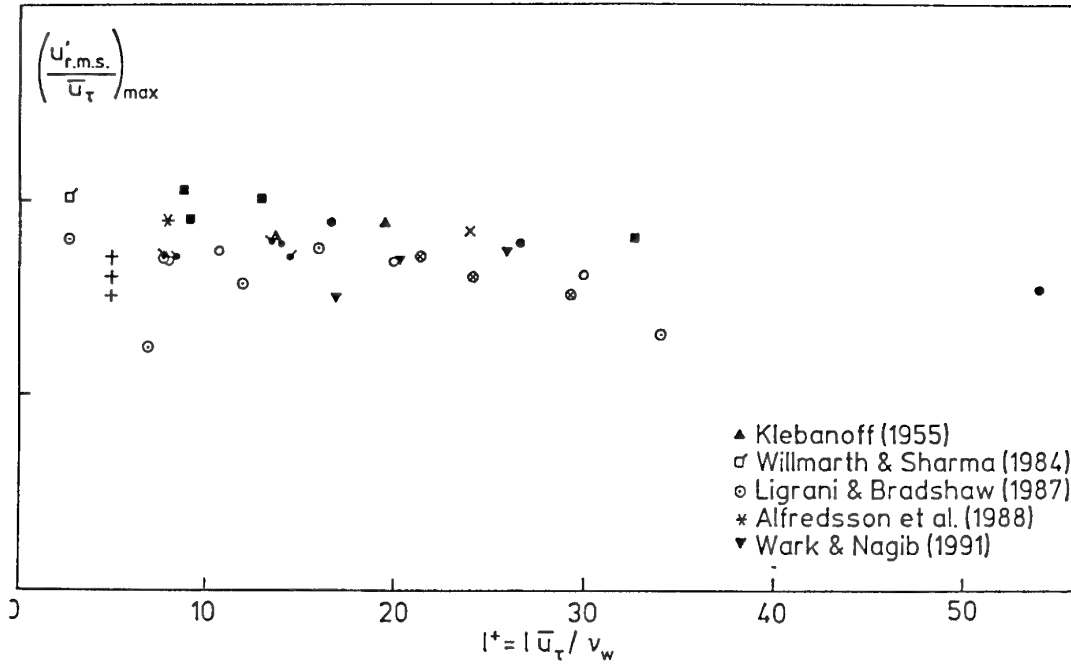
Figure 19: The influence of the characteristic dimensionless hot-wire length scale l^+ on the maximum value of $\sqrt{\overline{u'^2}}/u_\tau$ in subsonic boundary layers. $Re_\theta > 700$ and $l/\delta > 180$. For additional symbols see Table 1. Figure from Fernholz & Finley (1995).
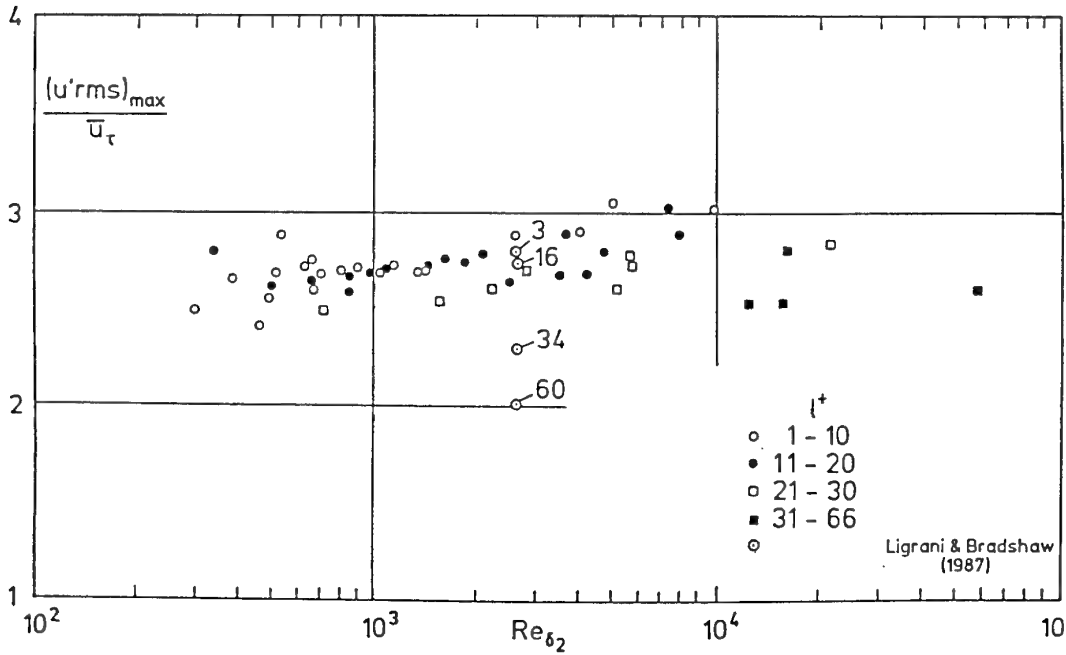
Figure 20: The influence of l^+ and Reynolds number on the maximum value of $\sqrt{\overline{u'^2}}/u_\tau$. Data from 13 experiments. Figure from Fernholz & Finley (1995).
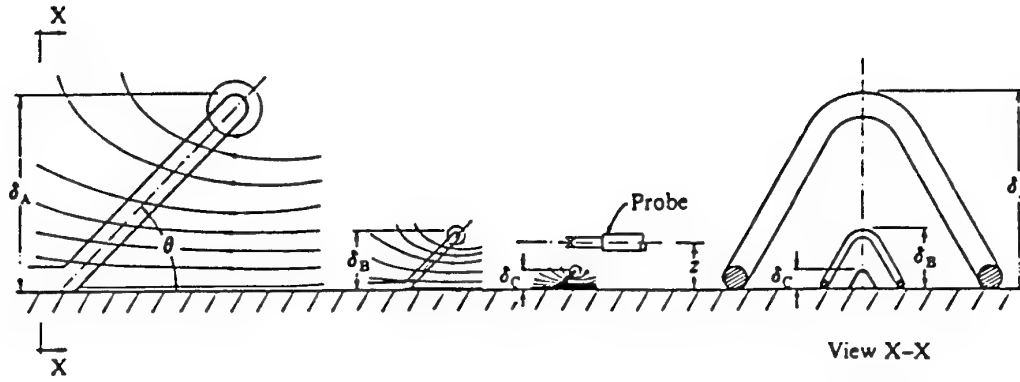
Figure 21: Sketch of the streamline patterns and spatial influence of attached eddies at three different scales (reproduced from Perry *et al.* , 1986).

3.2.2 Scaling laws for turbulence

To find the scaling laws for the turbulent stresses, it is useful to begin by considering the scaling of the turbulence spectra. The most consistent and successful scaling laws for the turbulence energy spectra were first suggested by Townsend and developed extensively by Perry and his co-workers. Based upon Townsend's (Townsend, 1976) "attached eddy" hypothesis and the flow visualization results of Head & Bandyopadhyay (1981) (see Section 3.3.2), Perry & Chong (1982) developed a physical model for near-wall turbulence. They assumed that a turbulent boundary layer may be modelled as a forest of hairpin or Λ-shaped vortices, which originate at the wall and grow outward. Figure 21 shows three Λ-shaped vortices of different scales, and indicates their influence on the velocity field sensed by a probe at a position y. The probe will sense contributions to u' and w' from all eddies of scale y and larger. However, only eddies of scale y will contribute to v'. Therefore, u' and w' should follow similar scaling laws, while v' may follow a somewhat different scaling law. Using these ideas in conjunction with dimensional analysis, Perry *et al.* (1985), Perry *et al.* (1986) derived scaling laws for the energy spectra in the turbulent wall region, defined as $\nu/u_\tau \ll y \ll \delta$. In general, it is the region beginning far enough from the wall such that direct wall effects, such as the damping of the velocity components, are unimportant, and extending to a point far enough inward from the boundary layer edge such that the direct influence of the large scale flow geometry and outer boundary conditions are also unimportant. Thus, at sufficiently high Reynolds numbers, any wall-bounded turbulent shear flow should have a turbulent wall region, where the following analysis will apply.

First consider the u' component of the turbulence fluctuations. Eddies of scale δ will contribute only to the large-scale, low-wavenumber (low-frequency) region of the energy spectrum, Φ_{11}. For the large-scale eddies, viscosity is less important, and the spectrum in the low-wavenumber region should depend only on u_τ, k_1, y and δ, where k_1 is the streamwise component of the three-dimensional wavenumber vector $\vec{k}$. Thus, from dimensional analysis, the spectrum of u' at low wavenumbers should have the

form

$$\frac{\Phi_{11}(k_1\delta)}{u_\tau^2} = g_1(k_1\delta) = \frac{\Phi_{11}(k_1)}{\delta u_\tau^2}. \tag{36}$$

Throughout this section, the argument of Φ_{ii} will denote the unit quantity over which the energy spectral density is measured, following Perry *et al.* (1986). Perry *et al.* call Equation 36 an "outer-flow" scaling, since it describes the effects of the large scale eddies.

Eddies of scale y will contribute to the intermediate wavenumber range of the spectrum, while eddies of scale δ will not contribute to this range. Thus, in this range the spectrum should have the following "inner-flow" scaling form:

$$\frac{\Phi_{11}(k_1y)}{u_\tau^2} = g_2(k_1y) = \frac{\Phi_{11}(k_1)}{yu_\tau^2}. \tag{37}$$

The smallest-scale motions, which contribute to the high-wavenumber range of the spectrum, are dependent on viscosity. Kolmogorov (1961) assumed that these small-scale motions are locally isotropic, and that their energy content will depend only on the local rate of turbulence energy dissipation, ϵ, and the kinematic viscosity, ν. Dimensional analysis leads to

$$\frac{\Phi_{11}(k_1\eta)}{v^2} = g_3(k_1\eta) = \frac{\Phi_{11}(k_1)}{\eta v^2}, \tag{38}$$

where η and v are the Kolmogorov length and velocity scales respectively, and are defined as

$$\eta = \left(\frac{\nu^3}{\epsilon}\right)^{1/4}, \tag{39}$$

$$v = (\nu\epsilon)^{1/4}. \tag{40}$$

Equation 38 is valid in the high wavenumber region of the spectrum and is commonly referred to as Kolmogorov scaling. The region in which Equation 38 is valid is called the *inertial subrange*.

Just as the mean flow exhibited an inner and outer scaling with a region of overlap, it is expected that Equations 36 and 37 will have a region of overlap (overlap region I), and that Equations 37 and 38 will also have a region of overlap (overlap region II). Perry *et al.* (1986) have shown that in overlap region I, the spectrum must have the form

$$\frac{\Phi_{11}(k_1\delta)}{u_\tau^2} = \frac{A_1}{k_1\delta} = g_1(k_1\delta), \tag{41}$$

or

$$\frac{\Phi_{11}(k_1 y)}{u_\tau^2} = \frac{A_1}{k_1 y} = g_2(k_1 y), \qquad (42)$$

where A_1 is a universal constant.

In overlap region II, the spectrum follows the same form derived by Kolmogorov (1961),

$$\frac{\Phi_{11}(k_1 \eta)}{v^2} = \frac{K_o}{(k_1 \eta)^{5/3}} = g_3(k_1 \eta), \qquad (43)$$

where K_o is the universal Kolmogorov constant. Following the suggestion of Townsend (1976), Perry et al. (1986) assumed that in the turbulent wall region dissipation is equal to production, thus

$$\epsilon = -\overline{u'v'}\frac{\partial \overline{U}}{\partial y}. \qquad (44)$$

They also assumed that in the turbulent wall region 1) the velocity profile is logarithmic as given by Equation 24, and 2) $-\overline{u'v'} = u_\tau^2$. These assumptions can be used with Equations 39 and 40 to show that, in the turbulent wall region,

$$\eta = \left(\frac{\nu^3 \kappa y}{u_\tau^3}\right)^{1/4} \qquad (45)$$

$$v = \left(\frac{\nu u_\tau^3}{\kappa y}\right)^{1/4}. \qquad (46)$$

Substitution of Equations 45 and 46 into Equation 38 and forcing it to match with Equation 37 yields

$$\frac{\Phi_{11}(k_1 y)}{u_\tau^2} = \frac{K_o}{\kappa^{2/3}(k_1 y)^{5/3}} = g_2(k_1 y). \qquad (47)$$

Figure 22 shows an example energy spectrum plotted using Kolmogorov scaling. The spectrum shown was obtained in a tidal channel by Grant et al. (1962). The extremely high Reynolds number results in a very long $-5/3$ range in the spectrum.

According to these arguments, the spectra of w', Φ_{33}, will follow similar scaling laws with A_1 replaced by A_3. Figure 23a summarizes the spectral scaling laws for Φ_{11} and Φ_{33}. The boundaries of the overlap regions are denoted by P, N, M, and F. P, N, and M are universal constants, and F is a large scale characteristic constant, and is thus likely to be Reynolds number dependent. Figures 23b and 23c illustrate the deduced form of Φ_{11} and Φ_{33} using inner and outer flow scaling.

For v', figure 21 suggests that there will be no contributions from δ-scale eddies, and thus there will be no outer-flow scaling for Φ_{22}. There will only be inner-flow and Kolmogorov scaling, with one region of overlap. Φ_{22} is described by Equations 37, 38, and 43. Figure 24a summarizes the scaling laws for Φ_{22}, and figures 24b and 24c illustrate the expected form of the spectrum using inner and outer flow scaling. Energy spectra measured by Perry & Abell (1975), Perry & Abell (1977), Perry et al. (1986), Perry et al. (1985), Li (1989), Perry & Li (1990), Erm (1988), Erm et al. (1985) and Smith (1994) have all shown encouraging agreement with these spectral scaling laws (see also Section 4.7).
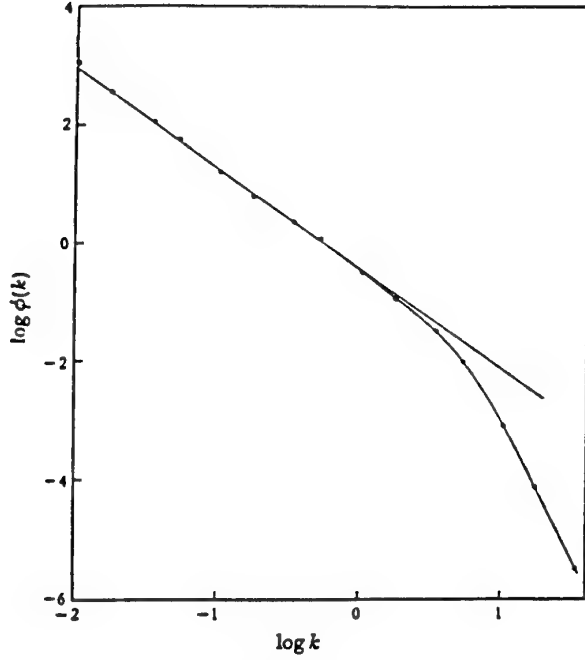
Figure 22: Longitudinal energy spectrum, $\Phi_{11}(k_1)$, measured in a tidal channel at $Re \approx 10^8$. The straight line has a slope of $-5/3$. Figure from Grant et al. (1962).

By integrating these spectral forms, Li (1989) and Perry & Li (1990) derived the following expressions for the turbulence normal stresses:

$$\frac{\overline{u'^2}}{u_\tau^2} = B_1 - A_1 \ln\left(\frac{y}{\delta}\right) - V(y^+), \qquad (48)$$

$$\frac{\overline{w'^2}}{u_\tau^2} = \cdot \, B_3 - A_3 \ln\left(\frac{y}{\delta}\right) - V(y^+), \qquad (49)$$

$$\frac{\overline{v'^2}}{u_\tau^2} = A_2 - V(y^+), \qquad (50)$$

where B_1 and B_2 are large-scale characteristic constants, particular to the flow geometry, and A_1, A_2, and A_3 are expected to be universal constants. $V(y^+)$ is a Reynolds-number-dependent viscous correction term, which accounts for the dissipation region of the spectrum at finite Reynolds numbers. Equations 48–50 are valid only in the turbulent wall region, defined as $\nu/u_\tau \ll y \ll \delta$ (corresponding roughly to the logarithmic overlap region of the mean velocity profile).

By comparison, Equations 34 and 35 neglect the mixed scaling in that the inner and outer regions have a contribution from inner and outer scales at all finite Reynolds numbers. Note, however, that by matching the gradients of the turbulence intensity in the inner and outer regions, Equations 34 and 35 will yield a logarithmic term in y/δ. This may represent an infinite Reynolds number limit.

To extend these scaling laws to regions outside the overlap region in the mean velocity profile, Uddin (1994) considered the distribution of the turbulence intensities for the entire region outside the viscous sublayer. He noted that the broadband turbulence intensities for the streamwise and spanwise velocity fluctuations follow a logarithmic distribution at sufficiently high Reynolds numbers. As

a)

Motions that are independent of viscosity
(i.e. Townsend's Reynolds-number-similarity hypothesis)

Viscosity-
dependent
motions

$\dfrac{\Phi_{11}(k_1 \Delta_E)}{U_\tau^2} = g_1(k_1 \Delta_E)$

('Outer-flow' scaling)

$\dfrac{\Phi_{11}(k_1 \eta)}{v^2} = g_3(k_1 \eta)$

(Kolmogoroff scaling)

0

$k_1 \Delta_E = F$

$k_1 z = P \quad k_1 z = N$

$k_1 \eta = M$
or $k_1 z = M \kappa^{-1} z_+^{\frac{1}{4}}$

k_1

Overlap
region I

Overlap
region II

$(z_+ = z U_\tau / v)$

$\dfrac{\Phi_{11}(k_1 z)}{U_\tau^2} = g_2(k_1 z)$

('Inner-flow' scaling)

b)

$k_1 z = \dfrac{Fz}{\Delta_E}$

-1

$\log \dfrac{\Phi_{11}(k_1 z)}{U_\tau^2}$

$-\frac{2}{3}$

$k_1 z = M(\kappa)^{-1}(z_+)^{\frac{1}{4}}$

$\log P \quad \log N$

$\log (k_1 z)$

c)

-1

$\log \dfrac{\Phi_{11}(k_1 \Delta_E)}{U_\tau^2}$

$k_1 z = \dfrac{P \Delta_E}{z}$

$\log F$

$\log (k_1 \Delta_E)$

Figure 23: Behavior of the energy spectra of the longitudinal and spanwise velocity fluctuations, $\Phi_{11}(k_1)$, according to Perry *et al.* (see text). $\Phi_{33}(k_1)$ is expected to behave similarly. a) Chart showing the different scaling regions, b) inner scaling behavior, and c) outer scaling behavior. Note that in Perry *et al.* 's notation, z is distance from the wall, and Δ_E is a boundary layer thickness, similar to δ. Figure from Perry *et al.* (1986).

a)

Motions that are independent of viscosity
(i.e. Townsend's Reynolds-number-similarity hypothesis)

Viscosity-
dependent
motions

$$\frac{\Phi_{22}(k_1\eta)}{v^2} = h_3(k_1\,\eta)$$

(Kolmogoroff scaling)

0

$k_1 z = N$

$k_1\eta = M$
or $k_1 z = M\kappa - |z|_*$

k_1

Overlap
region

$$\frac{\Phi_{22}(k_1 z)}{u_\tau^2} = h_2(k_1 z)$$

('Inner-flow' scaling)

b)

$$\log\frac{\Phi_{22}(k_1 z)}{u_\tau^2}$$

$k_1 z = M(\kappa)^{-\frac{1}{2}}(z_*)^{\frac{1}{2}}$

$-\frac{5}{3}$

$\log N$

$\log(k_1 z)$

c)

$$\log\frac{\Phi_{22}(k_1\Delta_E)}{u_\tau^2}$$

$\log(k_1\Delta_E)$

Figure 24: Behavior of the energy spectra of the wall-normal velocity fluctuations, $\Phi_{22}(k_1)$, according to Perry *et al.* (see text). a) Chart showing the different scaling regions, b) inner scaling behavior, and c) outer scaling behavior. Note that in Perry *et al.* 's notation, z is distance from the wall, and Δ_E is a boundary layer thickness, similar to δ. Figure from Perry *et al.* (1986).
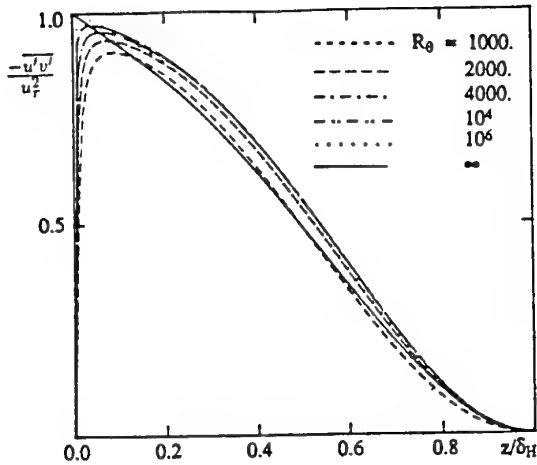
Figure 25: Theoretical Reynolds shear-stress profiles, $-\overline{u'v'}/u_\tau^2$, derived by Li & Perry (1989), form which this figure is taken. In their notation, z is the distance from the wall, and δ_H ($=\Delta_E$) is a boundary layer thickness similar to δ.

with the mean flow, the deviation from the logarithmic profile near the wall is attributed to viscous effects, and the deviation in the outer part of the layer is due to wake effects. He suggested that a wall-wake type of distribution where, for example,

$$\frac{\overline{u'^2}}{u_\tau^2} = B_1 - A_1 \ln\left(\frac{y}{\delta}\right) - V_{g1}(y^+) - W_{g1}\left(\frac{y}{\delta}\right) \ . \quad (51)$$

Here V_{g1} is called the *viscous deviation*, and W_{g1} is called the *wake deviation*. Uddin gave empirical forms for V_{g1} and W_{g1} which agreed well with data over the range $6,570 \leq Re_\theta \leq 35,100$.

Li (1989) (see also Perry *et al.* , 1991, Li & Perry, 1989)) also derived an expression for the total stress, $\tau = \mu\frac{\partial \overline{U}}{\partial y} - \rho\overline{u'v'}$. If the mean velocity profile is assumed known, then the boundary-layer equations may be used to solve for the total stress. For the derivation, Li used the traditional logarithmic law and Coles' law-of-the-wake (Equations 24 and 27) for the mean velocity profile. Li also assumed that the logarithmic law is valid down to the wall, thus introducing a small error by ignoring the buffer layer and viscous sublayer. He then subtracted the viscous stress, $\mu\frac{\partial \overline{U}}{\partial y}$, to obtain an equation for the Reynolds shear stress. Figure 25 shows several Reynolds shear-stress profiles calculated from Li's equation. Note that the variation of the Reynolds shear stress with Reynolds number is *not* monotonic.

Klewicki & Falco (1990), Falco (1991) proposed a different scaling for the streamwise turbulence intensity and Reynolds shear stresses. Instead of starting with arguments on spectral scaling, they used Falco's concept of "typical eddies" (discussed in Section 3.3.2). They first obtained empirical correlations for the length and velocity scales of the typical eddies as functions of Reynolds number. They then scaled the lon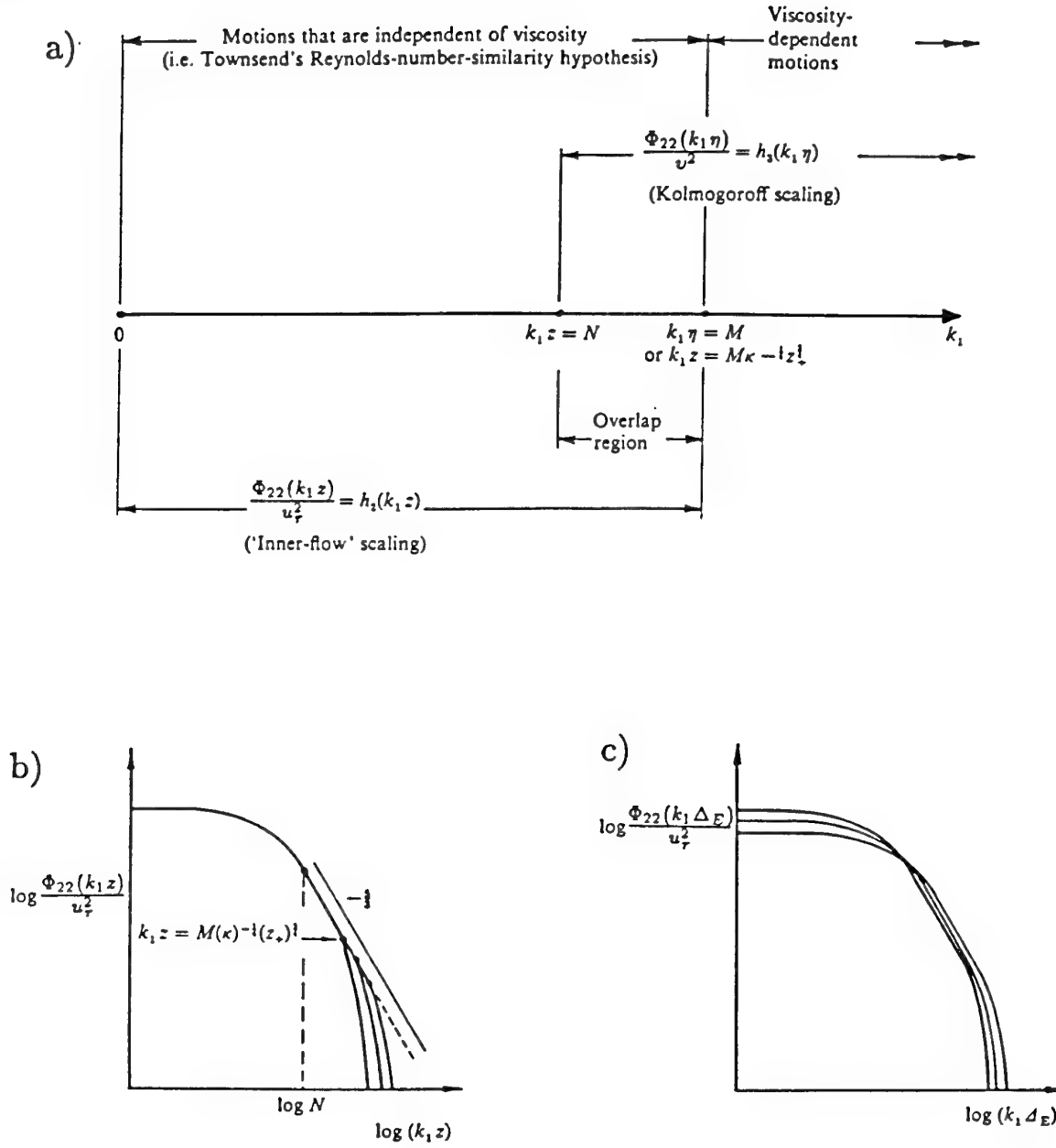gitudinal turbulence intensity and Reynolds shear stress using these typical eddy scales. Data were collected from several sources spanning

the Reynolds number range $1,010 < Re_\theta < 39,000$, and plotted in the form of u'_{rms}/u_{TE} vs. y/l_{TE}, and $\overline{u'v'}/u_{TE}^2$ vs. y/l_{TE}. As shown in figure 26, the data collapsed very well for $y/l_{TE} < 30$, and followed a power law in the range corresponding to the logarithmic region of the mean velocity. It would be interesting to see how well Falco's typical eddy scales correlate the mean flow data over the same wide range of Reynolds numbers but such a study is outside the scope of this AGARDograph.

3.2.3 Reynolds-stress data

The discussion in this section was adapted from that first given by Fernholz & Finley (1995) where further details of the analysis may be found.

Figures 27 and 28 show the distributions of $\overline{u'^2}$ normalised with wall variables. Even at very low Reynolds numbers, similarity can be observed in the range $3 \leq y^+ \leq 50$, even for the cases with high freestream turbulence levels. However, the maximum value of $\overline{u'^2}/u_\tau^2$ tends to increase slightly with Reynolds number. The data shown in figure 20 clearly suggest that if all results are extrapolated to zero sensor length the peak value of u'_{rms}/u_τ increases with Reynolds number, ranging from about 2.8 at $Re_\theta = 1,000$ to about 3.2 at $Re_\theta = 10,000$. The position where this maximum occurs seems to be, however, at $y^+ \approx 15$ (see also Sreenivasan, 1988).

The highest Reynolds number case [DNW 57720] shows some deviations from similarity, but the value of l^+ is unacceptably high. The data are all from single normal wire observations excepting those for $Re_\theta = 41,260$, where an X-wire was used, so that the data do not approach the wall so closely. For values of $y^+ > 100$ large departures are observed in inner scaling, with a tendency for the intensity to form a second maximum in region corresponding to the mean-profile log-law-region, which becomes more pronounced as Re_θ increases. Such second peaks are often observed in high Reynolds number compressible boundary layers (figures 3.1.1 and 3.1.2 in Fernholz & Finley, 1981), although generally not so pronounced.

The $\overline{u'^2}$ data plotted using the Rotta thickness as the outer length scale are shown in figures 29 and 30. It can be seen that with this scaling the data collapse well for $y/\Delta > 0.4$ ($y/\delta > 0.1$) for $Re_\theta > 5,000$ in the same way as the mean velocity profile (figures 14 to 16). The second maximum shown in figure 28 can be seen to represent a further extension of outer similarity towards the wall as Re_θ rises. Figure 29 shows the convergence of the $\overline{u'^2}$ profiles towards this universal behaviour at lower Reynolds numbers.

We conclude, therefore that at high enough Re_θ, the $\overline{u'^2}$ profiles display similarity in the viscous sublayer and buffer layer in inner scaling, while similarity in outer scaling is observed in the logarithmic layer and the outer region.

Smith (1994) found that all three non-dimensional Reynolds normal stresses $\overline{u'^2}/u_\tau^2$, $\overline{v'^2}/u_\tau^2$ and $\overline{w'^2}/u_\tau^2$ were found to increase with Reynolds number throughout the boundary layer. Comparisons with the predictions by Perry *et al.* (Equations 48 – 50) in the overlap region
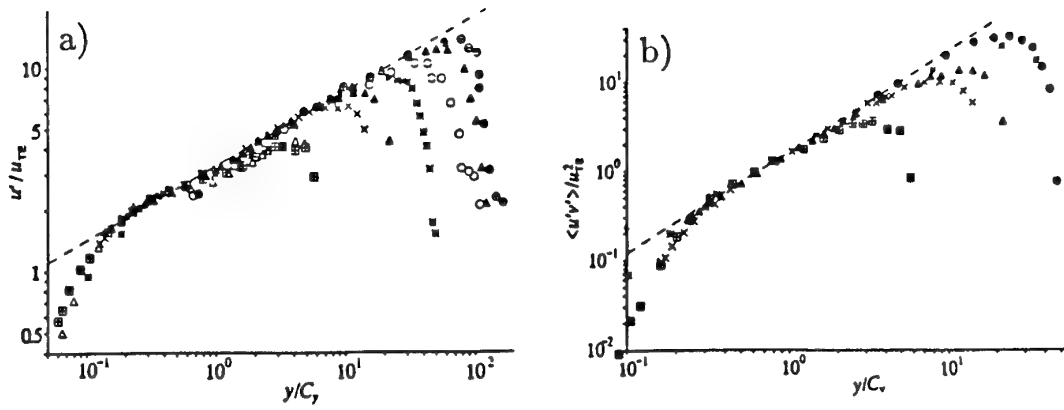
Figure 26: Turbulence stresses scaled on "typical" eddy velocity and length scales, u_{TE} and C_y, respectively: a) u'_{rms} for $1,010 \leq Re_\theta \leq 39,000$. b) $-\overline{u'v'}$ for $1,010 \leq Re_\theta \leq 14,500$. See Falco (1991) for data sources (reproduced from Falco, 1991).
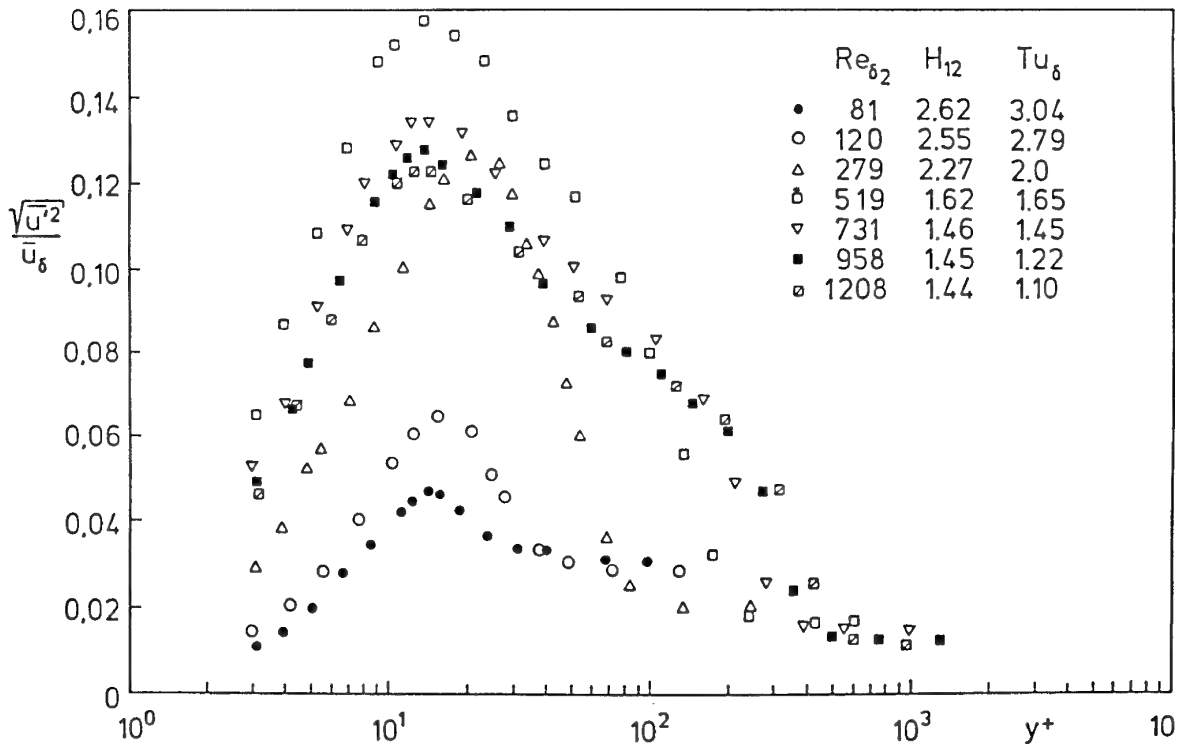
Figure 27: Development of $\sqrt{\overline{u'^2}}\big/u_\tau$ in a zero pressure gradient laminar-transitional-turbulent boundary layer. Tu_δ is the freestream turbulence level. Figure from Fernholz & Finley (1995).

27

Figure 28: Distribution of the longitudinal Reynolds stress in inner-layer scaling at medium to high Reynolds numbers. Data from Bruns *et al.* (1992) and Nockemann *et al.* (1994). ——————, equation 48 for $Re_{\delta 2} = 5,023$; ————————-, $Re_{\delta 2} = 57,720$. Figure adapted from Fernholz & Finley (1995).

Figure 29: Distribution of the longitudinal Reynolds stress in outer-layer scaling at low to medium Reynolds numbers. ——————, equation 48 for $Re_{\delta 2} = 5,023$. Figure adapted from Fernholz & Finley (1995).

Figure 30: Distribution of the longitudinal Reynolds stress in outer-layer scaling at medium to high Reynolds numbers. Data from Bruns *et al.* (1992) and Nockemann *et al.* (1994). ——————, equation 48 for $Re_{\delta 2} = 5,023$; ──────── -, $Re_{\delta 2} = 57,720$. Figure adapted from Fernholz & Finley (1995).

indicated that their additive "constants" are, in fact, Reynolds number dependent. The profiles of $\overline{v'^2}/u_\tau^2$ and $\overline{w'^2}/u_\tau^2$ plotted against y^+ for the studies listed in Table 1 show little or no sign of similarity. Now, v' and w' measurements using an X-wire probe are subject to errors due to spatial averaging errors caused by the separation L of the two wires. The dimensionless distance L^+ is likely to have as great an influence as l^+, and as a result v' and w' measurements are usually less precise than u' measurements (see also Section 3.2.1).

Figures 31 and 32 show these data plotted against y/Δ. As with the u' and v' profiles, an orderly similarity behavior is found, though again the peak values are functions of Re_θ. The value of $\overline{v'^2}/u_\tau^2$ increases from about 1 to 1.6 as Re_θ increases from about 600 to 60,000 (for details see Fernholz & Finley, 1995). Similarly, the value of $\overline{w'^2}/u_\tau^2$ increases from about 2 to 3 as Re_θ increases from about 700 to 40,000. In contrast, Perry & Li (1990) and Erm (1988) found that the peak value of $\overline{v'^2}$ was almost independent of Reynolds number, although they agreed on the trend observed here for $\overline{w'^2}$. The y^+ location of the peak for $\overline{v'^2}$ moves away from the wall as Re_θ increases, in agreement with the findings of Sreenivasan (1988), approximately as $y_{max}^+ = 0.071 Re_\theta$. For $\overline{w'^2}$ the location of the peak can not be determined with sufficient precision to make any meaningful conclusions.

As far as the Reynolds shear stress is concerned, Sreenivasan (1988) suggested "that the location of the peak Reynolds stress in a zero pressure gradient boundary layer

is something like a critical layer for the flow and that it shares some of the properties of the transitional critical layer". One of these properties is that the velocity of the mean flow in the transitional critical layer appears to be a constant fraction of the freestream velocity. For several wall-bounded shear flows Sreenivasan found $U_{crit} = 0.65 U_e$, so that the position of this "critical" layer is in the logarithmic region of the boundary layer. Since the convection velocity of the large-scale motions is almost the same as the local mean velocity (see figure 67), this proposition is promising. Now, the errors in measurements of the Reynolds shear stress in boundary layers are related to the size of the X-wire probe (which makes measurements close to the wall difficult), spatial averaging effects, the separation L^+ of the two wires, gradient effects near the wall and variations in the approach angle of the instantaneous velocity vector relative to the sensor wires.

The shear stress in inner-layer scaling shows a plateau in the vicinity of the peak value where the scaled Reynolds shear stress lies approximately between 0.92 and 0.95 (for details see Fernholz & Finley, 1995). The near wall observations are, however, not precise enough to confirm Spalart (1988) suggestion that the total shear stress approaches the wall with a finite slope of approximately -0.6, with the slope falling to zero only in the buffer layer. Figure 33 shows the data in outer layer scaling. The data collapse for $y/\Delta > 0.09$. Li & Perry (1989) also found this to hold for Re_θ up to 11,000. The peak value of the shear stress shows almost no dependence on Reynolds number,

29
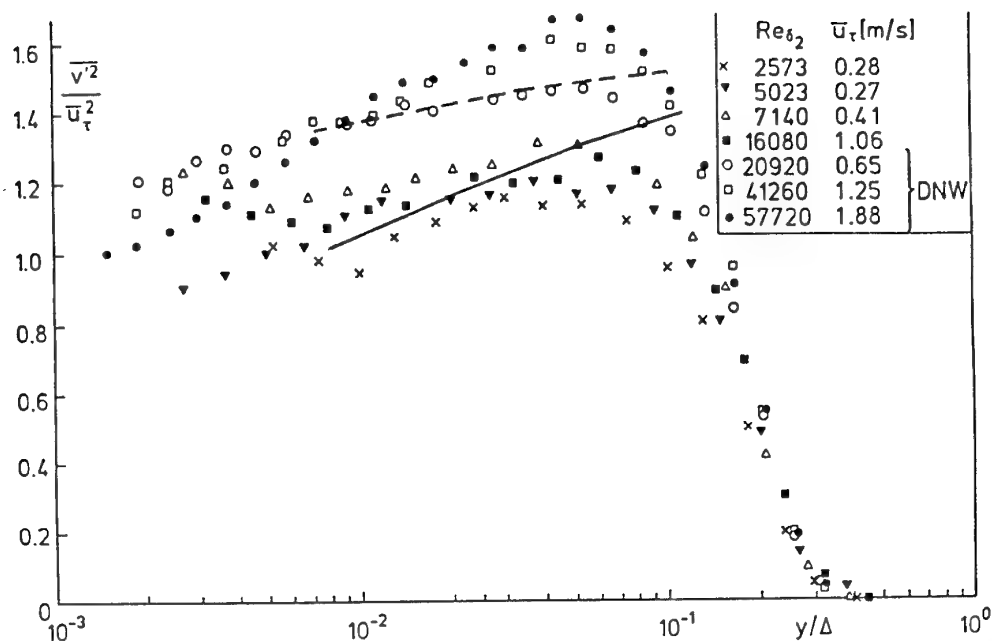
Figure 31: Distribution of the wall-normal Reynolds stress in outer-layer scaling at medium to high Reynolds numbers. ———————, equation 50 for $Re_{\delta 2} = 5,023$; — — — — —, $Re_{\delta 2} = 57,720$. Figure adapted from Fernholz & Finley (1995). For symbols see Table 1.
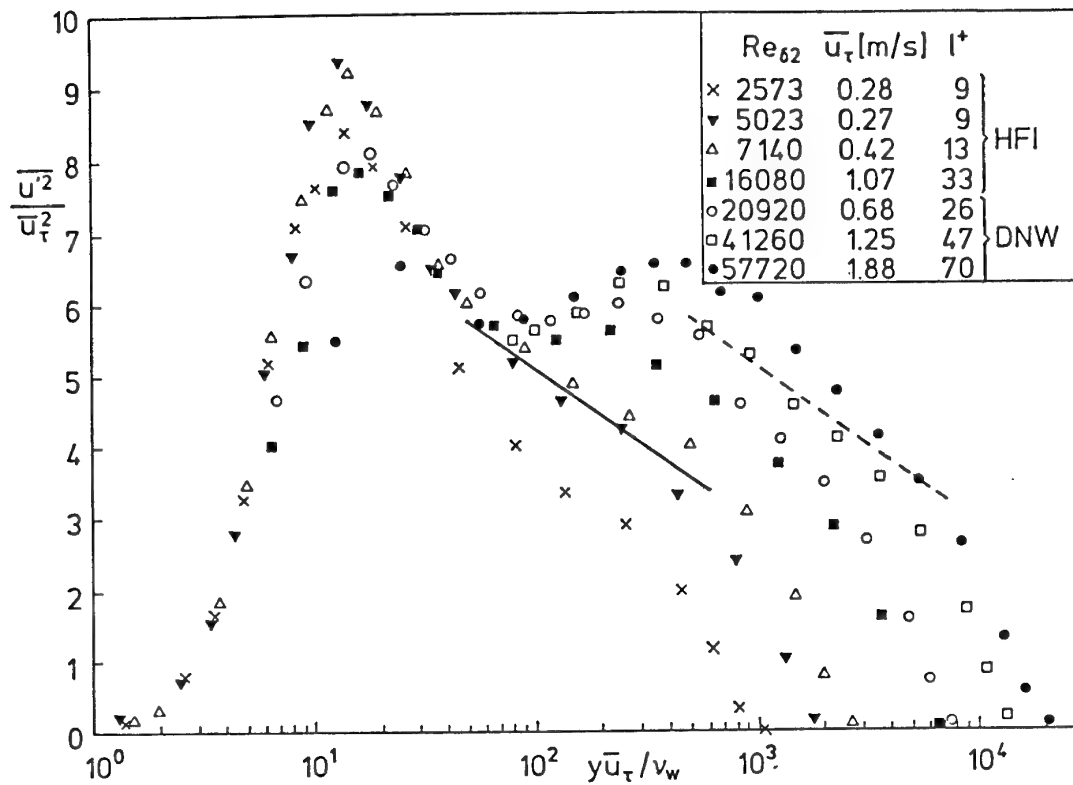

Figure 32: Distribution of the spanwise Reynolds stress in outer-layer scaling at medium to high Reynolds numbers. Data from Bruns et al. (1992) and Nockemann et al. (1994). ———————, equation 49 for $Re_{\delta 2} = 5,023$; — — — — — — —, $Re_{\delta 2} = 57,720$. Figure adapted from Fernholz & Finley (1995).
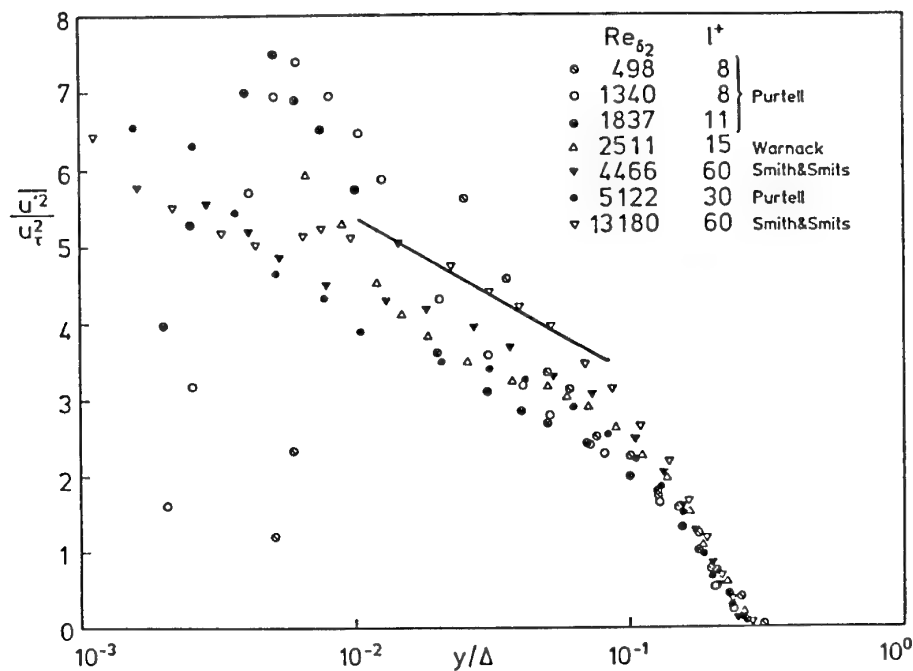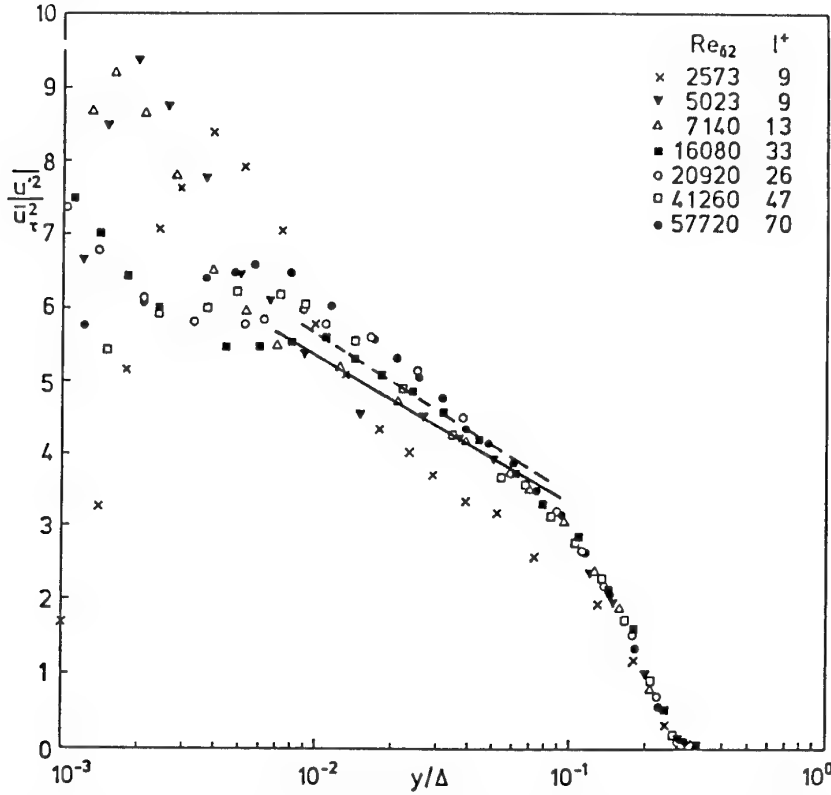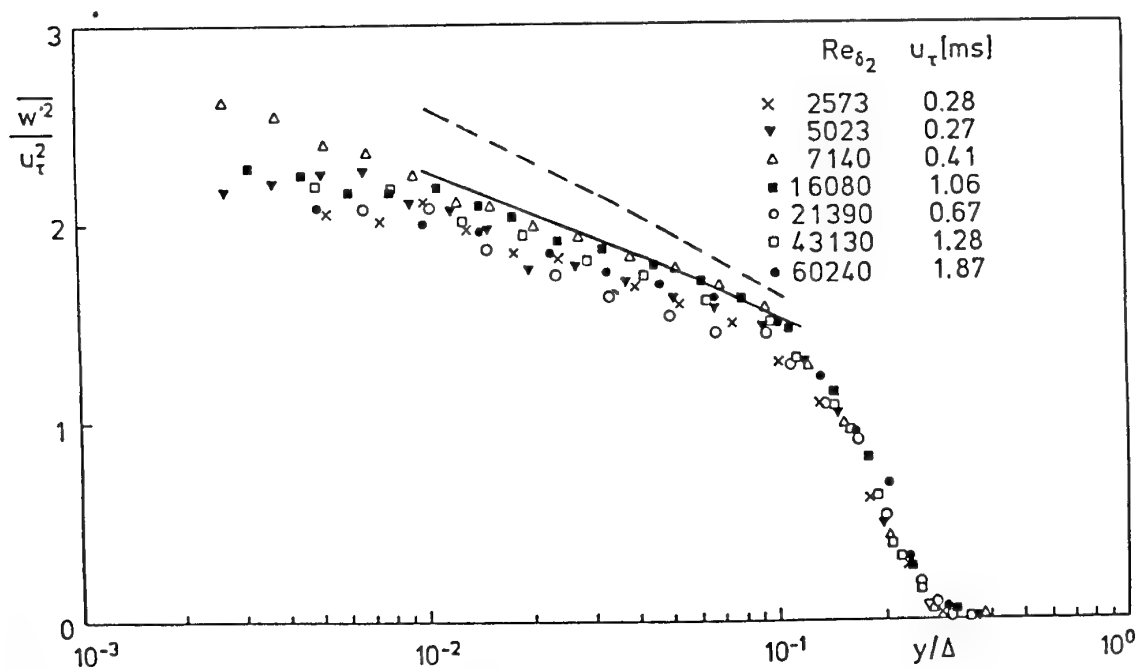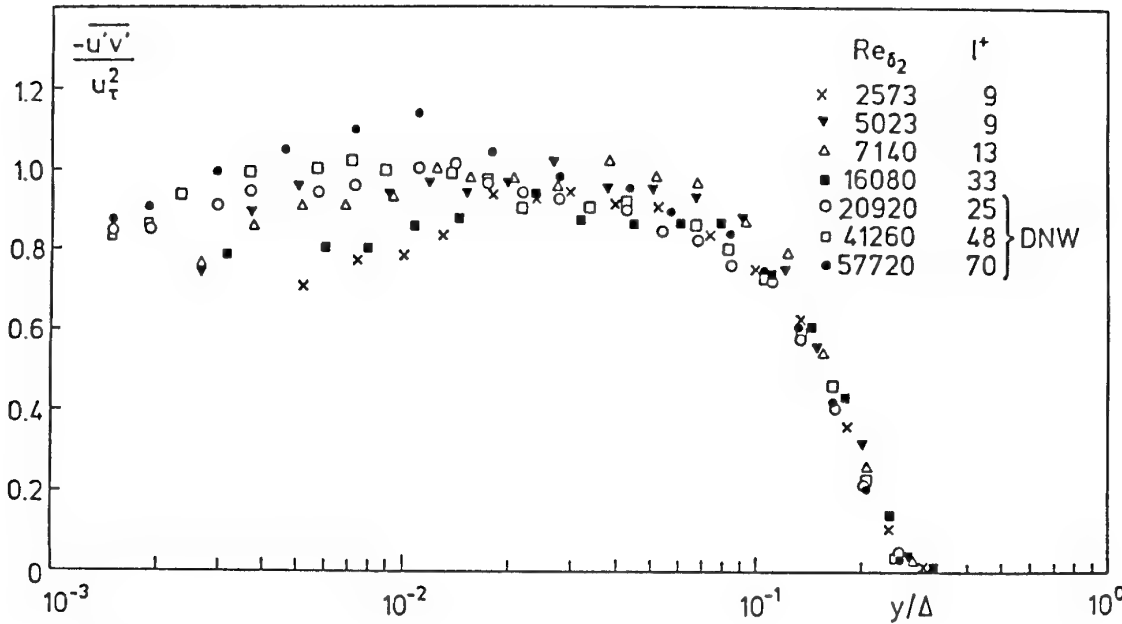
Figure 33: Distribution of the Reynolds shear-stress in outer-layer scaling at medium to high Reynolds numbers. Data from Bruns *et al.* (1992) and Nockemann *et al.* (1994). Figure from Fernholz & Finley (1995).

but the location of the peak is described approximately by $y_{max}^+ = Re_\theta^{0.61}$, showing that the peak location of $\overline{u'v'}$ is a weaker function of Reynolds number than that of $\overline{v'^2}$. This is in qualitative agreement with the results collected by Sreenivasan (1988), who also noted that the peak in the Reynolds shear stress moves inwards in terms of outer scaling as Re_θ increases (see figure 33) and that the part of the dynamics contributing to the Reynolds shear stress does not reside either at constant y^+ or at constant y/Δ.

It is interesting to note that Direct Numerical Simulations (DNS) of turbulent boundary layers give shear stress values near the wall which are generally in good agreement with the experimental values obtained at the same Reynolds number. For example, at $Re_\theta = 670$ Spalart (1988) finds a maximum value of $\overline{u'v'}/u_\tau^2$ of about 0.95 (compared with the value of 0.87 found by Erm & Joubert, 1991), and Yeung *et al.* (1993) finds a maximum value of about 0.89. The position of the maximum value also agrees well with the experiment (for further details see Fernholz & Finley, 1995). In all other respects, as for example in the turbulent stress and skewness and flatness distributions, the DNS results also agree well with experiment (see Erm *et al.* , 1994).

Some particular stress ratios are also of interest, in particular the "structure parameter" a_1, the correlation coefficient R_{uv} and the anisotropy ratios $\sqrt{\overline{v'^2}}/\sqrt{\overline{u'^2}}$ and $\sqrt{\overline{w'^2}}/\sqrt{\overline{u'^2}}$. The parameter a_1 is the ratio of the Reynolds shear stress to the turbulent kinetic energy $\overline{q^2}/2$, and Klebanoff (1955) found it to be approximately constant in a range $0.1 \leq y/\delta \leq 0.8$, at a Reynolds number $Re_\theta = 7,660$. Erm (1988) found similar results in the range $697 \leq Re_\theta \leq 2,788$, with a_1 taking values between 0.14 and 0.16. Higher Reynolds number data are shown in figure 34 in outer law scaling. The location of the peak value is approximately constant, and the magnitude of the

peak value lies between 0.14 and 0.17, increasing slightly with Re_θ.

As for the other stress ratios, the correlation coefficient R_{uv} increases from about 0.3 near the wall to about 0.45 in the outer part of the layer (see, for example Klebanoff (1955)'s results in figure 61), and there is a weak tendency for these values to decrease with Reynolds number. The anisotropy ratio $\sqrt{\overline{v'^2}}/\sqrt{\overline{u'^2}}$ increases across the boundary layer from a value of about 0.4 to about 0.8, and shows little Reynolds number dependence (see also Smith, 1994), and $\sqrt{\overline{w'^2}}/\sqrt{\overline{u'^2}}$ is nearly constant at a value of between 0.6 and 0.7 at all y-locations and Reynolds numbers.

The Reynolds number dependence of the higher moments of the fluctuating quantities was also studied by Fernholz & Finley (1995). In summary, the skewness and flatness of u' ($\overline{u'^3}/\left(\sqrt{\overline{u'^2}}\right)^3$ and $\overline{u'^4}/\left(\overline{u'^2}\right)^2$, respectively) appear to be independent of Reynolds number when scaled using the appropriate scaling parameters for each region, as found by Smith (1994). The behavior of the triple correlations and production terms is discussed by Murlis *et al.* (1982), Erm (1988), Fernholz & Finley (1995) and Morrison *et al.* (1992). Note also that Johansson & Alfredsson (1983) investigated the influence of l^+ on the skewness and flatness factors of u' in the range $1.4 \leq l^+ \leq 33$. They found little effect on the flatness, but substantial differences in the skewness factor which varied from - 0.20 to 0 as l^+ varied from 14 to 33. They also found that the skewness was sensitive to the value of l^+ at much greater distances from the wall than for the moments of u'.

Although the distribution of the shear stress among the four quadrants in the u'-v' plane did not vary with Reynolds number, the shear correlation coefficient R_{uv} and the non-dimensional shear rate $S^* = \left(q^2/\varepsilon\right)\left(\partial U/\partial y\right) \approx -q^2/\overline{u'v'}$ indicated that the large-
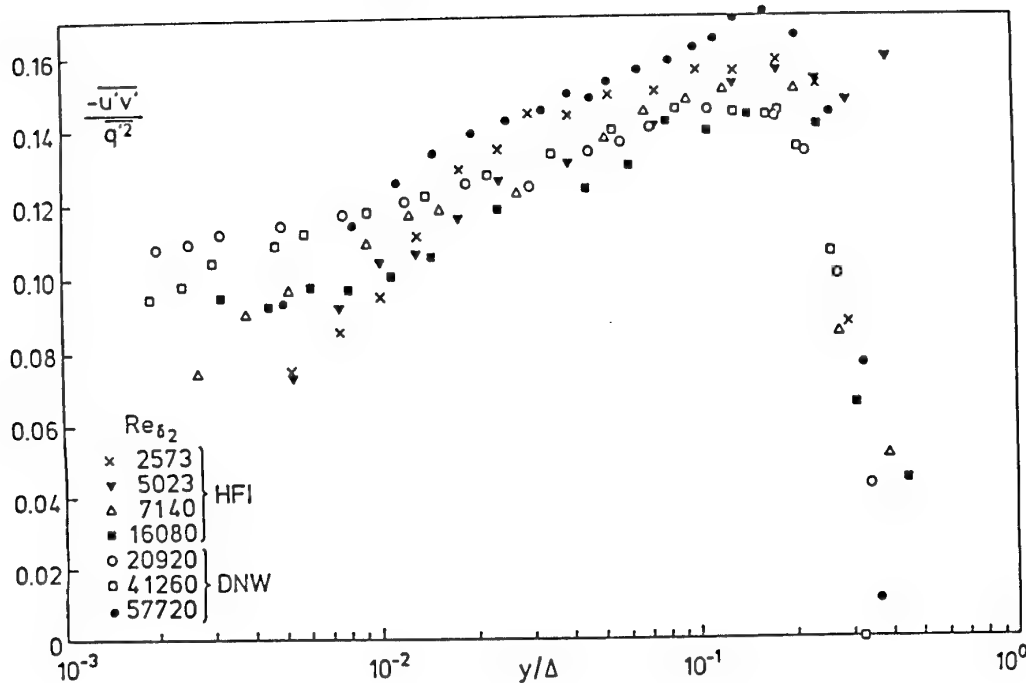
Figure 34: Distribution of the structure parameter $a_1 = -\overline{uv}/q^2$ in outer-layer scaling at medium to high Reynolds numbers. Data from Bruns *et al.* (1992) and Nockemann *et al.* (1994). Figure from Fernholz & Finley (1995).

scale structure plays a less active role in near-wall turbulence production as the Reynolds number increases (Smith, 1994): with increasing scale disparity the large-scale motions have a decreasing influence on near-wall events. This is not unexpected, but what is surprising is that the large-scale motions continue to have an influence at Reynolds numbers where the boundary layer is often thought to be fully-turbulent.

If the Reynolds number dependence can be empirically quantified by examining available data over a wide range of Reynolds numbers (for example, if the peak value of $\overline{u'^2}$ can be expressed as a function of Reynolds number), then, in principle, it is possible to suggest velocity and length scales which will also have the same Reynolds number dependence. Thus, when the turbulence quantities are nondimensionalized using these new scales, the Reynolds number dependence will cancel out, and all of the data will collapse onto a single curve. This is, in effect, what Falco's typical eddy scales do. Falco obtained a correlation for u_{TE}; for a fixed value of y^+, $u_{TE}/u_\tau \propto Re_\theta^{0.159}$. Thus, if the value of u'_{rms}/u_{TE} at a fixed y^+ is independent of Reynolds number, the value of u'_{rms}/u_τ will increase with Reynolds number, which agrees with the majority of available data (see figure 26). Note that u_{TE} and l_{TE} were obtained from combined flow visualization and hot-wire measurements.

3.3 Organized motions in turbulent boundary layers

This section is concerned with the structure of turbulent boundary layers, in the sense of organized, spatially cor-

related motions. it was adapted from the review given by Smith (1994), and further details are given there. There are several additional reviews of turbulent flow structure in the literature, including Willmarth (1975), Cantwell (1981), and Robinson (1991)a. More personal interpretations are offered by Coles (1987), Hussain (1983), and Sreenivasan (1989). The emphasis here is on Reynolds number effects and scaling laws.

In turbulence research, the term "structure" has been used to denote two different ideas. First, it is used to describe the behavior of the mean flow and Reynolds stresses. The scaling of the mean flow and Reynolds stresses, the composition of Reynolds stresses (*e.g.* as deduced from quadrant analysis), anisotropy ratios, the shear correlation coefficient, the structure parameter, and intermittency profiles, can all be viewed as describing the "structure" of a turbulent boundary layer. Second, the term "structure" is used to describe coherent, organized motions occurring in the flow. Robinson (1991)a defines a coherent motion, or structure, as

> "a three-dimensional region of the flow over which at least one fundamental flow variable (velocity component, density, temperature, etc.) exhibits significant correlation with itself or with another flow variable over a range of space and/or time that is significantly larger than the smallest local scales of the flow."

This definition is quite general. More specific definitions have been proposed (*e.g.* Hussain, 1983), but in essence they are just restricted forms of Robinson's definition. Both definitions of structure are used here, but the distinction should be clear from the context.

3.3.1 Inner-layer structure

Klebanoff (1955) showed that in a turbulent boundary layer about 75% of the total turbulence production in the entire layer occurs in the inner region, $y/\delta < 0.2$. Therefore, most investigations of turbulent boundary layer structure have focussed on the near wall region, primarily the viscous sublayer and buffer layer. Because of practical considerations, such as the small scales involved, and the need for adequate resolution, these studies have been limited predominantly to low Reynolds numbers, that is, $Re_\theta < 5,000$.

In 1967, Kline et al. (1967), in a culmination of work initiated by Runstadler et al. (1963), reported the results of a study of the near-wall structure of a turbulent boundary layer in the range $545 < Re_\theta < 1,680$. Using hydrogen bubble flow-visualization in a water channel, Kline et al. found that the viscous sublayer is occupied by alternating streaks of high- and low-speed (relative to the mean) fluid. The spanwise spacing of the streaks was found to scale on inner variables and to have a non-dimensional mean value of $\lambda_s^+ \approx 100$. The streaks were presumed to be the result of elongated streamwise vortices very near the wall. H.P. & Lumley (1967), using correlation measurements in a pipe flow ($Re = \overline{U}d/\nu = 8700$, $d =$ pipe diameter) together with the technique of proper orthogonal decomposition, also concluded that the dominant structures in the sublayer are pairs of counter-rotating vortices with an average spanwise wavelength of $\lambda_s^+ \approx 90 - 100$. Kline et al. observed that the low-speed streaks would gradually lift up from the wall, oscillate, and then break up violently, ejecting fluid away from the wall and into the outer layer. They coined the term "bursting" to describe this sequence of events. Kline et al. concluded that all the events comprising the bursting process were consistent with a stretched and lifted vortex. Later, Kim et al. (1971) performed further investigations in the same facility. They determined that in the wall region, $0 < y^+ < 100$, nearly all of the turbulence production occurs during bursting, thus establishing the dynamical significance of the near-wall region and the bursting process.

Corino & Brodkey (1969) performed a visual study of the near-wall region of fully developed pipe flow. They seeded the flow with a suspension of colloidal particles, illuminated the flow field, and photographed the flow with a high-speed camera moving with the flow velocity. Thus, they were able to follow the development of interesting events. Corino & Brodkey observed a recurring sequence of events which closely resembled the bursting process observed by Kline et al. . They found that a large scale disturbance would frequently impinge upon a near-wall region of low-speed fluid. This would be followed by one or more ejections of low-speed fluid up into the large scale disturbance, resulting in violent, chaotic interaction. Once the ejection(s) had subsided, a large region of high-speed fluid would cleanse the area of the debris of the interaction. Corino & Brodkey called this latter event a "sweep". They further found that, as the Reynolds number was increased, the frequency and intensity of the ejection events increased. At high Reynolds numbers ($Re = 52,000$), it was difficult to distinguish between individual events.

Since these initial studies, many other researchers have investigated the near-wall flow structure. Two of the most widely studied aspects of the near-wall structure are the mean spanwise streak spacing, λ_s, and the mean bursting period, T_b (or mean bursting frequency, $f_b \sim 1/T_b$). Kim et al. collected the results of several independent measurements of streak spacing, and the results generally agreed with Kline et al. 's value of $\lambda_s^+ \approx 100$. Smith & Metzler (1983) showed that λ_s^+ is independent of Reynolds number over the range $740 < Re_\theta < 5,830$. The value of $\lambda_s^+ \approx 100$ is now widely accepted.

In contrast, the scaling of the bursting period is highly controversial. Initially, Kline et al. suggested that, since the bursting process is a wall layer phenomenon, T_b should scale with inner variables. Subsequent research has provided many conflicting results. Rao et al. (1971), working in a turbulent boundary layer in the range $600 < Re_\theta < 9,000$, concluded that outer scaling is appropriate, and that $T_b U_e/\delta \approx 5$ (or $T_b U_e/\delta^* \approx 30$), independent of Reynolds number. Alfredsson et al. (1988), working in a fully developed channel flow in the range $13,800 < Re_c < 123,000$ (Re_c based on channel height and centerline velocity), found that T_b was independent of Re when nondimensionalized by a mixed time scale equal to the geometric mean of the inner and outer time scales. Thus, three different scalings for T_b (and thus f_b) have been proposed, and each has its own proponents. Those who obtained results in favor of outer scaling include Rao et al. (1971), Kim et al. (1971), Lu & Willmarth (1973) (turbulent boundary layer, $Re_\theta = 4,230$ and $38,000$), Blackwelder & Kaplan (1976) (turbulent boundary layer, $Re_\theta = 2,550$), Brodkey et al. (1974) (fully developed channel flow, $Re = 7,700$, equivalent to $Re_\theta \approx 430$), and Narasimha & Kailas (1987) (atmospheric boundary layer). Proponents of inner scaling include Blackwelder & Haritonidis (1983) (turbulent boundary layer, $10^3 < Re_\theta < 10^4$), Luchik & Tiederman (1987) (fully developed channel flow $9,400 < Re_a < 17,800$, Re_a based on mass-averaged velocity and channel height), Kim & Spalart (1987) (numerically simulated turbulent boundary layer, $Re_\theta = 300, 670$, and $1,410$), and Willmarth & Sharma (1984) (turbulent boundary layer, $Re_\theta = 6,480$ and $9,840$).

There are many reasons for the discrepancy among the various results. First, in order to measure the bursting period, it is necessary to devise a criterion for detecting the bursting process. Visual methods, as used by Kline et al. , Corino & Brodkey, and Kim et al. , are limited to very low Reynolds numbers. Therefore, several researchers have developed methods based upon measurements of fluctuating velocities. Lu & Willmarth (1973) introduced the u-level method, in which low values of u, relative to the mean, were used to detect ejections, and high levels of u were used to detect sweeps. Wallace et al. (1972) and Lu & Willmarth (1973) proposed splitting the u'-v' velocity plane into four quadrants, as shown in figure 35. Instantaneous values of $u'v'$ can then be associated with a certain quadrant and a corresponding event. Blackwelder & Kaplan (1976) developed the variable interval time averaging (VITA) technique, whereby the variance of the velocity, u', is computed over a short time interval. If the short time variance exceeds a preset threshold level, then an event is detected. The goal of these detection schemes is to identify segments of the velocity signal which corre-
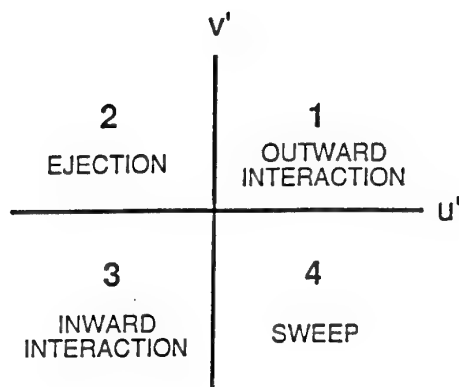
Figure 35: The four quadrants of the u'-v' plane, and the common terms for the events corresponding to each quadrant (from Robinson, 1991b).

spond to events of interest (*e.g.* ejections and sweeps), and to analyse these segments separately from the remaining signal, that is, by conditional sampling and averaging. All detection methods are quite subjective, requiring the user to choose threshold levels and/or averaging times. Willmarth & Sharma (1984) state that the bursting period determined using the VITA technique is highly sensitive to the threshold level and the averaging time. They found that when the threshold level was changed by 5%, the measured bursting frequency changed by 40%, and a 20% change in the averaging time resulted in a 15% change in measured bursting frequency. More disturbing is the fact that it is not even certain what relation the detected events have with the actual events of the bursting process. Bogard & Tiederman (1986), Bogard & Tiederman (1987) evaluated several detection methods and found that different methods could yield values of T_b which differed by an order of magnitude. They also found that different techniques detected different phases of the bursting process. Corino & Brodkey (1969) had observed earlier that more than one ejection may occur during a single burst. Luchik & Tiederman (1987) introduced the idea of grouping multiple ejections into a single burst, but most other researchers did not do this, resulting in further variation among reported results.

A further difficulty in measuring bursting frequency is related to spatial averaging effects, as discussed in Section 3.2.1 For example, Blackwelder & Haritonidis (1983) showed that the measured value of f_b drops sharply for wire lengths $l^+ > 20$.

Another difficulty arises from the fact that it is possible that the structure of fully-developed internal flows and that of turbulent boundary layers are different. As discussed in Section 3.1.4, it is possible that the mean flow can follow different scaling laws in the outer region of different flow geometries. In fully-developed internal flows, the inner and outer layers are intimately connected through the relation between the pressure drop and the wall shear stress. Luchik & Tiederman (1987) accounted for this connection when they concluded that inner scaling of T_b is more appropriate than either mixed or outer scaling. However, the outer layer of an internal flow does not

have the same highly intermittent character as do boundary layers. Therefore, a comparison of results obtained in fully developed internal flows and in turbulent boundary layers may not be valid.

Finally, Reynolds number effects are quite possibly causing some of the disagreement among the data. Shah & Antonia (1989) specifically addressed this issue. They measured T_b in fully developed channel flow for $3,300 < Re < 33,000$, and in a turbulent boundary layer for $650 < Re_\theta < 13,000$, using both the VITA and the u-level techniques. They found that inner scaling is effective for $Re < 20,000$ in the channel flow, and $Re_\theta < 6,000$ in the boundary layer. It is interesting to note that $Re_\theta = 6,000$ is the value above which Coles' wake parameter, Π, is constant. Shah & Antonia conclude that above these Reynolds numbers, mixed scaling is more appropriate for both flows. However, they emphasize that their data do not preclude the validity of outer scaling at Reynolds numbers greater than $Re_\theta \approx 10,000$.

Another interesting issue, indirectly raised by Shah & Antonia (1989), is related to the work of Luchik & Tiederman (1987). Luchik & Tiederman measured u_τ in their flow using two techniques: 1) by measuring the velocity gradient in the viscous (linear) sublayer, and 2) using the Clauser method. They found that the second method yielded values typically 15% higher than the first method. When they concluded that T_b scales on inner variables up to $Re_\theta = 10^4$, they had used u_τ determined from the first method. Shah & Antonia reanalysed Luchik & Tiederman's results using u_τ from the Clauser method, and found that the data scaled better with mixed or outer variables for $Re_\theta > 6,000$, in support of their own conclusions.

Tinh (1982) used hot-wire anemometry to study the near-wall structure in a channel flow for $43,200 < Re < 177,100$ (Re based on channel height and centerline velocity). He found that, for $y^+ < 50$, the skewness and flatness of the streamwise velocity fluctuations exhibited some Reynolds number dependence. Using conditional sampling techniques, he also showed that the relative importance of the ejection and sweep motions changed with Reynolds number. At $Re = 43,200$, ejections contributed more than sweeps to the total $\overline{u'^2}$ for $y^+ > 10$, while for $y^+ < 10$, sweeps dominated. At $Re = 177,100$, sweeps contributed more than ejections to $\overline{u'^2}$ over the entire range $0 < y^+ < 50$. The nondimensional hot-wire lengths for van Tinh's experiments varied from $l^+ \approx 12$ to $l^+ \approx 42$ over the range of Reynolds numbers investigated. Therefore, spatial averaging effects may have created an artificial Reynolds number dependence in the data. Similar results were obtained by Andreopoulos *et al.* (1984), in a boundary layer with $3,642 < Re_\theta < 15,406$, also found that sweeps become stronger relative to ejections with increasing Reynolds number, but, as noted in Section 3.2.2, their data also suffer from severe spatial averaging effects.

In summary, the spanwise spacing of the near-wall streaks has been established to be $\lambda_s^+ \approx 100$ for low to medium Reynolds numbers, but with a standard deviation of approximately 50 (Smith & Metzler, 1983). The scaling of the bursting period remains unresolved, and may be Reynolds number dependent. Resolution of the issue may come when we have a better understanding of the turbu-

Figure 36: Flow visualization by Falco (1977), of a boundary layer at $Re_\theta \approx 4,000$, obtained by seeding the flow with a fog of oil droplets, and illuminating the flow with a planar laser sheet. Flow is from left to right. Figure from Van Dyke (1982).

lence production cycle, and better techniques to study it. A knowledge of the scaling of T_b is important to an understanding of the overall dynamics of the turbulent boundary layer. If T_b scales on inner variables, this suggests that the inner layer controls the dynamics of the boundary layer, and the outer layer structure may be merely the debris of the bursting process. Alternatively, if T_b follows outer scaling, this implies that the bursting process is controlled or modulated by (and may be responding passively to) the outer layer structure. In between these two extremes, if T_b scales on mixed variables, this implies an important mutual interaction between the inner and outer structure.

3.3.2 Outer-layer structure

There is also considerable controversy regarding the nature of the outer-layer structure. Nevertheless, a general picture has emerged. A specific characteristic component of the outer layer is believed to be the large scale turbulent "bulge", also referred to as a "large scale motion" (LSM). The large scale motions evolve and decay slowly as they convect downstream, and, on average, they are inclined to the wall at an acute angle, leaning in the downstream direction. Between neighboring bulges, the flow is irrotational, resulting in the intermittent character of the outer layer. Figure 36 shows several LSM's. The structures are seen to vary greatly in size and inclination angle. The properties of the large scale motions, such as length scales, time scales, convection velocity, and stucture angle, as well their internal structure, such as velocity, vorticity, and pressure fields, remain the subject of controversy and active research. Furthermore, the Reynolds number dependence, if any, of the LSM's is not known.

Part of the difficulty in experimental studies of the outer-layer structure, as it is in studies of the inner-layer structure, is finding an unambiguous criterion for ensemble-averaging. One method is based on discriminating between "turbulent" and "non-turbulent" fluid, and using the intermittency function (a box-car logic function) to
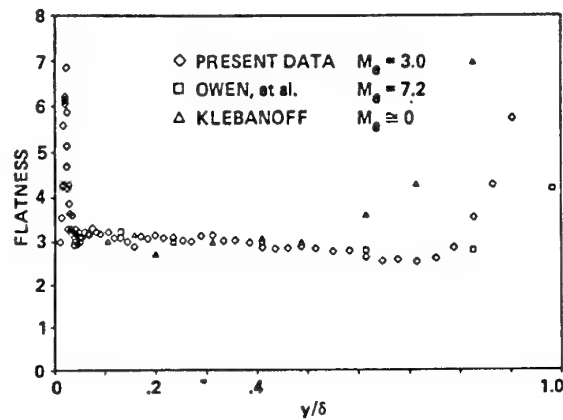
Figure 37: Comparison of flatness distributions: $\square$, Owen et al. (1975) ($Re_\theta = 8,500$, $M = 7$), based on mass flux; $\diamondsuit$, Robinson (1986) ($Re_\theta = 15,000$, $M = 3.0$, based on mass flow; $\triangle$, Klebanoff (1955) ($Re_\theta = 7,100$, $M \approx 0$), based on velocity. Figure from Robinson (1986).

sort the data. The most basic output is the intermittency itself, γ, which is the fraction of the time the flow is judged to be turbulent. One definition of γ is $3/F$, where the flatness $F = \overline{u'^4}\big/\overline{(u'^2)^2}$. The distribution of F is shown in figure 37 for a number of different freestream Mach numbers. The results imply that the intermittency in the outer part of the layer decreases with Mach number. Another method uses the VITA technique originally developed by Blackwelder & Kaplan (1976) for studies of the near-wall bursting process. A variety of similar techniques have been developed (for example, VISA by Kim & Spalart (1987), WAG by Antonia et al. (1990a), Antonia et al. (1990b)), but they are all subject to ambiguities related to the uncertainties in setting threshold levels. Nevertheless, they may still give useful insights if carefully used.

Before the advent of conditional sampling methods, sev-
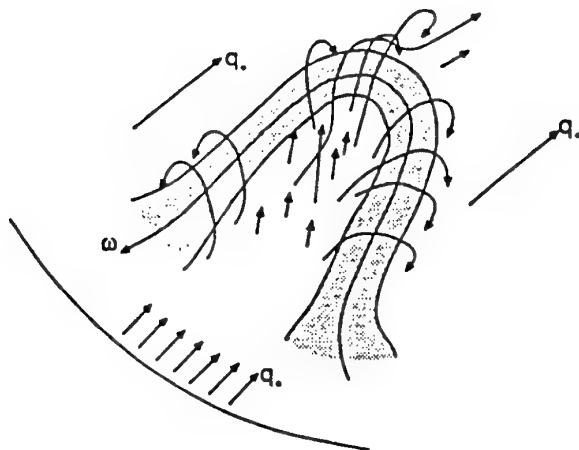
Figure 38: The horseshoe vortex proposed by Theodorsen (1955) as the basic structure in wall-bounded turbulent flows. Figure from Spina (1988).

eral fundamental observations were made regarding the nature of the LSM's in turbulent boundary layers. The first physical model of the large scale structure of turbulent boundary layers was proposed as early as 1955 by Theodorsen (1955). He hypothesized that the basic structure of all turbulent shear flows is the inclined horseshoe vortex, as shown in figure 38. Using the vorticity transport equation, Theodorsen attempted to prove that the only vortical structures which can sustain a non-decaying turbulent field must have a horseshoe shape. As seen in figure 38, the model can certainly account for the generation of Reynolds stress. Between the legs of the vortex, the induced velocity ejects low-speed fluid up, away from the wall, into a region of higher mean velocity, hence $u' < 0, v' > 0$ (a Quadrant II event). On the outboard sides of the legs, high speed fluid is swept toward the wall, hence $u' > 0, v' < 0$ (a Quadrant IV event).

Townsend (1976) did not regard the LSM's as having any particular shape, but he made two important hypotheses about the large scale motions based upon theoretical considerations. First, he concluded that

"... the main eddies of the flow have diameters proportional to the distance of their centers from the wall, because the motion is directly influenced by its presence. In other words, the velocity fields of the main eddies, regarded as persistent, organized flow patterns, extend to the wall and, in a sense they are attached to the wall."

This is commonly known as Townsend's *attached eddy hypothesis*. Second he assumed that the interaction between a large eddy and a smaller, viscous-dominated eddy occurs over several intermediate steps. Due to this highly indirect interaction, Townsend proposed that the large-scale motion is essentially inviscid, and thus independent of Reynolds number. This is known as Townsend's *Reynolds number similarity hypothesis*. It should be noted that the idea that eddies of largely dissimilar scale do not directly

interact is currently being challenged (see, for example, Brasseur, 1991, Praskovsky, 1993).

Despite the extensive literature on the subject of the large-scale structure of turbulent boundary layers, only a few studies have specifically addressed the issue of Reynolds-number effects. This is primarily due to the general acceptance of Townsend's Reynolds number similarity hypothesis.

The flow visualization work of Head & Bandyopadhyay (1981) provided strong support for the concept that at least some of the LSM's are loop-shaped vortical structures. Head and Bandyopadhyay showed that the aspect ratio of these vortical structures is Reynolds-number dependent. Figure 39 shows that at $Re_\theta = 600$, the structures have the proposed horseshoe shape, with a low aspect ratio. As Re_θ increases, the structures are elongated, and at $Re_\theta = 9,400$, they appear more as hairpins, with a large aspect ratio. At all Reynolds numbers, the spacing between the legs of the structures is similar to the spacing between the near-wall streaks ($\approx 100\nu/u_\tau$). The structures appear to extend to the wall, in support of the attached eddy hypothesis. Head and Bandyopadhyay also suggested that, at low Reynolds numbers, the LSM's were merely single horseshoe elements. At higher Reynolds numbers, the LSMs were actually agglomerations of many elongated hairpin vortices. At low Reynolds numbers, the LSM's exhibited a "brisk" overturning motion, while at higher Reynolds numbers, they overturned slowly. This suggests that entrainment decreases with increasing Reynolds number, which is in agreement with the observation that the boundary layer grows more slowly with increasing Reynolds number.

Other visualizations of turbulent boundary layers reveal that, as Reynolds number increases, the outer-layer bulges appear to be comprised of, or contain, a wider range of scales (Falco, 1977, Fiedler & Head, 1966). This is in accord with the fact that the ratio of the outer to inner length scale, δ^+, increases with increasing Reynolds number.

Another useful method for investigating the large scale structure is multiple-point measurements of one or more flow variables, typically velocity, wall pressure, and wall shear stress. The data are then analysed in the context of space-time correlations. The correlation of two variables measured at two points in the flow field is given by

$$R_{ab}(\xi_x, \xi_y, \xi_z, \tau) =$$

$$\frac{\overline{a(x,y,z,t)b(x+\xi_x, y+\xi_y, z+\xi_z, t+\tau)}}{a_{rms}b_{rms}} \quad (52)$$

where a and b are the two flow variables being correlated, ξ_x, ξ_y, and ξ_z are the separations between the two points in the three coordinate directions x, y, and z, respectively, and τ is the time delay applied to the signal of variable b. For the case when both a and b are velocities, R_{ab} is typically denoted by R_{ij}, where i and j are the indices of the velocity components ($R_{11} = R_{uu}$, $R_{12} = R_{uv}$, etc...). When any of ξ_i are nonzero in Equation 52, R_{ab} is called a space-time correlation. Space-time correlations generally have a single well-defined peak, which occurs at $\tau = \tau_{max}$, the optimum time delay, which may be nonzero.
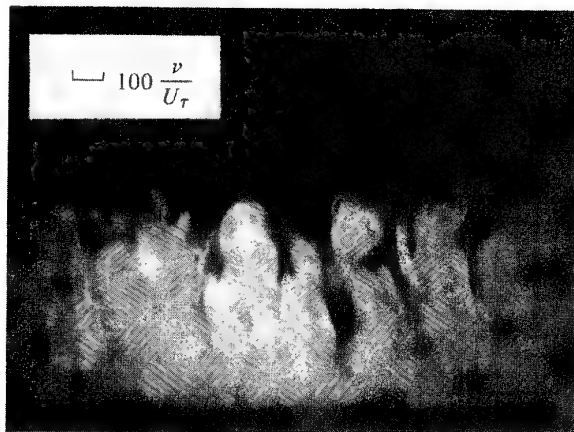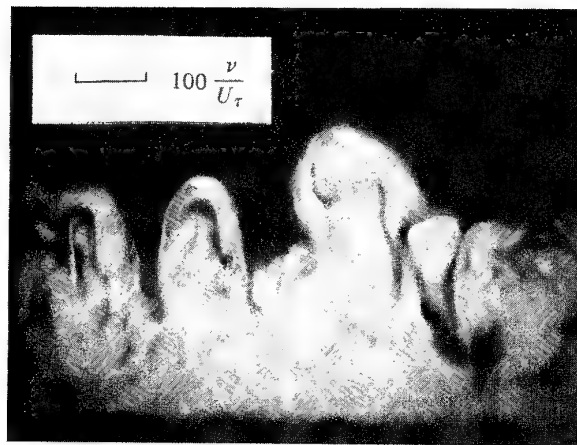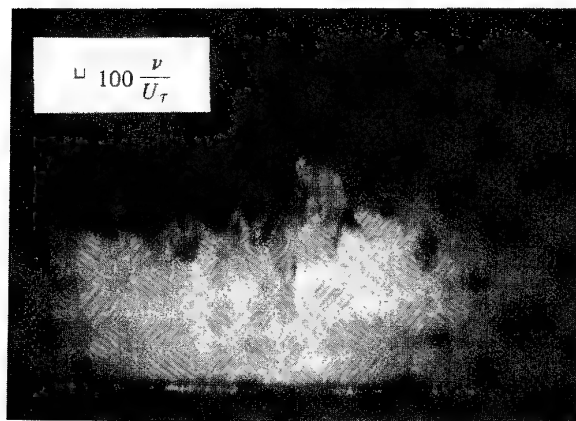
Figure 39: Flow visualizations by Head & Bandyopadhyay (1981), showing the Reynolds number dependence of vortex loop structures in a turbulent boundary layer. The visualizations were obtained by filling the boundary layer with smoke, and illuminating the flow with a laser sheet inclined 45° downstream. a) $Re_\theta = 600$; b) $Re_\theta = 1,700$; c) $Re_\theta = 9,400$. Figure from Head & Bandyopadhyay (1981).

Favre *et al.* (1957), Favre *et al.* (1958) pioneered the use of velocity space-time correlations. Their results, for $Re_\theta \approx 1,400$ and $2,700$, showed that the fluctuating velocities in the outer layer are correlated over distances comparable to the boundary layer thickness, δ, in the spanwise and wall-normal directions, and over several δ in the streamwise direction. Favre *et al.* 's space-time correlations at optimum time delay clearly showed that in the outer-layer flow structures are convected downstream several $(O(10))$ δ before decaying. Nearer the wall, the structures decay more rapidly than farther from the wall. Sternberg (1967) noted that Favre *et al.* 's results also indicated that the large eddies are inclined to the wall in the downstream direction.

In a later paper, Favre *et al.* (1967) used space-time correlations to measure convection velocities of the large scale motions in a turbulent boundary layer with $Re_\theta \approx 8,700$. To complement their broadband results, they band-pass filtered the data to measure the convection velocities of structures within a narrow range of scales. Their results are reproduced in figure 40, which shows that the smallest scales convect at about the local mean velocity throughout the boundary layer. For $y/\delta > 0.2$, large scale structures convect at speeds less than the local mean velocity, and the convection velocity decreases with scale. For $y/\delta < 0.2$, the opposite behavior is observed. At $y/\delta \approx 0.2$, all scales convect at the local mean velocity. This behavior could be explained as follows. A large structure will extend across a significant fraction of the boundary layer, and will convect at a speed which is a weighted average of the local mean velocity acting over the vertical span of the structure. This convection velocity will be greater than the local mean near the wall, and less than the local mean in the outer layer. The greater the vertical extent of the structure, the greater will be this effect. Based upon space-time correlations of wall pressure fluctuations, Tu & Willmarth (1966) and Corcos (1963) reached similar conclusions regarding the difference in convection velocity between large and small scale structures. Spina *et al.* (1991b) obtained similar results in a compressible flow, and their results are discussed in greater detail later in Section 4.9.

Grant (1958) measured all nine components of the correlation tensor R_{ij} in a turbulent boundary layer at $Re_\theta \approx 2,200$. His results, shown in figure 41, indicate that the correlation tensor is quite complex. Grant stated that such complex behavior could only occur if the large eddy structure of the flow was highly organized. Grant attempted to deduce a simple model of the large scale eddies which was consistent with the measured correlations, but was not entirely successful. However, through a detailed and insightful interpretation of his data, he postulated the existence of "stress relieving motions originating very near the wall, perhaps involving the boundary of the laminar sublayer (*sic*). The motion would be in the nature of an outward eruption originating near the wall." Grant's paper is in remarkable agreement with the later flow visualization results of Kline *et al.* (1967). Tritton (1967) extended the measurements of Grant, but did not deduce a simple eddy model to explain the features of the correlations.

Townsend (1961) also suggested that the large-eddy structure is likely to be simple, but added that the structures undergo a cycle of growth, decay and renewal. He warned that time averaging will superpose contributions from eddies at all stages of this cycle, and thus the results will appear to suggest a more complicated structure than is actually present in the flow.

Kovasznay *et al.* (1970) and Blackwelder & Kovasznay (1972) obtained space-time correlation measurements of velocity in the outer region of a turbulent boundary layer at $Re_\theta = 2,970$. Using conditional-averaging techniques based on the intermittency, their measurements revealed the presence of a stagnation point on the back (upstream) side of the turbulent bulges. Because the large bulges convect at a speed less than the freestream velocity (see figure fig:favreuc), the high-speed, freestream fluid in the regions between the bulges will impinge on the backs of the bulges, resulting in a stagnation point in the convected frame of reference, as shown in figure 42. Similar to the results of Favre *et al.* (1957), Favre *et al.* (1958), Kovasznay *et al.* found that isocontours of the space-time correlations of the streamwise velocity, shown in figure 43, were elongated in the streamwise direction and spanned the entire boundary-layer thickness, and that the large eddies lean downstream. The contours were generated by correlating the velocity measured by a probe at a fixed point in the middle of the boundary layer with the velocity measured by a probe which was traversed in both the y and z directions while maintaining a constant longitudinal probe separation of 3.8δ. The isocorrelation contours shown in figure 43 indicate that the large eddies are inclined with an average angle of approximately $16°$. At the location of the fixed point, the streamwise extent of the correlations is about 0.4δ (based on a minimum correlation value of 0.5).

Additional examples of such boundary layer data do not exist, but Liu *et al.* (1992) recently constructed isocorrelation contours of the large scale structure in a fully developed turbulent channel flow for $Re = 2,872$, $5,378$, and $29,935$ (Re based on channel half-height and bulk velocity). They used particle image velocimetry to obtain several realizations of the instantaneous velocity field in the x-y plane. The isocorrelation contours were computed by mapping the correlation of the velocity at each point in the plane with the velocity of a fixed point located at $y/H \approx 0.40$ (H is the channel half-height), and ensemble averaging the results for all realizations. Liu *et al.* 's results were very similar to those of Kovasznay *et al.* . For the two highest Reynolds numbers, the streamwise extent of the correlations at the position of the fixed point (based on a minimum correlation value of 0.5) increased from approximately $0.9H$ at $Re = 5,378$ to about $1.4H$ at $Re = 29,935$. Note that these length scales are larger than those obtained by Kovasznay *et al.* probably because the large streamwise probe separation used by Kovasznay *et al.* reduced the measured correlation values. Liu *et al.* 's contours also indicated that the structures leaned downstream, and that the angle of inclination, which did not differ appreciably between the two highest Reynolds numbers, was about $10°$.

Brown & Thomas (1977) used space-time correlations and conditional sampling techniques to investigate the relationship between the large-scale motion and the wall shear stress in a boundary layer at $Re_\theta = 4,940$ and $10,160$. They found that large-scale motions were inclined at an
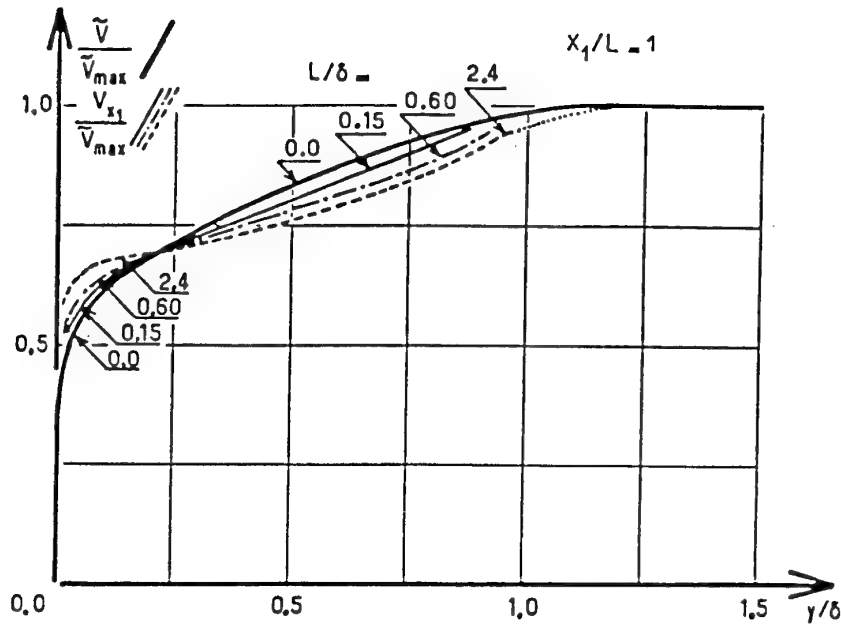
Figure 40: Scale-dependent convection velocity profiles measured by Favre *et al.* (1967) in a turbulent boundary layer at $Re_\theta \approx 8,700$. In Favre *et al.* 's notation, $\widetilde{V}$ is the local mean velocity, $\widetilde{V}_{max}$ is the freestream velocity, V_{x1} is the scale dependent convection velocity, and L is a length scale corresponding to the center frequency of the standard third-octave band filters used to filter the velocity time series before calculating convection velocity. Figure from Favre *et al.* (1967).
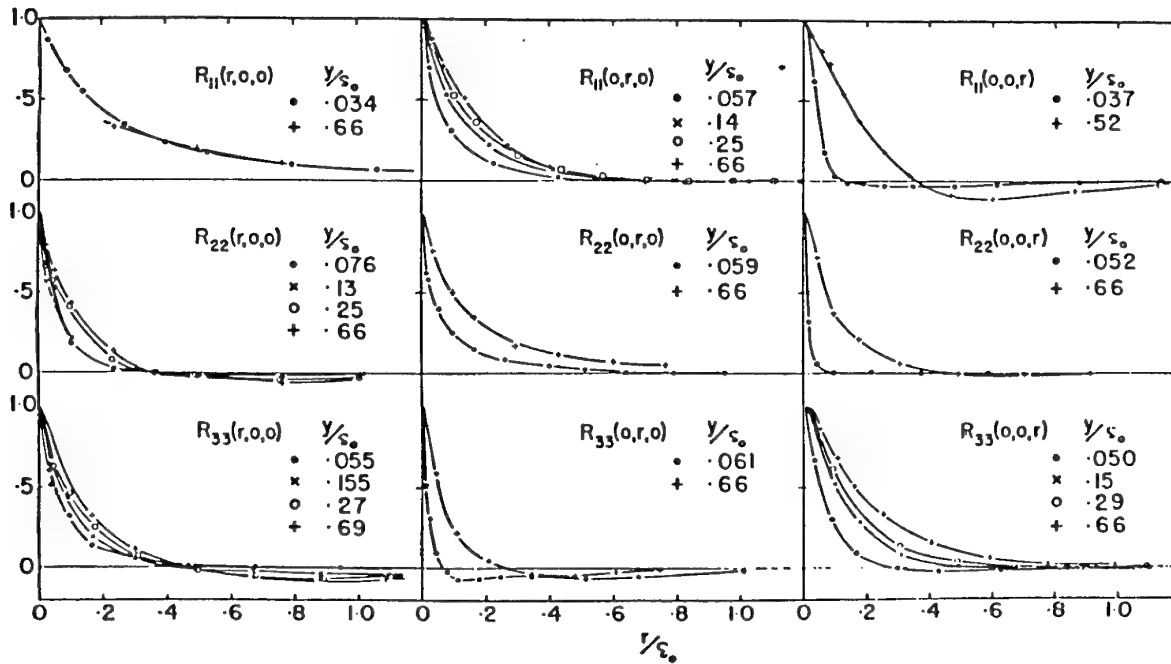
Figure 41: Space-time correlations measured by Grant (1958) in a turbulent boundary layer at $Re_\theta \approx 2,200$. In Grant's notation, r is the probe separation, and δ_o is the boundary layer thickness. Figure from Grant (1958).
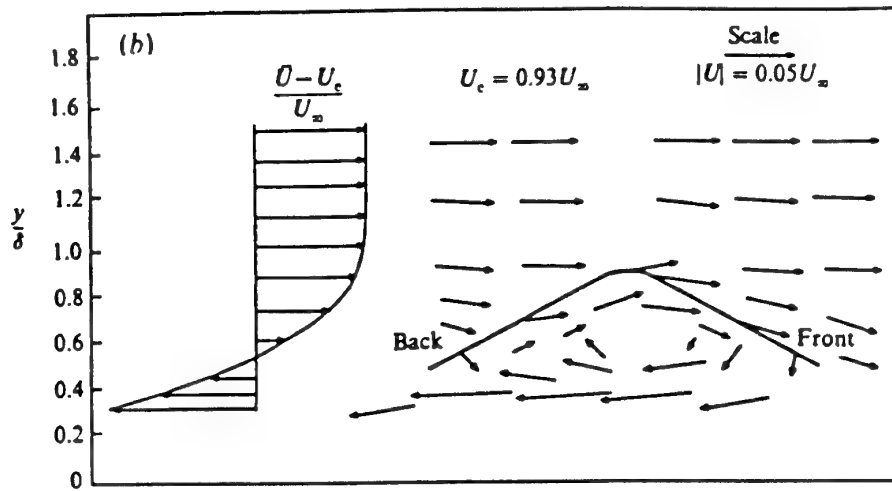
Figure 42: Schematic of the flowfield within and surrounding a large scale motion in a turbulent boundary layer, according to Blackwelder & Kovasznay (1972). Figure from Spina *et al.* (1991a).
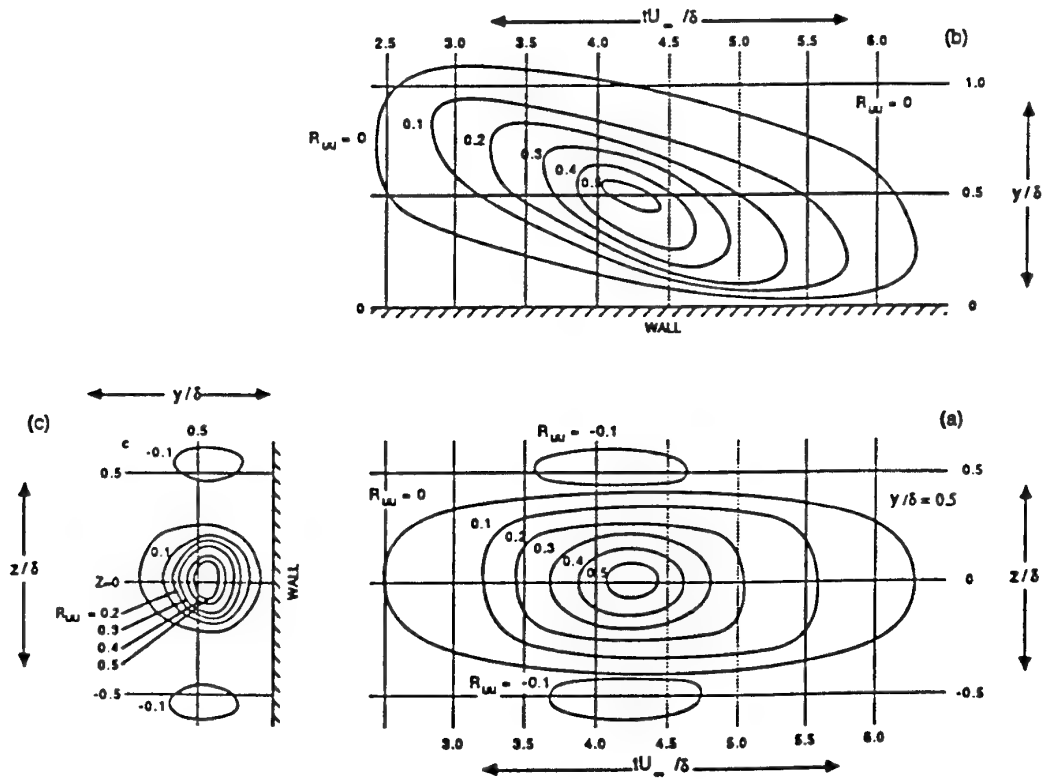
Figure 43: Isocorrelation contours of space-time correlations of the streamwise velocity component measured by Kovasznay *et al.* (1970). a) x-z plane, b) x-y plane, and c) y-z plane. The position of one probe was fixed at $y/\delta = 0.5$. Figure from Smits *et al.* (1989).

angle of 18° to the wall and extended $\approx 2\delta$ in the stream-wise direction. As the structures passed over the wall, they created a characteristic wall-shear-stress signature. Brown & Thomas concluded that this wall-shear-stress pattern was related to the bursting process, and hence that the large scale, outer-layer structure influenced the near-wall structure and dynamics. Although they only reported results for $Re_\theta = 10,160$ in Brown & Thomas (1977), they stated that the results were the same at $Re_\theta = 4,940$ when scaled on outer variables (U_e and δ).

Falco (1977) used combined flow visualization and hot-wire measurements to study the large-scale motions over a range of Reynolds numbers. His flow visualizations showed two distinct scales of motions in the outer layer — LSM's and "typical eddies." Falco found that the typical eddies are small scale motions, which scale on wall variables and are responsible for a significant fraction of the total Reynolds shear stress in the outer layer. Falco determined that the average streamwise extent of the LSM's was about 1.6δ at $Re_\theta \approx 1,000$. The streamwise length scale of the typical eddies was a constant value of $200\nu/u_\tau$ for $1,000 < Re_\theta < 10,000$. The vertical length scale varied nearly linearly from $100\nu/u_\tau$ at $Re_\theta \approx 1,000$, to $150\nu/u_\tau$ at $Re_\theta \approx 10,000$. Falco found that the typical eddies generally appear on the backs of the LSM's, and propagate toward the wall, thus acting as sweeps very near the wall.

Falco (1977) claimed that the typical eddies may be an intermediate link between the inner and outer layers; however, this is difficult to justify. As discussed by Smith & Smits (1991), if the typical eddies scale on wall variables, then at very high Reynolds number, when δ^+ is very large, the typical eddies will become vanishingly small compared to the boundary layer thickness, and are unlikely to be dynamically significant (*i.e.* they will not carry significant levels of shear stress). Furthermore, flow visualizations at very high Reynolds numbers, as shown in figure 44, show features which appear to be very similar to the typical eddies observed by Falco at lower Reynolds numbers, but which are at least an order of magnitude larger (in terms of inner variables), even taking into account the variations in fluid properties, as expressed by the difference between Re_θ and R_{δ_2}. Nevertheless, Falco (1991) has recently used measured typical eddy length and velocity scales to collapse turbulence intensities and Reynolds shear stress data over a very wide range of Reynolds number, as discussed in Section 3.2.2. In light of the objections raised here, the success of the typical eddy scaling is somewhat surprising.

Antonia *et al.* (1982) and Chen & Blackwelder (1978) studied coherent structures using cold-wires in a turbulent boundary layer developing over a slightly heated wall. Chen & Blackwelder's experiments were performed at $Re_\theta = 2,800$, and Antonia *et al.* examined three cases, $Re_\theta = 990, 3,100$, and $7,100$. Both studies used conditional sampling and found that the temperature traces showed characteristic features wherein a slow increase in temperature was followed by a rapid decrease. This suggests that the downstream side of the large structures is not as well defined as the upstream side. The upstream side appears as a sharp interface between high temperature fluid inside the structure, and low temperature fluid behind the structure (note that this interpre-

tation assumes that the Prandtl number is near unity). The interface was found to extend down to the wall, and the convection speed at any location along the interface was approximately equal to the local mean velocity. Antonia *et al.* measured the average inclination angle of the interface to be about 35° for $0.2 < y/\delta < 0.8$. Above and below this range, the angle decreased. These angles are lower, by about 10 - 15°, than those measured by Chen & Blackwelder, and higher, by about 15°, than those measured by Brown & Thomas (1977). Within the scatter of Antonia *et al.* 's results, the average inclination angle appears to be independent of Reynolds number for the range they investigated. They also found that the ensemble averaged velocity and temperature signatures of the large-scale structures are independent of Reynolds number for $Re_\theta > 1,000$. Furthermore, the contribution of the large-scale structures to the Reynolds shear stress seemed to increase with Reynolds number in the range $0.1 < y/\delta < 0.5$.

Antonia *et al.* (1990a), Antonia *et al.* (1990b) studied the effect of Reynolds number on the topology of the organized motion over the range $1,360 < Re_\theta < 9,630$. Broadband isocorrelation contours of u' showed that the average structure extends in the wall-normal direction across most of the boundary layer, has a streamwise extent on the order of δ, and is inclined to the wall, leaning in the downstream direction. Isocorrelation contours for v' also extend across most of the boundary layer, but are narrower in the streamwise direction, and are oriented perpendicular to the wall. The contours show a slight Reynolds number dependence for $Re_\theta < 5,000$, but are independent of Reynolds number for $Re_\theta > 5,000$, as shown in figure 45. Instantaneous streamline patterns showed no significant changes over the entire range of Reynolds numbers.

Using what they called a "window average gradient" (WAG) detection scheme, Antonia *et al.* (1990a), Antonia *et al.* (1990b) found that the time period of occurrence of detected events is independent of Reynolds number when scaled on outer variables and has a value of $\approx 2.5\delta/U_e$. This value is similar to that obtained by Corrsin & Kistler (1955) and Ueda & Hinze (1975), as noted by Falco (1977). Conditionally averaged isovorticity contours were observed to extend further from the wall and have a larger inclination angle (*i.e.* were more upright) at lower Reynolds numbers. Antonia and his coworkers also found that the contribution of the organized motion to the turbulence stresses decreases as Re_θ increases. This is in contrast to the earlier results of Antonia *et al.* (1982) in which the conditional averages were based upon visual identification of characteristic temperature signatures. The difference is most likely due to the difference in detection method.

Murlis *et al.* (1982) used hot-wire anemometry and temperature "tagging" methods to study the effect of Reynolds number on boundary-layer structure for $791 < Re_\theta < 4,750$. Using temperature signals to determine intermittency factors, assuming a Prandtl number near unity, they found that the intermittency profile is essentially independent of Reynolds number. However, the average length of zones of turbulent motion was found to decrease with increasing Reynolds number up to $Re_\theta \approx 5,000$. Their data suggested that, beyond this Reynolds
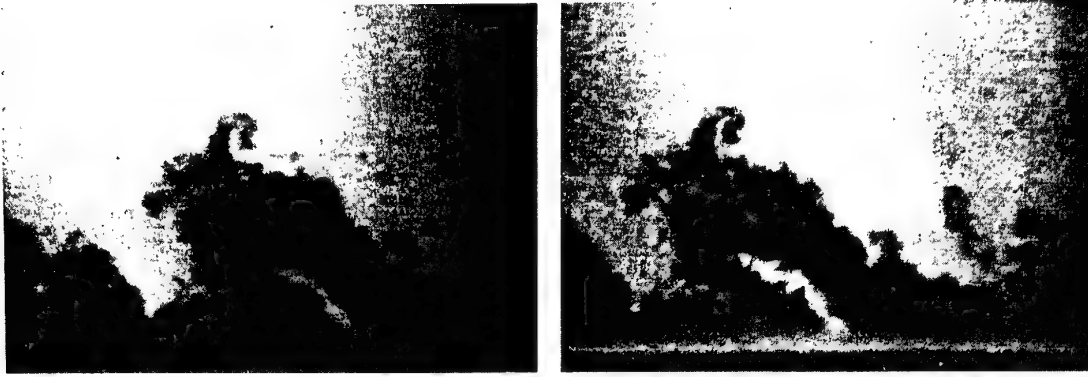
Figure 44: Double-pulsed Rayleigh images from a Mach 3 turbulent boundary layer ($Re_\theta = 80,000$, $R_{\delta 2} = 35,000$); Left: time $= t$; Right: time $= t + 20\mu s$. The flow is from right to left. Figure from Cogne et al. (1993).
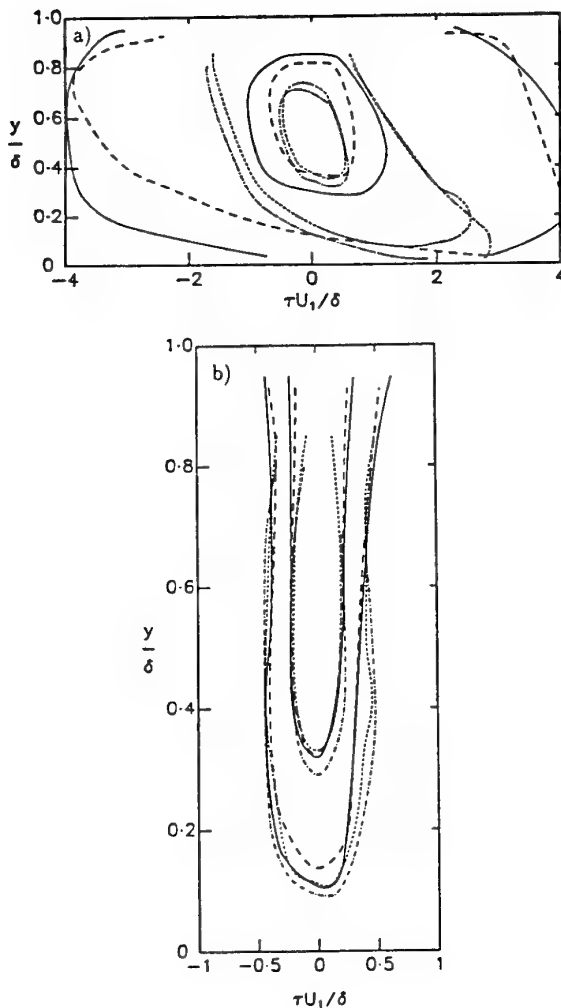
Figure 45: Reynolds number dependence of isocorrelation contours of: a) R_{uu}, b) R_{vv}. $Re_\theta = 1,360$ ————; $2,180$ --------; $6,030$ ················· -; $9,630$ —·—·—. One probe was fixed at $y/\delta = 0.56$. Two contour levels, 0.05 and 0.2, are shown for each Reynolds number. Figure from Antonia et al. (1990b).

number, the turbulent zone length remained constant. Through a detailed analysis of the turbulence statistics, Murlis et al. also concluded that there is a large variation of eddy structure with Reynolds number, but that the basic transport mechanisms did not vary appreciably. This conclusion was based on the finding that the second-order statistics showed significant Reynolds-number dependence, while the triple products, which describe the turbulent transport of the turbulence stresses, were approximately independent of Reynolds number. Murlis et al. also suggested that the large-scale motions carry more shear stress at higher Reynolds numbers, owing to the diminishing importance of the "typical eddies."

Alving & Smits (1990a), Alving et al. (1990b) measured the broad-band structure angle of the LSM's by using two probes separated by a distance ξ_y in the wall-normal direction. The structure angle was defined by $\theta = \tan^{-1}(\xi_y/U_c\tau_{max})$, where U_c is the convection velocity (assumed to be equal to the local mean velocity) and $U_c\tau_{max}$ is the time delay to the maximum in the space-time correlation. The results are shown in figure 46 and they indicate that θ is a strong function of probe separation when ξ_y is small. It appears, however, that θ reaches a limit as ξ_y increases, where it becomes independent of probe separation. The angles in the middle of the layer are about 30°, considerably higher than the values found by Brown & Thomas (1977) and Kovasznay et al. (1970). Perry et al. (1992) later measured structure angle by fixing the wall-normal separation of two probes and varying the streamwise separation until the value of the crosscorrelation of the signals from the two probes attained a peak. This method has the advantage of not depending on the validity of Taylor's hypothesis. The results agreed well with the data of Alving et al. (1990b), for which the probes were separated in only the wall-normal direction and Taylor's hypothesis was used. Thus, Perry et al. concluded that the use of Taylor's hypothesis is an accurate approximation for measurements of turbulence structure in a boundary layer (at least for reasonable Reynolds numbers and large-scale features).

MacAulay & Gartshore (1991) determined that the major contributions to the broadband crosscorrelations in a turbulent boundary layer at $Re_\theta = 8,390$ came from δ-scale segments of the velocity signals, which encompass many aspects of the flow structure, rather than from individual

Figure 46: Broadband structure angle in a subsonic boundary layer, as a function of probe-separation distance. Figure from Alving *et al.* (1990b).

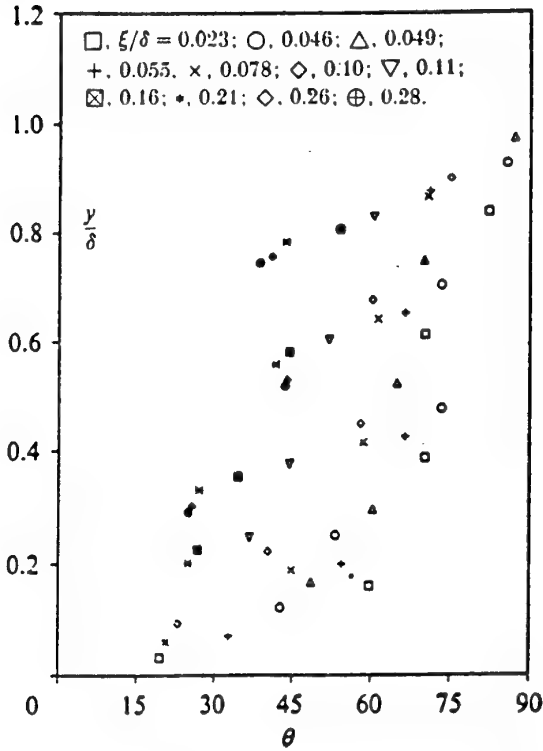Figure 47: Structure angles measured by MacAulay & Gartshore (1991) in a turbulent boundary layer at $Re_\theta = 8,390$: $\square$, broadband general structure angle; $\triangle$, structure angle of the trailing (upstream) interface of the large-scale motions as detected using the VITA technique. Figure from MacAulay & Gartshore (1991).

hairpin eddies, which are an order of magnitude smaller than δ, in the streamwise and spanwise directions, at this Reynolds number. Using conditional sampling, they were able to measure the inclination angle of the sharp interface at the backs of the large-scale motions. This interface angle is compared to their measurements of the broadband structure angle in figure 47, and the difference is significant.

Based upon their own data and a review of the literature, MacAulay & Gartshore developed a conceptual model illustrating the Reynolds number dependence of the outer-layer structure, which is shown in figure 48. As in the visualizations of Head & Bandyopadhyay (1981) at low Reynolds numbers, the horseshoe vortices are of the same magnitude as the boundary-layer thickness in the spanwise and wall-normal directions. At high Reynolds numbers, the spanwise scale of the hairpin eddies is much smaller than the boundary-layer thickness. An interesting feature of the high-Reynolds-number model is the congregation of small-scale features near the backs of the large-scale structures. Due to their own self-induction, the hairpin vortices will propagate backwards (in a frame of reference moving at the mean velocity) through the low-speed fluid within the turbulent bulges. When they reach the back of a bulge, they encounter a sudden increase in streamwise velocity which balances their self-induced velocity. MacAulay & Gartshore suggest that stronger structures (with higher self-induced velocities) will penetrate the rear interface further than weaker structures. This results in the appearance of small scale struc-

tures on the backs of the large scale motions, similar to Falco's typical eddies. When the hairpin vortices cease their backward propagation, their self-induction will continue to carry them up, away from the wall, resulting in a slow overturning motion.

Wark *et al.* (1991) and Naguib & Wark (1992) used Spalart (1988) DNS data ($670 < Re_\theta < 1,410$) together with their own data for $1,579 < Re_\theta < 5,961$ to investigate the scaling of space-time correlations between the fluctuating wall shear stress and the streamwise velocity component. Their study concentrated on the near-wall region (the overlap layer and below). Close to the wall, the correlations for different Reynolds numbers scaled on inner variables for spanwise probe separations $\xi_z^+ \leq 40$. For $\xi_z/\theta > 0.5$, the correlations scaled on outer variables. This would seem obvious, since the spatial separation of the probes acts as a spatial filter. At larger separations, small-scale motions, which scale on inner variables, do not contribute to the corrrelation, since they do not pass by both probes. Only large-scale motions, which scale on outer variables, will contribute to the correlation. In the overlap layer, the correlations were found to scale on outer variables for all spanwise probe separations.

Wark *et al.* (1991) found that the commonly observed negative correlation region in the spanwise correlations disappeared at higher Reynolds numbers. Naguib & Wark (1992) filtered the data to show that the region of negative correlation is due to the small structures which scale on inner variables. They also found that, as Re_θ increases, the larger, lower-frequency structures make in increased contribution to $\overline{u'^2}$. However, at $y^+ = 35$, small-scale features were found to make the greatest contribution to Reynolds shear stress, and thus to the production of turbulence kinetic energy, at all Reynolds numbers.

Space-time correlation measurements by Smith (1994) at Reynolds numbers in the range $4,600 \leq Re_\theta \leq 13,200$ showed that the broad-band convection velocity and the decay of the large scales with increasing time delay scaled

on outer-layer variables (specifically U_e and δ) were only weakly dependent on Reynolds number. However, iso-correlation contours indicated that the streamwise length scales increased with Reynolds number, in agreement with the results by Liu *et al.* in a fully-developed channel flow. Furthermore, space-time correlations in the wall-normal direction revealed that the broadband structure angle *decreased* by about $10°$ over the same range in Re_θ.

Isocorrelation contour maps (figures 49 and 50) showed an *increase* of between 30 and 60% in the streamwise length scale over the same Reynolds number range, and this behavior may be related to the decrease in the structure angle. The spanwise length scale showed comparatively little variation.

These subsonic results provide an interesting contrast to the results obtained by Spina *et al.* (1991a) in a Mach 3 boundary layer with $Re_\theta = 80,000$ (see figures 51 and 52). In the supersonic flow, the streamwise length scales were two to three times *smaller* than in the subsonic flow, and the structure angles were about $10°$ *larger*. The spanwise scales were almost independent of the Mach number. Now, the smaller streamwise scales correlate well with the increased structure angle, but the trend with Reynolds number seen in the subsonic data does not seem to hold for the supersonic flow. Therefore it seems that the streamwise length scale and the structure angle depend on the Mach number and the Reynolds number. These observations have important implications for developing turbulence models for high speed flows, where it is commonly assumed that length scales follow the same scaling as in subsonic flow, and only fluid proerty variations are important. The fact that some characteristics of the turbulence depend on Mach number in a more subtle way, even at supersonic speeds where these assumptions work reasonably well, indicate that at higher Mach numbers the scaling will need to include compressibility effects directly.

4 Supersonic Flows

4.1 Introduction

At supersonic Mach numbers, viscous energy dissipation makes a significant contribution to the energy budget. As a result, the temperature rises and significant temperature gradients occur within the boundary layer. In a turbulent boundary layer in supersonic flow, therefore, the mean temperature and velocity vary, and significant temperature and velocity fluctuations occur. Pressure fluctuations are usually small at supersonic speeds but may become important at Mach numbers exceeding 5.

The increased influence of viscous dissipation is illustrated by the evolution of the mass-flux profile with Mach number. The elevated static temperature at the wall creates a low-density region that shifts the majority of the mass flux toward the outer part of the boundary layer, and the profile becomes more skewed as the freestream Mach number becomes larger. In addition to affecting the density profile, the mean static temperature variation also creates fluid-property gradients across the boundary layer. For an adiabatic wall, the temperature at the wall T_{aw} depends
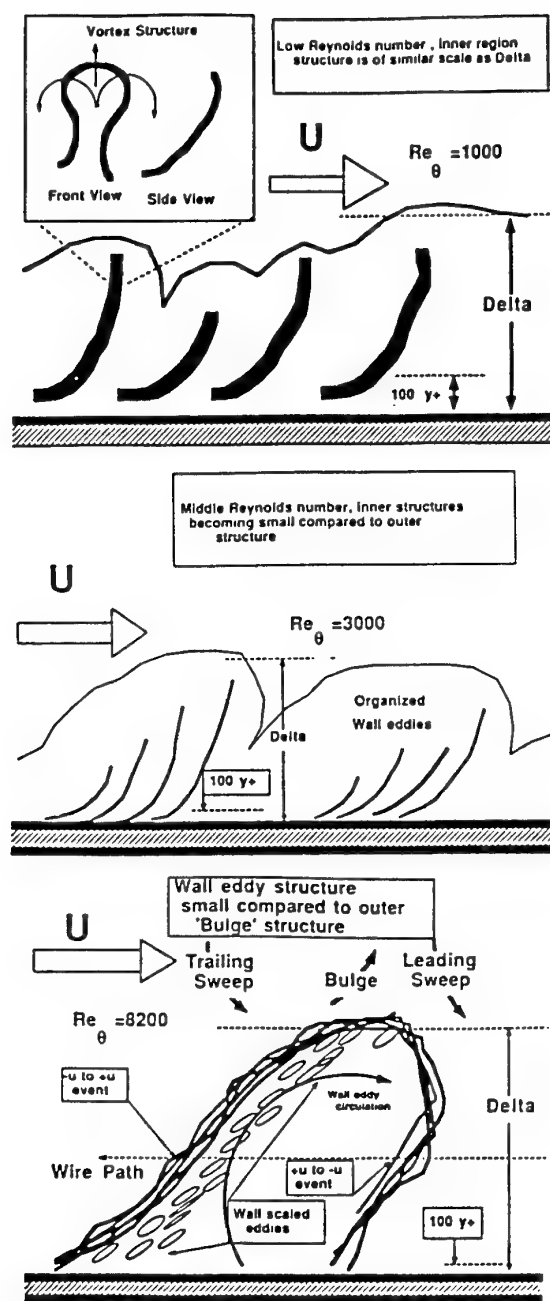

Figure 48: Conceptual model of the Reynolds number dependence of the structure of turbulent boundary layers. Figure from MacAulay & Gartshore (1991).

Figure 49: Isocorrelation contour maps in the x-y plane, as measured by Smith (1994), in a turbulent boundary layer at $Re_\theta = 4,981$ and $13,052$ using different wall-normal probe separations: a) $\xi_y/\delta \approx 0.1$. Figure from Smith (1994).

Figure 49 (cont.) c) $\xi_y/\delta \approx 0.3$.

Figure 49 (cont.) b) $\xi_y/\delta \approx 0.2$.

Figure 50: Isocorrelation contour maps in the x-z plane, as measured by Smith (1994), in a turbulent boundary layer at $y/\delta = 0.09, 0.42, 0.80$. (a) $Re_\theta \approx 4,600$. Figure from Smith (1994).
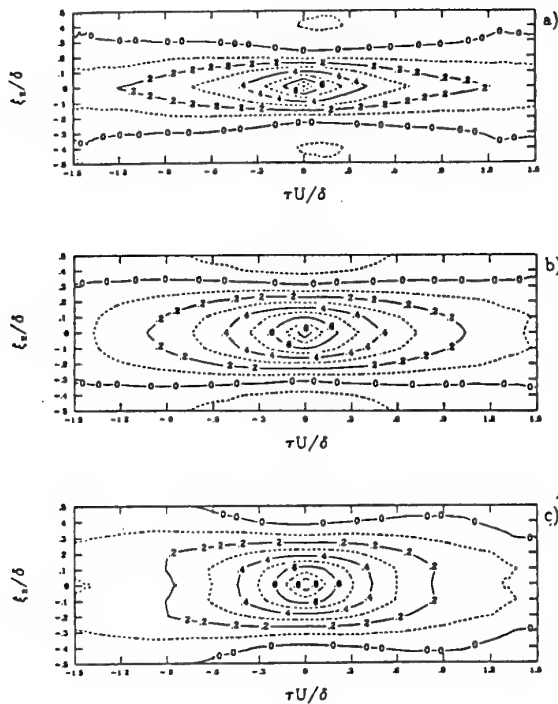
Figure 50 (cont.) (b) $Re_\theta \approx 13,200$.

on the recovery factor r and the freestream Mach number, but it is always within 10 to 12% of the freestream total temperature. Typical wall-to-freestream ratios of some flow properties are provided in Table 3 for three different Mach numbers. Since the density of gases decreases and the viscosity increases with temperature, the ratio of ν_w/ν_e can become very large. Of course, when the wall is heated or when the flow is perturbed so that normal pressure gradients exist, the gradients of ρ, μ, and k may be even more severe. As a result of the fluid-property gradients, the low Reynolds number effects usually found only very near the wall will encompass a larger portion of the boundary layer as M_∞ increases, and the influence of the viscous sublayer will increase. Such considerations indicate the physical basis for preferring the use of $R_{\delta 2}$

M_∞	T_w/T_∞	ρ_w/ρ_∞	μ_w/μ_∞	ν_w/ν_∞
2.9 (air)[a]	3	0.33	1.4	4.2
4.5 (air)[b]	5	0.2	2.9	14
10.3 (He)[c]	33	0.03	9.6	320

[a] Spina & Smits 1987.
[b] Mabey et al 1974.
[c] Watson et al 1973.

Table 3: The ratio of fluid properties across three boundary layers in supersonic flow on adiabatic walls. Table from Spina et al. (1994).

in the desription of supersonic boundary layers over the conventional Re_θ.

4.2 Stagnation-Temperature Distribution

The stagnation-temperature profile must be known to calculate the velocity distribution. Measurements and theory often seem to conflict, however, and a truly representative stagnation-temperature profile is difficult to define, particularly at high Mach number. The measurement difficulty stems from the compromise that must be made between spatial resolution and accuracy when selecting a stagnation-temperature probe (see, for example, Fernholz & Finley, 1980). Since approximately one-half of the decrease in $\overline{T_0}$ to the wall-recovery value occurs in the inner layer of near-unity Prandtl-number gases (Morkovin, 1962), this compromise leads to a kind of uncertainty principle on the accuracy of the data.

As for theoretical stagnation-temperature distributions, Fernholz & Finley (1980) present and discuss many of the energy-equation solutions commonly applied to supersonic turbulent boundary layers. They note that many of the relations are applied beyond their range of validity when used to benchmark experimental data. The two most widely discussed stagnation-temperature distributions in the literature are the "linear" and "quadratic" solutions. It has been commonly assumed that $(T_0 - T_w)/(T_{0_e} - T_w) \equiv \Theta = U/U_e$ is the proper distribution for flat-plate flows, while $\Theta = (U/U_e)^2$ is the appropriate tunnel/nozzle wall solution. It has been claimed that the quadratic nature of the measurements along tunnel walls is due to the upstream history of the flow (significant dT/dx and dp/dx) and the resultant local non-equilibrium. While Feller (1973), Bushnell et al. (1969), and Beckwith (1970) offer convincing arguments for flow-history effects, there is little experimental evidence that the linear profile is the equilibrium stagnation-temperature distribution in supersonic, turbulent boundary layers.

The classic (linear) Crocco solution, $\Theta = U/U_e$, is derived from the energy and momentum equations for laminar flow with $Pr = 1$, zero pressure gradient, and an isothermal wall. The Crocco solution is extended to turbulent flows under the same conditions with the additional assumption of unity turbulent Prandtl number (Pr_t). However, it has been shown that Pr_t is less than 1.0 across the outer layer for both near-adiabatic walls (Meier & Rotta, 1971) and cold walls (Owen et al., 1975). Fernholz & Finley (1980) show that the origins of a quadratic profile for turbulent flow lie in a solution by Walz (1966):

$$\Theta = \beta \frac{U}{U_e} + (1 - \beta)\left(\frac{U}{U_e}\right)^2, \qquad (53)$$

where $\beta = (T_{aw} - T_w)/(T_{0_e} - T_w)$. The assumptions inherent in this solution are zero pressure gradient, isothermal wall, and a constant "mixed" Prandtl number, $Pr_M \equiv c_p(\mu + \mu_t)/(k + k_t)$ between 0.7 and 1.0. The linear profile therefore holds only for $\beta = 1$, that is, $T_{0_e} = T_{aw}$, and the purely quadratic profile holds only for a zero-pressure-gradient flow, with constrained Pr_M, and an isothermal
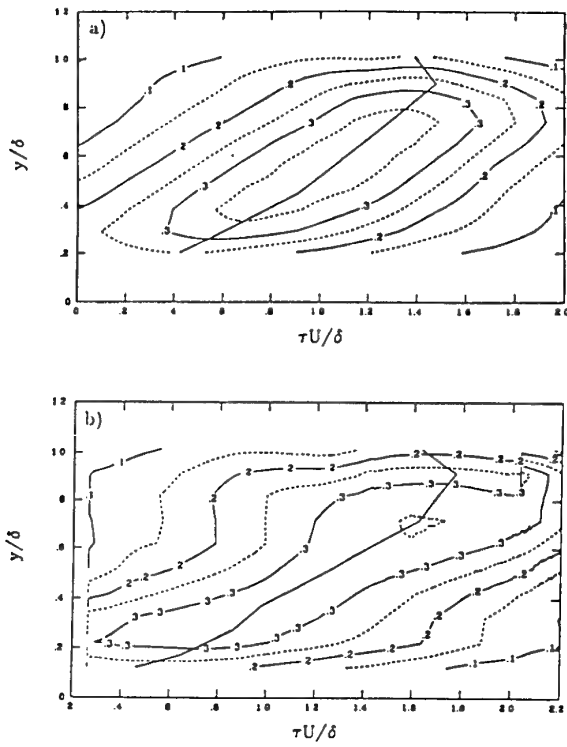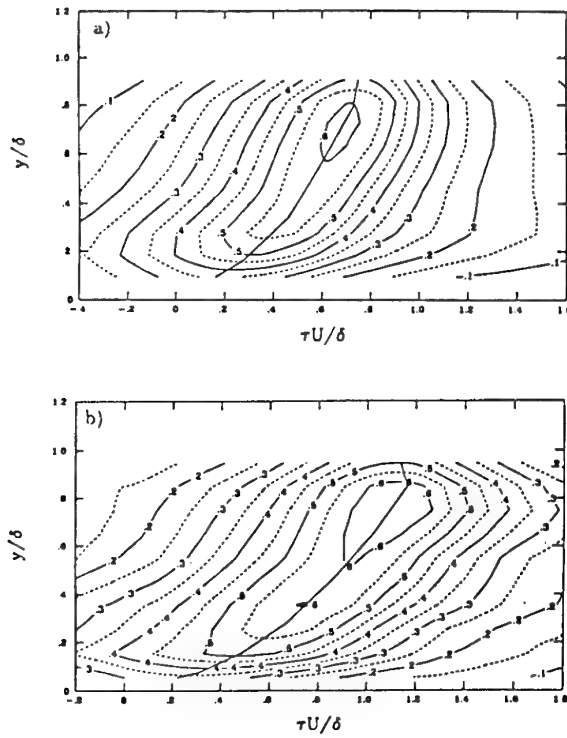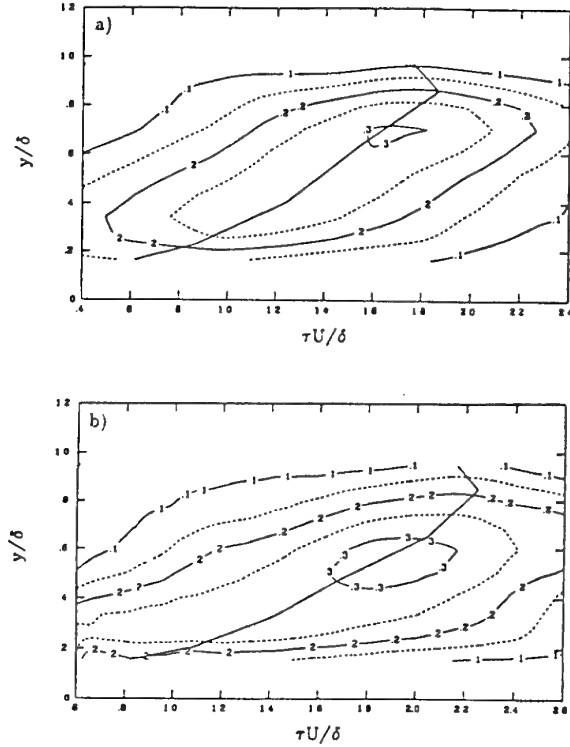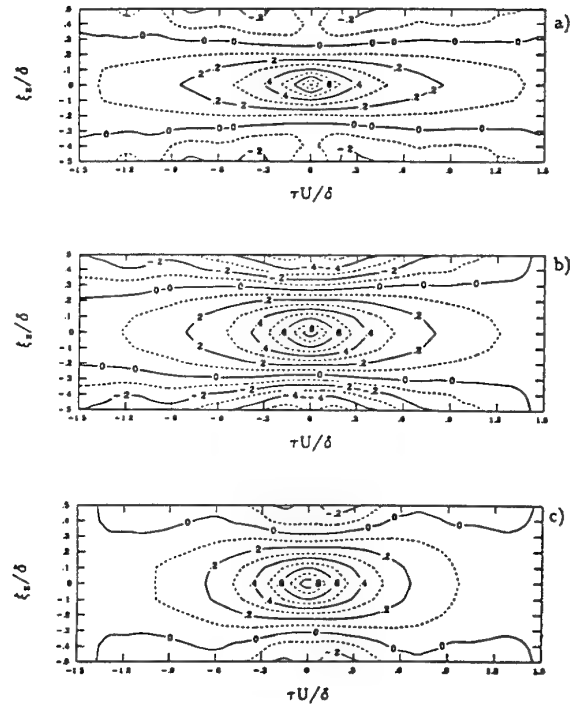
Figure 51: Isocorrelation contour maps in the x-y plane, as measured by Spina (1988), in a turbulent boundary layer at $Re_\theta = 81,000$ and $M = 2.9$ using different wall-normal probe separations: a) $\xi_y/\delta = 0.09$; b) $\xi_y/\delta = 0.30$; c) $\xi_y/\delta = 0.51$. Figure from Spina (1988).
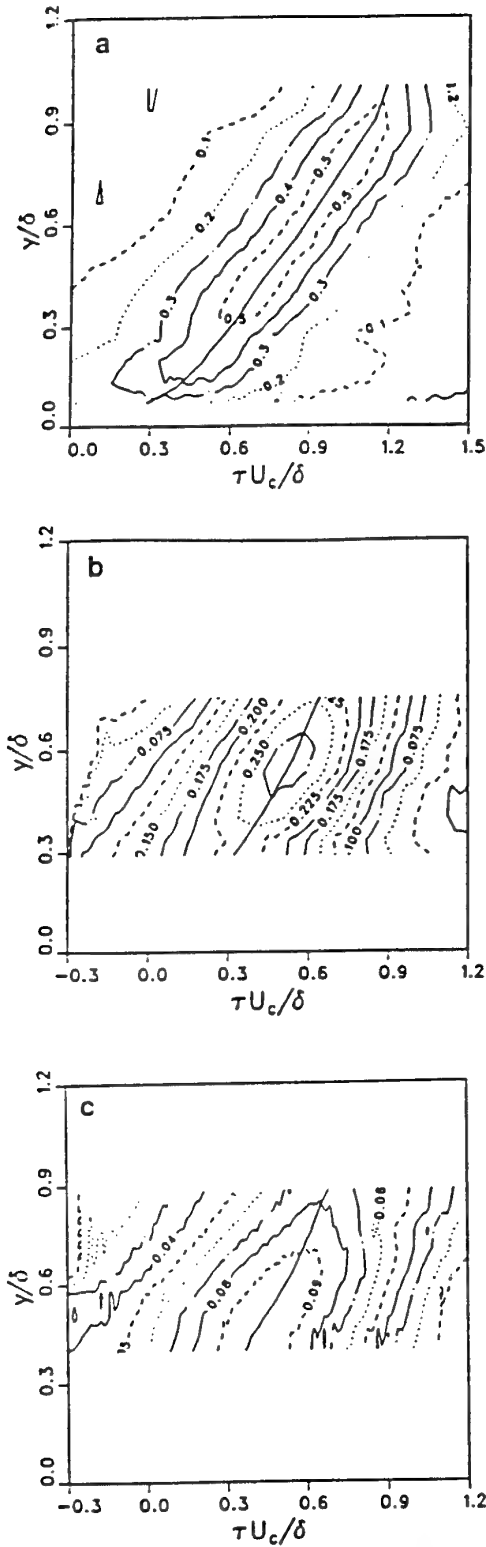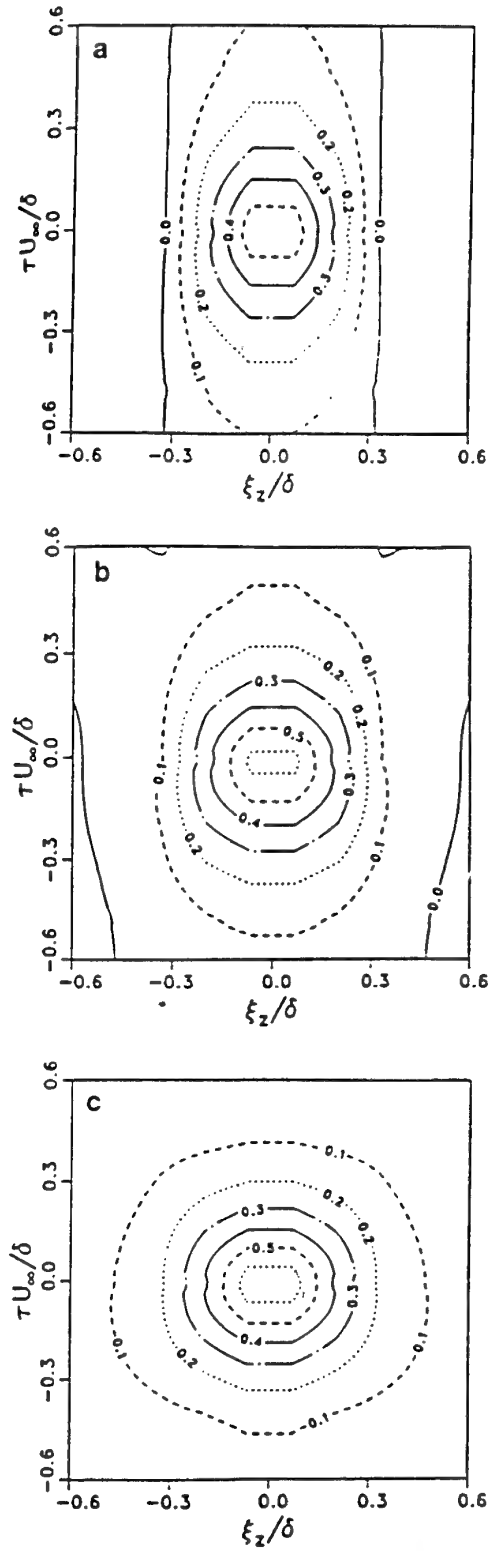
Figure 52: Isocorrelation contour maps in the x-z plane, as measured by Spina (1988), in a turbulent boundary layer at $Re_\theta = 81,000$ and $M = 2.9$ at three positions in the boundary layer: a) $y/\delta = 0.20$; b) $y/\delta = 0.51$; c) $y/\delta = 0.82$. Figure from Spina (1988).

(also adiabatic) wall ($\beta = 0$). The range of validity of the quadratic relation is often extended improperly to flows with pressure gradients because of the similarity of the equation to one that is valid for laminar and turbulent adiabatic flows with pressure gradients. Perhaps due to the relaxed constraint on the Prandtl number (as compared to the linear solution), much of the stagnation-temperature data appears to be characterized by a quadratic trend (Bushnell *et al.* , 1969, Bertram & Neal, 1965, Wallace, 1969, Hopkins & Keener, 1972).

A critical shortcoming is the dearth of near-wall T_0 measurements, which are critical for determination of the wall heat-transfer rate. The lack of data makes it impossible to determine whether these temperature-velocity relations, or even those provided by Bradshaw (1977) to represent the inner layer, accurately describe the near-wall behavior of the stagnation temperature. For flows with non-isothermal walls and significant pressure gradients the situation is much worse, however, as no theoretical temperature-velocity relations exist for these conditions. Much of the confusion surrounding stagnation-temperature distributions is due to comparison between data taken under these conditions and theoretical relations that are applied beyond their range of validity.

4.3   Mean-Velocity Scaling

When the mean velocity in a supersonic boundary layer is plotted as U/U_e *vs.* y/δ, the profile appears qualitatively similar to that of an incompressible flow. When the velocity is replotted in classic inner- or outer-layer coordinates, however, the velocity does not follow the familiar incompressible scaling laws for these regions. But a modified scaling that accounts for the fluid-property variations correlates much of the existing compressible mean-velocity data with the "universal" incompressible distribution. This velocity scaling was first employed in the viscous sublayer and the logarithmic region by van Driest (1951), was extended to the wake region and to velocity-defect scaling by Maise & McDonald (1968), and to Coles' universal wall-wake scaling by Mathews *et al.* (1970). The following outline of the scaling arguments for supersonic turbulent boundary layers is based largely on the discussion given by Fernholz & Finley (1980).

The usual derivation of the velocity distribution in the inner region is based on the assumptions:

(1) that the convective term $\partial/\partial x$ in the equation of motion is small compared with the viscous term,

(2) that the pressure gradient term can be ignored so as to simplify the discussion, and

(3) that the total stress $\tau_T = \mu\left(\partial\bar{U}/\partial y\right) - \bar{\rho}\overline{u'v'}$ is constant in the inner region and equals τ_w.

(4) Morkovin's hypothesis holds, in that the structure of the turbulence does not change significantly due to compressibility effects up to about a freestream Mach number of about 5.

"The dominating factor in the compressible turbulent-boundary layer problem is apparently then the effect of high temperature on the velocity profile near the wall and therefore on

the shear stress. This latter observation was first advanced by von Kármán in 1935 but has been somewhat neglected in favour of interpolation formulae or of elaborate generalizations of the mixing length hypothesis" (Part I of Coles, 1953).

The increased dissipation rate in the viscous sublayer has the effect that at a fixed Reynolds number the sublayer thickness increases with increasing Mach number. The same effect is of course responsible for the observed increase in the thickness of the laminar boundary layer at high Mach numbers (see, for example, van Driest, 1951).

If one assumes that in the viscous sublayer the molecular shear stress $\mu\left(\partial\bar{U}/\partial y\right)$ is large compared with the Reynolds shear stress $-\bar{\rho}\overline{u'v'}$ and equal to the skin friction τ_w, then one obtains for the velocity gradient

$$\frac{\partial\bar{U}}{\partial y} = \frac{u_\tau^2}{\nu_w}\left(\frac{T_w}{\bar{T}}\right)^\omega \tag{54}$$

in which the variation of the viscosity with temperature is taken to be given by

$$\frac{\mu}{\mu_w} = \left(\frac{\bar{T}}{T_w}\right)^\omega \tag{55}$$

Using Equation 53 for the temperature distribution (valid under the assumptions $dp/dx = 0$ and $T_w = $ constant), Equation 54 yields:

$$\frac{\overline{U^s}}{u_\tau} = \frac{yu_\tau}{\nu_w} \tag{56}$$

where the transformed mean velocity in the sublayers $\overline{U^s}$ is defined by

$$\overline{U^s} = \int_0^U \left(\frac{T}{T_w}\right)^\omega dU. \tag{57}$$

Hence, with $\omega = 1$:

$$\overline{U^s} = \bar{U}\left[1 + \frac{1}{2}a\frac{\bar{U}}{U_e} - \frac{1}{3}b^2\left(\frac{\bar{U}}{U_e}\right)^2\right] \tag{58}$$

in which

$$a = \left(1 + r\frac{\gamma-1}{2}M_e^2\right)\frac{T_e}{T_w} - 1 \tag{59}$$

$$b^2 = r\frac{\gamma-1}{2}M_e^2\frac{T_e}{T_w}. \tag{60}$$

We see that the transformed velocity $\overline{U^s}$ has a linear distribution similar to the linear velocity distribution in the viscous sublayer of an incompressible turbulent boundary layer, and to which it reduces for $\bar{T} = T_w$ and $M_e = 0$.

Between the viscous sublayer and the outer layer there exist a region, defined by $y^+ >> 1$ and $\eta << 1$, where the Reynolds shear stress $-\bar{\rho}\overline{u'v'}$ is dominant and is approximately equal to the skin friction τ_w. If it is assumed that Prandtl's mixing length theory is also valid

for compressible turbulent boundary layers, then from $\tau_w = -\bar{\rho}\overline{u'v'} = \rho\ell^2\left(\partial\bar{U}/\partial y\right)^2$ we obtain:

$$\frac{\partial\bar{U}}{\partial y} = \frac{\sqrt{\tau_w/\rho}}{\kappa y} \tag{61}$$

where κ is von Kármán's constant and ℓ is Prandtl's mixing length (assumed to be equal to κy, as in subsonic flows). This result is independent of Mach number. Since the pressure is constant in the wall-normal direction, we have, for a perfect gas:

$$\frac{\partial\bar{U}}{\partial y} = \frac{u_\tau}{\kappa y}\sqrt{\left(\frac{\bar{T}}{T_w}\right)} \tag{62}$$

We can again use Equation 53 to substitute for the temperature ratio in Equation 57 and obtain (Fernholz, 1969):

$$\frac{\overline{U^*}}{u_\tau} = \frac{1}{\kappa}\ln\frac{yu_\tau}{\nu_w} + C^* \tag{63}$$

where

$$\overline{U^*} = \int_{U_1^+}^{U^+}\sqrt{\frac{T_w}{\bar{T}}}\,dU^+. \tag{64}$$

Hence:

$$\overline{U^*} = \frac{U_e}{b}\sin^{-1}\left[\frac{2b^2\frac{U}{U_e} - a}{\sqrt{(a^2 + 4b^2)}}\right] \tag{65}$$

and

$$C^* = \frac{1}{\kappa}\ln\frac{y_1 u_\tau}{\nu_w} + \frac{U_e}{u_\tau}\frac{1}{b}\sin^{-1}\left[\frac{2b^2\frac{\overline{U_1}}{U_e} - a}{\sqrt{(a^2 + 4b^2)}}\right]$$

where a and b are given by Equations 59 and 60, and the suffix 1 denotes a boundary condition at the lower end of the validity range of the log-law (which can in principle only be found by experiment).

For an adiabatic wall, T_w becomes the recovery temperature T_r, and $a = 0$. In this case experiments show that $\overline{U_1}/U_e$ lies in the range $0.3 \leq \overline{U_1}/U_e \leq 0.6$. With a value for $\overline{U_1}/U_e = 0.5$ one can show that arcsin can be replaced by its argument for Mach numbers up to 8 with a relative error of -4% or less. Then C^* reduces to

$$C_{ad}^* \approx \frac{\overline{U_1}}{u_\tau} - \frac{1}{\kappa}\ln\frac{yu_\tau}{\nu_w} \approx C, \tag{66}$$

that is, the same value as for the incompressible case. This result was also confirmed by the measurements discussed by Fernholz & Finley (1980) and by general computational experience (Bushnell et al. , 1976).

Fernholz & Finley (1980) concluded that velocity profiles in compressible turbulent boundary layers are well represented by Equation 63 within the limits set by the assumptions. A comparison between measurements in transformed and un-transformed coordinates is given in figure 53.

The first approach to this type of transformation was suggested by van Driest (1951) who derived a relationship

similar to Equation 63 also using the mixing length concept. He assumed Prandtl number unity and so a recovery factor equal to one and determined the constant C so that for the limit $M_e \to 0$ and $(T_w/T_e) \to 1$ the well-established relationship for the incompressible case should result. Van Driest's equation for the logarithmic law then reads the same as Equation 63, except that $r = 1$ in the definitions of a and b.

The differences likely to appear if the alternative transformation is used can be seen in figure 54. Here three sets of profile data are plotted using firstly Equation 65 with $r = 0.896$ and secondly Equation 65 with $r = 1.0$ which then reduces to van Driest's transformation. The differences, although systematic, are small when compared to experimental error, particularly in the determination of C_f. Given the uncertainties in the transformation approach, and the experimental difficulties in obtaining accurate values for C_f, there is little that can be said for any given set of log-law constants and their possible variation with Reynolds number or Mach number. It is equally difficult to say anything meaningful regarding the existence of power law similarity, rather than log-law similarity, as discussed in Section 3.1.5.

The empirical validity of Morkovin's hypothesis offers some support for the concept behind the van Driest transform (and similarly that by Fernholz & Finley) by suggesting that multi-layer scaling holds in compressible boundary layers. And despite the assumptions inherent to the mixing-length hypothesis, the underlying dimensional argument is sound as long as the length-scale distributions in supersonic boundary layers follow the same behavior as in subsonic flows. In fact, experimental data taken over a wide Mach-number range, with various wall-heating conditions and modest pressure gradients, and transformed via van Driest show good agreement with incompressible data correlations (for example, Kemp & Owen, 1972, Laderman & Demetriades, 1974, Owen et al. , 1975, Watson, 1977). The systematic discussion given by Fernholz & Finley (1980) is particularly persuasive.

It is important to note what the limits of applicability appear to be, however. Other than strong pressure gradients, the primary constraint is imposed by the dependence of similarity on large values of the Reynolds number, implying universality and independence from upstream history. Fernholz & Finley (1980) observe that the low-Reynolds-number region that begins to dominate the inner layer at high Mach number may eventually cause the failure of the velocity scaling laws that the transformed data follow. Hopkins et al. (1972) attribute the poor performance of van Driest at $M_e = 7.7$ to the low Reynolds number of the flow, $Re_\theta \approx 5,000$. This can be compared to a successful application of van Driest at $M_e = 9.4$ and $Re_\theta \approx 37,000$ by Laderman & Demetriades. It seems reasonable, however,that the transformation suggested by Fernholz & Finley offers a slightly more accurate variation of van Driest, since the temperature distribution is based on a Prandtl number assumption $(0.7 \leq Pr_M \leq 1.0)$ that is more realistic than van Driest's assumption of $Pr_t = Pr = 1$.

In the outer region, the similarity of the velocity profile can be verified by plotting the velocity defect $\left(U_e^* - \overline{U^*}\right)/u_\tau$ versus y/δ' where the transformation of

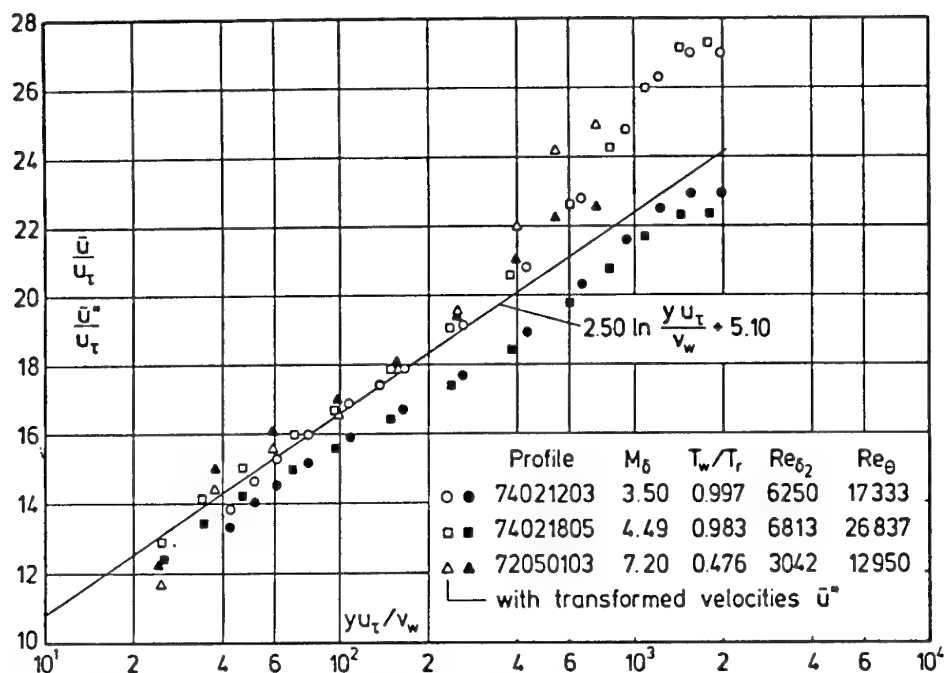Figure 53: Log-linear plots of the velocity profile for a compressible turbulent boundary layer. Natural and transformed velocities ($\bar{U}^*$). From Fernholz & Finley (1980), where catalog numbers are referenced.
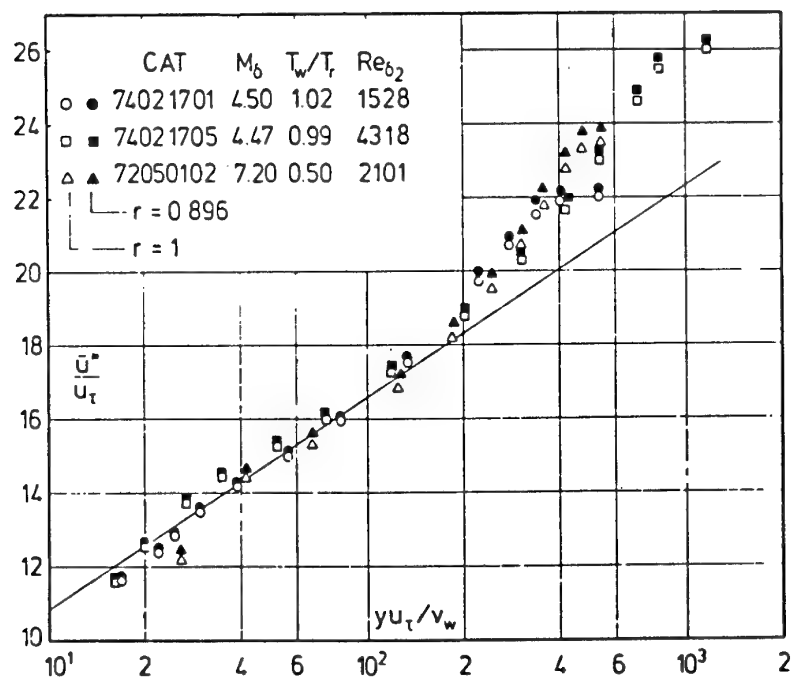

Figure 54: Comparison of velocity profiles transformed by using recovery factors of 1 and 0.896 (Mabey *et al.* , 1974, Horstman & Owen, 1972). From Fernholz & Finley (1980), where catalog numbers are referenced.

the velocities U_e^*, $\overline{U^*}$ and the characteristic length δ' have yet to be determined. Since the mean velocity approaches the velocity U_e asymptotically the boundary layer thickness is an ill-defined quantity, and it is sensible to use instead an integral length Δ as suggested by Rotta (1950) for incompressible boundary layers (see Equation 26). The only difficulty in using the reference length Δ is that both the velocity profile and the skin friction must be known which, unfortunately, is not always the case for the published measurements. If both are available then the velocity defect distribution and the integral length scale can be transformed and applied to compressible turbulent boundary layers. It is then hoped that the dimensionless velocity defect will be described by a function

$$\frac{U_e^* - \overline{U^*}}{u_\tau} = f\left(\frac{y}{\Delta^*}\right) \qquad (67)$$

(for zero pressure gradients), where

$$\frac{\Delta^*}{\delta} = \int\limits_0^1 \frac{U_e^* - \overline{U^*}}{u_\tau} d\left(\frac{y}{\delta}\right) \qquad (68)$$

There is no justification for the simple relationship of Equation 67 other than verification by experiment. However, an evaluation of a large number of experiments in zero-pressure gradient boundary layers, mainly along adiabatic walls appears to support this particular scaling scheme. The data suggest the following semi-empirical relation (Fernholz, 1971):

$$\frac{U_e^* - \overline{U^*}}{u_\tau} = -M \ln \frac{y}{\Delta^*} - N \qquad (69)$$

with $M = 4.70$ and $N = 6.74$ ($1.5 \times 10^3 \leq Re_\theta \leq 4 \times 10^4$).

More elaborate semi-empirical relationships of the type:

$$\frac{U_e^+ - \overline{U^+}}{u_\tau} = -\frac{1}{\kappa} \ln \frac{y}{\delta} + \kappa g\left(\frac{y}{\delta}\right) \qquad (70)$$

were suggested by Coles (1953), by Stalmach (1958) and by Maise & McDonald (1968), the latter two authors using van Driest's velocity transformation, that is, with Prandtl number one. Due to the different methods applied in specifying the boundary layer thickness δ, the authors of the semi-empirical relations mentioned above do not agree with each other nor do they agree with measurements if these are plotted using values as given by the experimentalists.

Figure 55 shows this comparison. Since the figure is meant only to illustrate the problem, the reader is referred to Fernholz (1969) for the identification of the experimental data.

Libby & Visich (1959), Mathews et al. (1970) and Sun & Childs (1973) extended the Coles (1956) wall-wake velocity profiles (Equation 27) to compressible turbulent boundary layers (a) for adiabatic flows with pressure gradient and (b) for isothermal wall and zero pressure gradient, using the van Driest transformation in the 1973 paper. Sun & Childs (1976) modified Coles's relationship to avoid the shortcomings basic to this formulation that the velocity gradient at the boundary edge has a non-zero

value. Though the basic elements of this "amalgamated" velocity profile look promising, no sufficient comparisons with experiments are available as yet. Transformed velocities according to van Driest were also used by Lewis et al. (1972) for a semi-empirical description of the velocity distribution in the inner and outer region.

Finally, it should be pointed out (as we did for incompressible flows) that the similarity scaling of the compressible boundary layer mean velocity profile is most usefully expressed in terms of the scaling for the mean velocity gradient $\partial U/\partial y$. That is, $\partial U/\partial y$ in the near-wall region scales with a length scale ν_w/u_τ and a velocity scale $u_\tau (T_w/T)^{\omega/2}$. In the outer region the length scale is δ, and the velocity scale is $u_\tau\sqrt{(T/T_w)}$. In the overlap region, the length scale becomes y, but the velocity scale is still $u_\tau\sqrt{(T/T_w)}$. So we see that the mean velocity profile in a compressible boundary layer scales with the same length scales used in scaling incompressible flows, but the velocity scale is modified by the variation in mean temperature.

4.4 Skin Friction

Skin-friction measurements are more difficult to make and to interpret in supersonic flows (Fernholz & Finley, 1980, Smith et al. , 1992). Floating-element gauges are susceptible to inaccuracies stemming from leakage, local variations in heat transfer, flushness, and moments applied by streamwise pressure gradients. Preston-tube data can be analyzed using a variety of calibration schemes, leading to considerable uncertainty in the results. Most schemes for reducing Preston-tube data rely on boundary-layer edge conditions (for example, Hopkins & Keener, 1966), and this can introduce additional errors, particularly in perturbed flows where the edge properties are often unrelated to the flow behavior near the wall. As Finley (1994) points out, calibration equations which involve an empirical "intermediate temperature", and/or freestream properties are functionally incorrect, since the Preston tube pressure should depend on wall variables only. He adds that as long as they are used in flows with small or negligible normal pressure gradients, this is not crucial. However, in many compressible flows there are significant normal pressure gradients and the calibration equations should be expressed in terms of wall variables. The only calibration which does so is that by Bradshaw & Unsworth (1974). Here, for adiabatic flows and for $u_\tau d/\nu_w > 100$:

$$\frac{\Delta p}{\tau_w} = 96 + 60 \log_{10}\left(\frac{u_\tau d}{50\nu_w}\right) + 23.7 \log_{10}^2\left(\frac{u_\tau d}{50\nu_w}\right)$$

$$- 10^4 M_\tau^2 \left[\left(\frac{u_\tau d}{\nu_w}\right)^{0.26} - 2.0\right] \qquad (71)$$

which reduces to a very good fit to the calibration data of Patel (1965) for incompressible flows as $M_\tau \to 0$.

Allen (1977) suggested that the constants used by Bradshaw & Unsworth were incorrect and proposed that the last term should read:

$$-10^4 M_\tau^2 \left[\left(\frac{u_\tau d}{\nu_w}\right)^{0.3} - 2.38\right] .$$
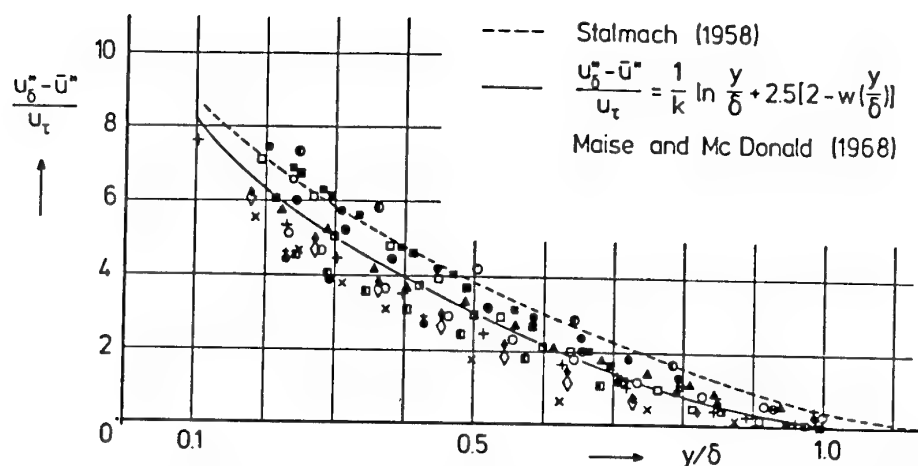
Figure 55: Mean velocity profiles in outer-layer scaling for zero pressure gradient compressible turbulent boundary layers . From Fernholz & Finley (1980). The key to the data is given in Fernholz (1969).

However, Finley (1994) concluded that these corrections were based on unreliable balance data, and on the basis of a detailed analysis of the available data recommended that the original constants as given in Equation 71 are more accurate than those given by Allen (1977). It should also be noted that Finley introduced a reduction procedure originally due to Gaudet (1993, private communication), in wall variables, which depends on the van Driest (1951) transformation, and not directly on balance measurements.

The Clauser method (Clauser, 1954) can also be used as long as a logarithmic region can be found, but the results obviously depend on the validity of the particular compressibility transformation used. In perturbed-flows, the compressibility transformation of Carvin et al. (1988) should be more reliable than that of van Driest because it does not have the additional requirement of a self-preserving boundary layer. In practice, for a wide variety of flows, including flows with strong pressure gradients and shock wave boundary layer interactions, the differences between the Clauser-chart results obtained using the two transformations seem to be within about ±15% of the Preston-tube results (Smith et al. , 1992). The laser interferometer skin friction meter (LISF) is a promising new technique that does not require assumptions about the character of the wall region to deduce the wall shear stress, and can thus provide direct measurement of the skin friction in a perturbed flow. Kim et al. (1991) compared LISF results to Preston tube measurements in a three-dimensional shock-wave boundary-layer interaction and found encouraging agreement.

As a result of the increased viscous dissipation in compressible boundary layers is a decrease in the skin-friction coefficient with increasing Mach number (at fixed Re). The low density of the fluid near the wall indirectly results in a decrease in the slope of the non-dimensionalized velocity profile relative to that for an equivalent-Reynolds-number incompressible boundary layer. Since density has a stronger dependence on temperature than viscosity does, the skin-friction coefficient decreases with Mach number (although the dimensional wall shear increases

due to the increase in velocity). The general trends for hot and cold walls can be predicted from these considerations, with heated walls leading to lower C_f (Hinze, 1975, Fernholz, 1971, Fernholz & Finley, 1980).

While the Howarth-Dorodnitsyn compressibility transformation provides an analytical solution for C_f in laminar boundary layers ($Pr = 1$), no such solution exists in turbulent compressible boundary layers. Instead, a variety of experimental correlations, transformations, and finite-difference solutions exist. Bradshaw (1977) critically reviewed the most widely-used skin-friction formulas and found that a variation of "van Driest II" (van Driest, 1956) exhibited the best agreement with reliable zero-pressure-gradient data, with less than 10% error for $0.2 \leq T_w/T_{aw} \leq 1$. Of course, the success of van Driest II is mainly due to the fact that for air the molecular and turbulent Prandtl numbers are close to unity.

4.5 Scales for Turbulent Transport

In the analysis of the mean velocity distributions in supersonic boundary layers it was assumed that the mixing length distribution was the same as in subsonic flows. This comprises essentially a variable fluid property assumption, that is, the mechanisms governing turbulent transport are the same as at low speed, and the variations of density are taken in account by scaling the local stress. This hypothesis is quite successful, since, as we have seen, experimental evidence supports that the log law is observed on the van Driest transformed velocity, with the same constant as in at low speed. Therefore it may be expected that the typical size of the energetic eddies producing turbulent transport obeys the same laws as in subsonic flows. Note that this scale is built on the shear stress $-\overline{uv}$, and that it is a scale related to turbulent diffusion.

The following discussion has been adapted from the recent work by Dussauge & Smits (1995). Consider the characteristic time scales of the turbulent and mean motions. The turbulent time scale t_t can be expressed as a

function of mean time scale, flow parameters such as the Reynolds and Mach numbers R and M, the position y and the length scale L. That is:

$$t_t = g\left(t_m, R, M, y, L, ...\right).$$

We know that the energetic structures and the mean motion have characteristic scales of the same order. This suggests that the previous relationship can be rewritten as

$$t_t = t_m g\left(R, M, y, L, ...\right) \tag{72}$$

where the function g is of order 1. If we assume Morkovin's hypothesis, then for weak compressibility effects, for example in boundary layers at moderate Mach numbers, the relation between the scales is the same as at low speeds. Equation 72 reduces to:

$$t_t = t_m g\left(R, y, L, ...\right). \tag{73}$$

The turbulent time scale is defined as usual by k/ε. The mean time scale is chosen as $(\partial U/\partial y)^{-1}$, the turnover time of the mean motion, as in low speed flows. This choice can be justified as follows. The main role of the mean inhomogeneity is to amplify turbulence through linear mechanisms described, for example, by rapid distortion theories. In general, a fluctuation subjected to mean shear obeys an equation of the form:

$$\frac{Du'}{Dt} + u'\frac{\partial U}{\partial y} = f.$$

In this equation, f represents the pressure, non-linear and viscous terms. It appears from the linear left hand side that the amplification of u' by linear mechanisms occurs with a time constant of order of $(\partial U/\partial y)^{-1}$ (for incompressible turbulence, the role of the pressure terms in f is to reduce $u'\partial U/\partial y$, but the order of magnitude remains unchanged). The mean time scale can therefore be interpreted as a response time of fluctuations to mean homogeneity, and it must therefore be of order $(\partial U/\partial y)^{-1}$. If we evaluate f in the zone where the shear is constant, and where production and dissipation are equal:

$$-\overline{\rho u'v'} \approx -\overline{\bar{\rho} u'v'} = \rho_w u_\tau^2 .$$

Moreover, in this region, we assume that similarity of the profile is achieved by using either a viscous length scale, or an external length scale. We denote L the scale, whatever the choice. Equation 73 can then be rewritten as:

$$\frac{\bar{\rho}k}{\rho_w u_\tau^2} = g\left(\frac{y}{L}, R, ...\right) \tag{74}$$

We recognize in Equation 74 the scaling proposed by Morkovin for the similarity of the Reynolds stresses: similarity is achieved if the local velocity scale in the constant stress region is now $\sqrt{(\rho_w/\rho)}u_\tau$ instead of u_τ. We can now define a length scale in the particular case when production is balanced by dissipation. The turbulent time scale is defined as Λ/u', where u' is a characteristic scale for velocity fluctuations, for example $\sqrt{k}$. Equating this time to k/ε, and setting ε equal to production gives the relation:

$$\frac{\Lambda}{u'} = \frac{\bar{\rho}k}{\rho_w u_\tau^2 \partial U/\partial y}$$

or, according to Equation 74,

$$\Lambda = g\left(\frac{y}{L}, R, ...\right)\frac{u'}{\partial U/\partial y} . \tag{75}$$

From Equation 75, it can be deduced that the length scale is the same in subsonic and supersonic flows when the ratio $u'/(\partial U/\partial y)$ is unchanged. This implies that the scaling for density effects should be the same for u' and $\partial U/\partial y$. We know from experiment (and from Equation 74) that in supersonic layers, u' varies like $\rho^{-1/2}$. We also know that $\partial U/\partial y$ varies as $\rho^{-1/2}$ since the van Driest transformed velocity obeys the same log-law as in subsonic flows. Therefore the characteristic length scales governing turbulent transport should not change in the supersonic regime.

To conclude these scaling considerations on turbulent transport, it should be emphasized that the presence of a logarithmic region in the mean velocity profile is a necessary condition, and that we have only considered a single velocity scale and a single length scale. This was applied to turbulent stresses, which are represented by a tensor. Therefore, it is likely that the results we obtained are related mainly to a single component or to the turbulent kinetic energy, but not to all of the components. Finally, Equations 72 and 74 may give some insight into the influence of compressible turbulence on the high speed boundary layers, and indicate some possible ways to investigate departures from Morkovin's hypothesis in these flows. In Equation 72, an acoustic time scale (or a Mach number) may be introduced, while the equilibrium condition should be modified by balancing the dissipation rate by the sum of production and pressure divergence terms, and by modifying Equation 74.

4.6   Mean Turbulence Behavior

Sandborn (1974) and Fernholz & Finley (1981) both critically reviewed turbulence measurements in supersonic boundary layers. While many data sets were acquired in the period between the two reviews, their conclusions were similar and they continue to be relevant. In particular, accurate, repeatable measurements of the Reynolds-stress tensor are still needed over a wide Mach-number range. The most well-documented component is the longitudinal normal stress, which has been widely measured and properly scaled. But there have been so few systematic investigations of the effects of Reynolds number and wall heat transfer in supersonic flow that their influence on the turbulence field is not well known. The reason for the scarcity of measurements and their generally poor quality is simple: the measurement of turbulence quantities in supersonic boundary layers is exceedingly difficult, with the level of difficulty increasing with flow complexity and Mach number. But furthermore, there are significant measurement and data-reduction errors associated with every technique designed to measure fluctuating velocities in supersonic flow: thermal anemometry (see Smits & Dussauge, 1989), laser-Doppler velocimetry (Johnson,
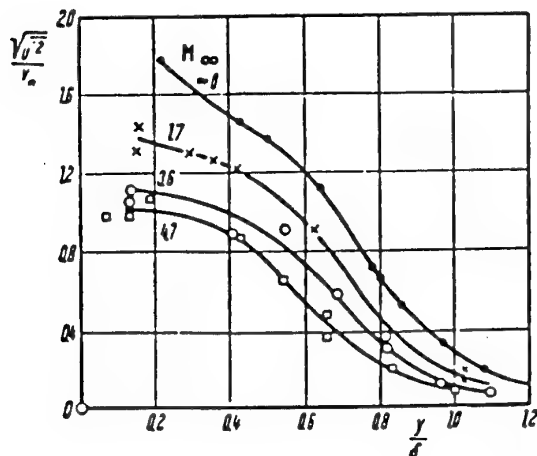
Figure 56: Distribution of turbulent velocity fluctuations in boundary layers. Measurements are from Kistler (1959) and Klebanoff (1955). Figure from Schlichting (1979).

Figure 57: Velocity fluctuation intensity in supersonic boundary layers: $*$, Dussauge & Gaviglio (1987); , $M = 1.72$; $\circ$, $M = 3.56$; $\circ$, $M = 4.67$, Kistler (1959); $\triangle$, hot wire; $\diamond$, laser, $M = 2.9$, Johnson & Rose (1975); , $M = 2.9$, Smits et al. (1989); $\blacksquare$, $M = 2.32$, Eléna & Lacharme (1988); $\square$, $M = 2.3$, Debiève (1983); , $M = 2.32$, Eléna & Gaviglio (1993); $\diamond$, $M = 3$, Yanta & Crapo (1976). Figure taken from Dussauge & Gaviglio (1987).

1989), and advanced laser-based techniques such as laser-induced fluorescence (Logan, 1987, Miles & Nosenchuck, 1989).

Despite these uncertainties in the measurements, certain trends can be distinguished. For example, when the longitudinal velocity fluctuations are normalized by the shear velocity, $\overline{u'^2}/u_\tau^2$, there is a clear decrease in fluctuation level with increasing Mach number (see Kistler, 1959, Fernholz & Finley, 1981). This is shown in figure 56.

However, when the streamwise normal stress is normalized by the wall shear stress, the data exhibit some degree of similarity (as suggested in Section 4.5), particularly in the outer layer (see figure 57). This formulation of the velocity fluctuations indicates the success of the scaling suggested by Morkovin (1962) to account for the mean-density variation, and provides some support for the discussion given in Section 4.5. In fairness, it should be mentioned that Fernholz & Finley (1981), in considering an earlier set of data, concluded that the streamwise Reynolds stress did not show a similar behavior in the outer region, no matter which velocity scale was used in the non-dimensionalization. It appears that the later data shown in figure 57 displays a more regular behavior. The streamwise normal stress distribution for supersonic flows is in fair agreement with the incompressible results of Klebanoff (1955), except near the wall where reduced accuracy affects the supersonic measurements. Morkovin's scaling appears to be appropriate to at least Mach 5. Measurements by Owen et al. (1975) at $M_e = 6.7$ and Laderman & Demetriades (1974) at $M_e = 9.4$ exhibit damped turbulent fluctuations, particularly near the wall. Since both of the hypersonic data sets are for cold-wall conditions, this may simply indicate the stabilizing effect of cooling.

Cross-wire measurements of both streamwise and wall-normal components of velocity have suggested additional apparent differences between Mach 3 and incompressible boundary-layer structure (Smits et al. , 1989). Measurements of $\overline{v'^2}$ and $\overline{w'^2}$ are less common than those of $\overline{u'^2}$, the data exhibit more scatter, and the conclusions are
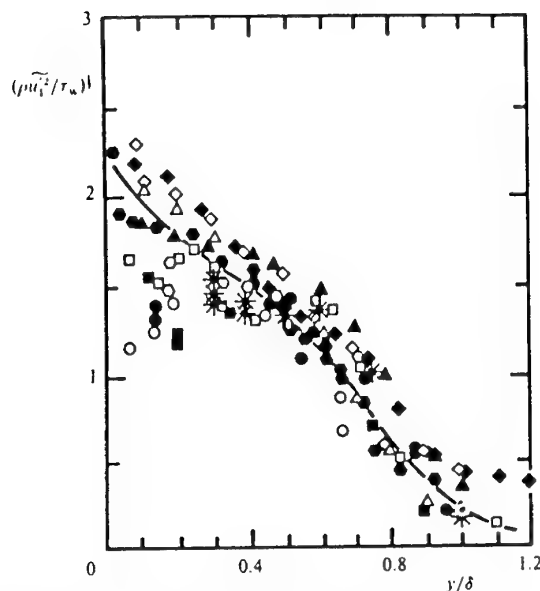
therefore less certain. In contrast to the streamwise turbulence intensity, both distributions appear to increase slightly with increasing Mach number (Fernholz & Finley, 1981). In this case, Morkovin's scaling does not collapse the data, and $\overline{\rho v'^2}/\tau_w$ and $\overline{\rho w'^2}/\tau_w$ show no real trend toward similarity. Konrad (1993) using hot-wire anemometry found that $\overline{w'^2}$ and $\overline{v'^2}$ in a Mach 2.9 boundary layer were approximately equal throughout the layer (see figure 58). In contrast, the measurements by Eléna & Lacharme (1988) in a Mach 2.3 boundary layer using laser Doppler anemometry indicate that the behavior of $\overline{v'^2}/u_\tau$ is almost identical to that found in subsonic flows (see figure 59). The behavior of the anisotropy parameter is therefore not clear: the measurements by Eléna & Lacharme (1988) indicate that $\sqrt{\overline{v'^2}}/\sqrt{\overline{u'^2}}$ is almost the same as in subsonic flows, whereas the hot-wire measurements by Fernando & Smits (1990) and Konrad (1993) indicate that this ratio increases with Mach number (Reynolds number effects were shown to be negligibly small in Section 3.2.3). The limited nature of the data precludes any conclusions regarding the effects of compressibility on this structure parameter.

Sandborn (1974) reviewed direct measurements and indirect evaluations of the zero-pressure-gradient Reynolds shear stress, $-\overline{\rho u'v'}$ (a later, more comprehensive study was provided by Fernholz & Finley, 1981). Sandborn constructed a 'best fit' of normalized shear stress profiles (τ/τ_w) from integrated mean-flow data taken by a variety of researchers over a wide Mach-number range, $2.5 < M_\infty < 7.2$ (extended to Mach 10 by Watson (1978)

Figure 59: Turbulence distributions in a Mach 2.3 boundary layer, measured using LDV ($Re_\theta = 5,650$). Figure from Eléna & Lacharme (1988).
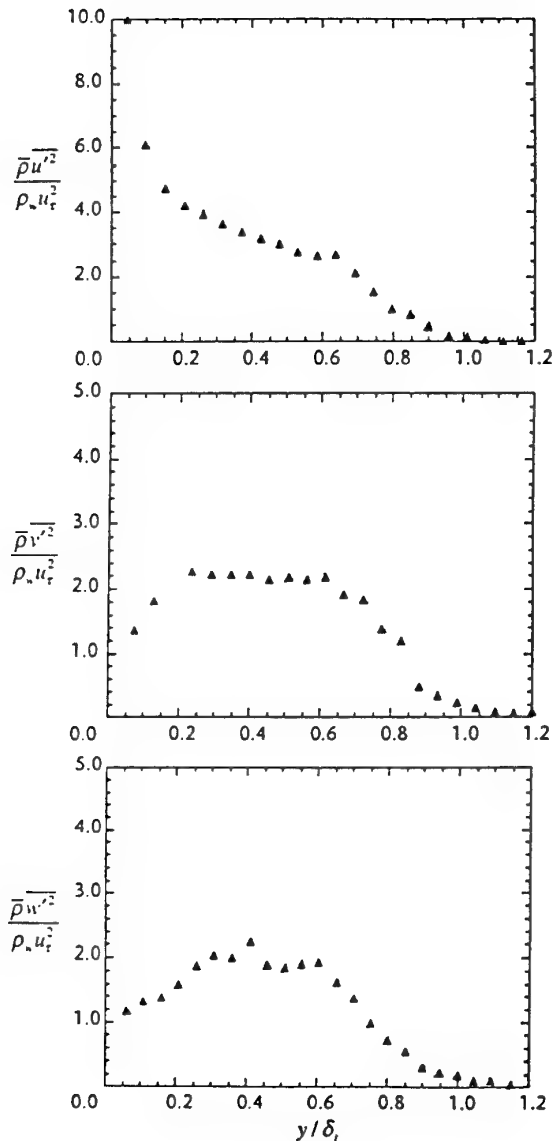

Figure 58: Turbulence distributions in a Mach 2.9 boundary layer, measured using hot-wire probes ($Re_\theta = 65,000$). Adapted from Konrad (1993).
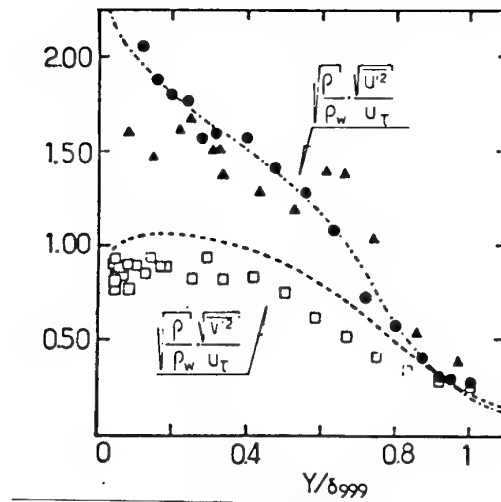
for adiabatic and cold walls). The data indicate a near-universal shear-stress profile that agrees well with the incompressible measurements of Klebanoff (1955) (see figure 60). As Sandborn pointed out, the universality of τ/τ_w over such a wide Mach-number range is not surprising in light of the fixed constraints on the values of the shear stress at the wall and in the freestream. Even so, the only Reynolds shear stress measurements to agree with the 'best fit' in 1974, and then only in the outer layer, were the LDV data of Rose & Johnson (1975). Subsequent Reynolds shear stress measurements by Mikulla & Horstman (1975), Kussoy et al. (1978), Robinson (1983), Smits & Muck (1984), and Donovan et al. (1994) (all using hot wires except Robinson) have exhibited modest agreement with Sandborn's best fit and the incompressible distribution. The agreement is limited to the outer layer, with great scatter in the inner layer and most profiles not tending toward $\tau/\tau_w = 1$ near the wall. The data in the inner layer do not scale with yu_τ/ν_w, almost certainly because of the difficulties with the measurements.

The behavior of the shear correlation coefficient R_{uv} is affected strongly by the level of $\overline{v'^2}$. In the measurements by, for example, Fernando & Smits (1990) at Mach 2.9, R_{uv} decreases significantly with distance from the wall, from a value of about 0.45 near the wall to about 0.2 near the boundary layer edge (see figure 61). This is in contrast to most subsonic flows where the correlation coefficient is nearly constant at a value of about 0.45 in the region between 0.1δ and 0.8δ. As can be seen in the figure, the data by Eléna & Lacharme (1988) at Mach 2.3 follow the subsonic distribution closely, and it is difficult to say what the effect of compressibility is on the level of R_{uv} without further experiments. However, the subsonic data showed that the maximum value of $\overline{v'^2}$ increases significantly with Reynolds number (see figure 32), and considering that there is about a factor of 15 difference in the Reynolds numbers between the results of Fernando & Smits (1990) and Eléna & Lacharme (1988), the differences seen in the distribution of R_{uv} may well indicate the effects of Reynolds number. Joint probability density dis-
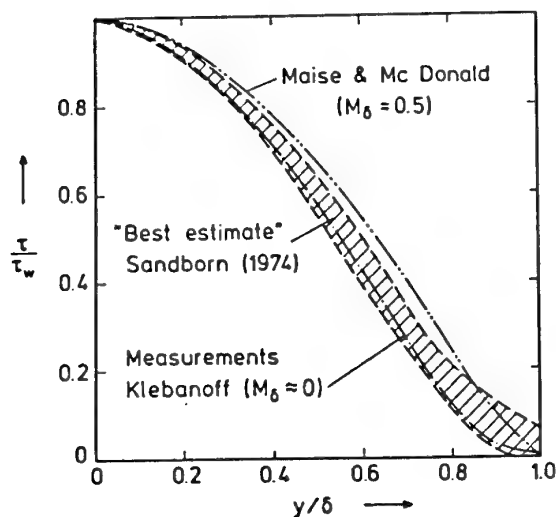
Figure 60: Distribution of turbulence shear stress in boundary layers at supersonic speed. Figure from Sandborn (1974).

Figure 62: Test of the Strong Reynolds Analogy in a supersonic boundary layer ($M_e = 2.32$, $Re_\theta = 5,650$). Data from Debiève (1983).
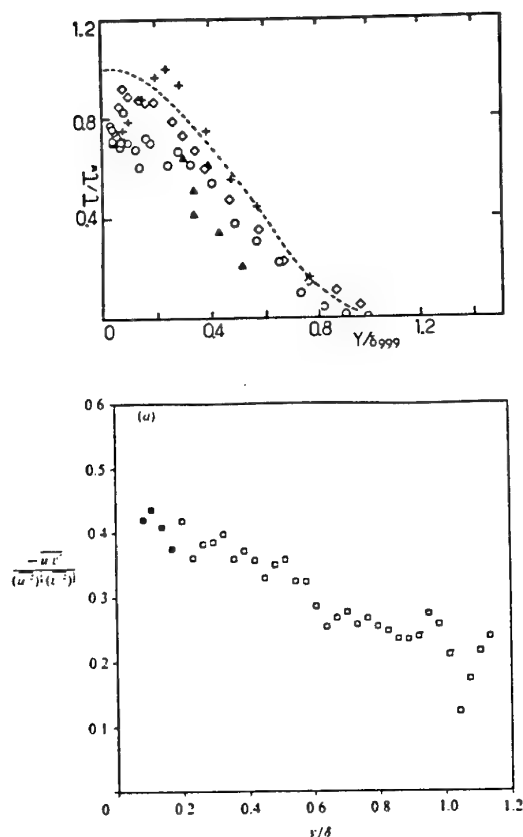

Figure 61: Distribution of R_{uv} in subsonic and supersonic boundary layer: (a) Data from Eléna & Lacharme (1988): the dotted line corresponds to the subsonic data of Klebanoff (1955). (b) Data from Fernando & Smits (1990): the filled-in symbols are subject to errors due to transonic effects.
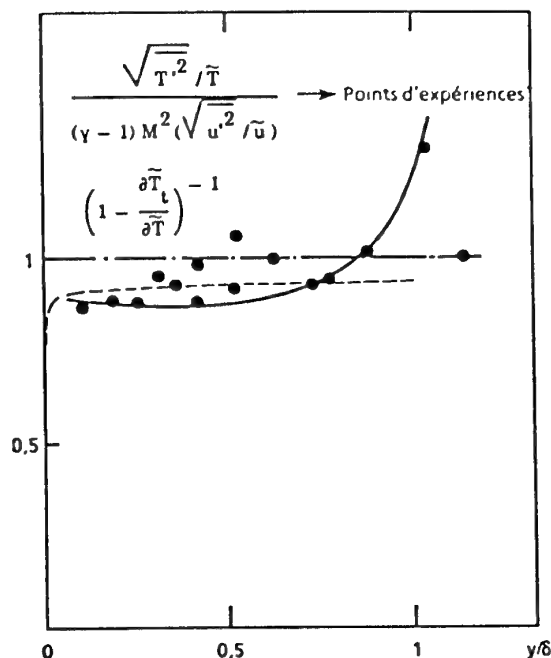
tributions of the two velocity (or mass-flux) components may also be somewhat different between subsonic and supersonic flows, with the supersonic case favoring vertical fluctuations in the mid-layer slightly more than the subsonic case (for further details see Fernando & Smits, 1990), but again the evidence is not conclusive.

In Section 2.3 the Strong Reynolds Analogy was discussed. Some measurements designed to test the validity of this analogy in adiabatic flows are presented in figures 62 and 63. The results indicate that the SRA is closely followed in supersonic boundary layers, and the correlation coefficient R_{uT} is close to the value of 0.8 throughout the layer (note that for $y/\delta > 0.8$, the assumptions used in the data reduction are probably invalid). This value is considerably higher than that found in slightly heated subsonic flows, as seen in figure 63, and the reason is not entirely clear. However, the SRA can be a very useful tool in describing the behavior of supersonic turbulent boundary layers, especially in formulating turbulence models. The SRA can also be extended to non-adiabatic flows, as discussed by Gaviglio (1987).

At hypersonic Mach numbers, it is possible that the triple correlation $\overline{\rho'u'v'}$ may become comparable to the 'incompressible' Reynolds shear stress, $\overline{\rho u'v'}$, since $\rho'/\overline{\rho} \sim M^2 u'/U$. Owen (1990) evaluated the various contributions to the 'compressible' Reynolds shear stress at Mach 6 through simultaneous use of two-component LDV and a normal hot wire. His results indicate that $\overline{\rho'u'v'}$ is negligible compared to $\overline{\rho u'v'}$. Even though density fluctuations increase with the square of the Mach number, it should be remembered that the main contribution to the Reynolds shear stress occurs in the region where the local Mach number is small compared to the freestream value, so this 'hypersonic effect' should only be important at very high freestream Mach number.
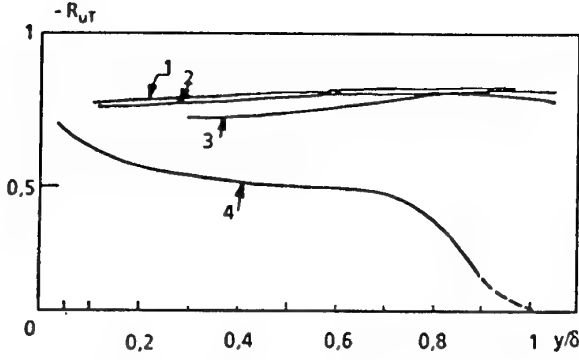
Figure 63: Distribution of R_{uT} in boundary layers. Curve 1: $M_e = 2.32$, $Re_\theta = 5,650$, from Debiève (1983). Curves 2 and 3: $M_e = 1.73$, $Re_\theta = 5,700$, from Dussauge (1981). Curve 4: $M_e \ll 1$, $Re_\theta = 5,000$, from Fulachier (1972). Figure from Eléna & Gaviglio (1993).

The stagnation-temperature fluctuation must be known to evaluate the turbulent heat-flux correlation, $-c_p \overline{\rho} \overline{v'T'}$. Kistler (1959) observed that $T'_{0_{rms}}/\overline{T_0}$ increased with Mach number, with maxima of 0.02 at $M_\infty = 1.72$ and 0.048 at $M_\infty = 4.67$. If Kistler's data is alternately non-dimensionalized by either T_w (Fernholz & Finley, 1981) or $T_r - T_e$ (Sandborn, 1974), the Mach-number dependence appears to be eliminated, but similarity of the stagnation-temperature distributions is not achieved. Similar conclusions are reached from measurements by Morkovin & Phinney (1958) and Horstman & Owen (1972). The maximum level of stagnation-temperature fluctuations is about 6% (for $M < 7$). Further analysis of these data shows that $T'_{0_{rms}}$ scales according to either $T_{0e} - T_w$ or $T_{0e} - T_r$. The fluctuations in total temperature appear to be produced by the difference in stagnation temperature between the wall and the freestream, and not, for example, by the unsteadiness in pressure, through the term $\partial p/\partial t$ in the total enthalpy equation. In these experiments, the maximum of $T_{0_{rms}}/(T_{0e} - T_r)$ is about 0.5, regardless of the Mach number, a rather satisfactory result since it shows that the total temperature fluctuations are of the order of (but less than) the total temperature difference across the boundary layer. Finally, $T'_{0_{rms}}$ is less than that of u'_{rms} and T'_{rms}, but not low enough to satisfy the strict Strong Reynolds Analogy (see Gaviglio, 1987). In fact, the SRA can be used to estimate that $T'_{0_{rms}}$ is about 60% of T'_{rms} at Mach 3 (Smits & Dussauge, 1989).

4.7 Spectral Scaling

We saw in Section 3.2.2 that two overlap regions in wavenumber space can be found by considering the scaling for the spectra of subsonic boundary layers in the logarithmic region, one where the spectra has a power law with exponent -1 and another with an exponent -5/3 (Perry et al. , 1986). Three spectral zones were considered. In the first zone the length scale was the layer thickness δ and the turbulent velocity scale was u_τ. In the second zone, the turbulent velocity scale was the same, but the

length scale was the distance from the wall y. And in the third zone, the scales were given by the Kolmogorov length and velocity scales η and v (see equations 39 and 40). Matching Zones 1 and 2 leads to a spectrum which varies as k_1^{-1}, and matching Zones 2 and 3 gives a $k_1^{-5/3}$ variation.

We will now extend these considerations to high speed boundary layers (for further details see Dussauge & Smits, 1995). The scales for zones 1 and 2 were discussed in Section 4.5, where it was shown that the local scale for $\overline{u'^2}$ is $(\rho_w u_\tau^2)/\bar{\rho}$. Again, the -1 power law is obtained as the result of the overlap between zones 1 and 2.

For the viscous zone, however, the Kolmogorov scales will change. We can define new length and velocity scales by considering the dynamic viscosity μ, the rate of dissipation per unit volume φ (and not per unit mass ε) and the density ρ. Dimensional analysis gives:

$$\eta' = \rho^{-1/2}\left(\frac{\mu^3}{\varphi}\right)^{1/4}$$

and

$$v' = \rho^{-1/2}(\mu\varphi)^{1/4} \ .$$

Equations 42 and 43 now have the form:

$$\frac{\Phi_{11}(k_1 y)}{\rho_w u_\tau^2/\rho} = g_2(k_1 y) = \frac{\Phi_{11}(k_1)}{y\rho_w u_\tau^2/\rho} \tag{76}$$

$$\frac{\Phi_{11}(k_1\eta')}{v'^2} = g_3(k_1\eta') = \frac{\Phi_{11}(k_1)}{\eta'v'^2}. \tag{77}$$

So the Kolmogorov scales are unchanged as long as $\bar{\nu} \approx \bar{\mu}/\bar{\rho}$ and $\bar{\varepsilon} \approx \bar{\varphi}/\bar{\rho}$. The analysis for the overlap region is the same as for low speed boundary layers: the Kolmogorov scales are determined in the equilibrium zone where production and dissipation are assumed to balance, where the turbulent shear stress is constant, and where the van Driest velocity is logarithmic. It is again found that the spectrum of $\overline{u'^2}$ should have a range in $k_1^{-5/3}$. Since the analysis can be performed using either the incompressible or compressible variables, the changes in the scales due to variations in the mean density are absorbed in the modified dissipation rate because of the density scaling of the velocity gradient. The differences between the incompressible and the compressible definitions of the Kolmogorov scales are mainly related to the link between velocity and density in the part of the layer where dissipation is maximum, and therefore it should scale with the friction Mach number $M_\tau = u_\tau/a_w$.

It may then be inferred that for weak compressibility effects, the spectra have two wave number ranges with power law variations in k_1^{-1} and in $k_1^{-5/3}$, as at low speeds. This analysis does not indicate where these wave number ranges are placed in the spectrum, that is, if high speeds produce larger or smaller energetic eddies, or induce a change in the orientation of these eddies. It appears also that the existence of a k_1^{-1} range seems to be a rather robust feature, since the only conditions are the existence of two domains where the wave numbers scale respectively with δ and with y. The $k_1^{-5/3}$ law is expected to have less generality, since the existence of a constant shear stress

zone with logarithmic velocity profiles is postulated, and the balance between production and dissipation is also required. As a last remark, it may be seen that the incompressible and the compressible definitions of the Kolmogorov scales are equivalent for moderate Mach numbers. However, in the buffer zone they may differ significantly from each other if the friction Mach number M_τ is not much less than 1. In this case, however it may be expected that the hypotheses required for the derivation of the power laws are no longer valid. In practice, friction Mach numbers are usually small (≤ 0.1), except at hypersonic Mach numbers and very high Reynolds numbers, or extremely cold walls.

4.8   Spectral Data

Experimentally, the integral scales are deduced mainly from one point hot-wire measurements, so that the spatial scales are deduced using Taylor's hypothesis. Even when measurements of two-point correlations are available ((see, for example, Spina & Smits, 1987, Robinson, 1986), it is often difficult to determine integral scales from the data. The types of data which are available also depend on the measurement technique. For instance, when constant current anemometers (CCA) are used, time histories are generally not measured. Spectral data for u' and T' can be obtained directly by processing the signal with the fluctuation diagram technique to separate the contributions of u' and T' (see Fulachier, 1972, Bestion, 1982, Debiève, 1982, Debiève, 1983, Bestion *et al.*, 1983, Audiffren, 1993). Bestion (1982), and Audiffren (1993) showed that for an adiabatic flat-plate boundary layer at a Mach numbers of 2.3 the shapes of the spectra of $(\rho u)'$ and u' are practically the same, but differ considerably from the spectrum of total temperature T'_0. Therefore, when anemometers are operated with a single overheat, a sufficiently high value of the resistance should be chosen to minimize the contribution of T'_0 and to obtain a signal practically proportional to $(\rho u)'$. When constant temperature hot-wire anemometers (CTA) are used at a high overheat ratio, the measured signal is practically proportional to $(\rho u)'$, which in turn gives spectral information on u'. Such data can be inaccurate at low wave numbers. The spectral measurements of velocity and temperature performed with a CCA in adiabatic boundary layers by Morkovin (1962), Bestion (1982), Audiffren (1993) show that the ratio $(u'/U)/(T'/T)$ at low frequencies is not a constant, and that the spectral correlation coefficient $R_{uT}(f)$ increases to unity at zero frequency. This may be the cause for the differences in the shapes of the spectra for u' and $(\rho u)'$ at low frequencies, depending on the Mach number. For higher frequencies, the ratio $(u'/U)/(T'/T)$ and the correlation coefficient are approximately constant, and the spectra are nearly proportional to each other.

Now, the classical integral scale can be determined from one-point measurements by integrating the autocorrelation coefficient of u'. It is then necessary to define the domain of integration, since the autocorrelation can become negative. When using hot-wire anemometry in supersonic flows, this question can be complicated by possible "strain-gauge" effects. These effects can cause peaks in the spectrum, which may be acceptable for measurements of the overall stress or the turbulence energy, but which can cause spurious oscillations in the autocorrelations, and make the estimates of the integral scale inaccurate.

To avoid this effect, the integral scale can be determined by finding the value of the energy spectrum at zero frequency. However, since the signal is usually filtered with a high-pass filter, it has zero mean and its spectrum has a zero value at zero frequency. The integral scale must then be found by extrapolating the spectrum to zero frequency. In practice, the value at a frequency slightly larger than the limit of the high-pass filter is taken as the best estimate. Moreover, it may be difficult to measure the low frequencies, because they can be affected by noise of the power supply, and by the peculiarities of each wind tunnel such as acoustic resonances. For CTA measurements, it has also been shown that, the spectra of u' and of $(\rho u)'$ may be different at very low frequencies.

For these reasons, an additional scale has also been used. Since we expect that the spectra have a region of k_1^{-1} dependence in the logarithmic zone, $E(k_1)$ varies as k_1^{-1}, and $k_1 E(k_1)$ is constant or presents a maximum. Here we have chosen the wave number for which this maximum occurs as the (inverse of the) characteristic space scale.

This probably has a clearer physical meaning than the integral scale, since for the incompressible part of the fluctuating motion it characterizes the eddies extracting energy from the mean field. As indicated earlier, experimentalists usually measure frequency spectra, so that a characteristic frequency is measured, and then a length scale is deduced using Taylor's hypothesis. There is usually a considerable amount of scatter because the location of the maximum is not always well defined. For the data considered here, a maximum was generally found in the external layer, but in the logarithmic zone of the subsonic boundary layer the spectra were frequently "double-humped" and the maximum was difficult to determine. Such shapes were also mentioned by Perry *et al.* (1986) who interpreted them to mean that Taylor's hypothesis failed for low frequencies. Uddin (1994) noted that the bump at low wavenumber became more prominent at higher Reynolds numbers (see also Smith, 1994). These double-humped profiles led to some difficulty in determining the length scale, and it was necessary to discard some points in the log-law region of the subsonic boundary layer data. However, the typical situation was that the higher frequency bump corresponds to scales comparable to the scales of the outer layer, and the other maximum occurs at frequencies an order of magnitude lower, corresponding to length scales five to ten times larger than the outer layer scales.

For supersonic boundary layers, there is another source of uncertainty. Generally, the point where the slope is -1 occurs at frequencies beyond the natural cut-off of the wire; this means that it occurs in a range where the shape of the spectrum depends on the system used to extend the system frequency response beyond the wire thermal lag (a feed-back loop is used for the CTA, and a compensation circuit is used for the CCA). In such conditions, it can be misleading to rely on one series of experiments. The data from supersonic flows, however, were obtained in different laboratories using different techniques (CTA and CCA).
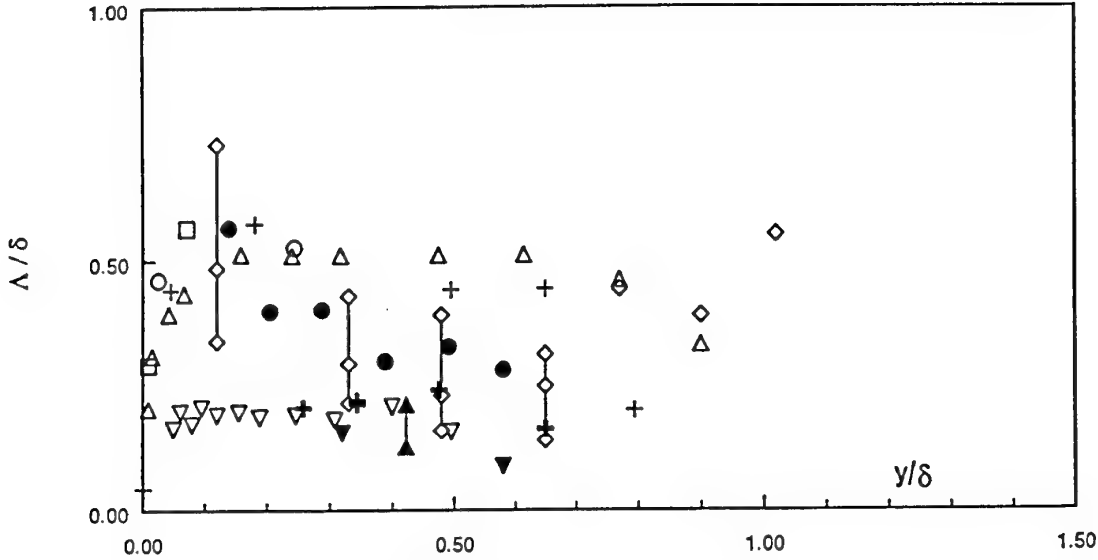
Figure 64: Integral scales in turbulent boundary layers. *Subsonic data*: +, Klebanoff (1955); △, Fulachier (1972); ○ $R_{\delta2} = 20,900$, Fernholz *et al.* (1995); □ $R_{\delta2} = 57,720$, Fernholz *et al.* (1995). *Supersonic data*: +, Debiève (1983); △, Bestion *et al.* (1983); ○, Spina & Smits (1987); ▽, Audiffren (1993); ◇ $R_{\delta2} = 633$, McGinley *et al.* (1994); ▽ $R_{\delta2} = 1,115$, McGinley *et al.* (1994). Figure from Dussauge & Smits (1995).

Authors	M	R_θ - $R_{\delta2}$	Measurement method	Remarks
Klebanoff (1954)	0.044	7000	CCA	
Fulachier (1972)	0.035	4750	CCA	
Fernholz et al 1994	0.06 and 0.17	20000 and 60000	CTA	
Spina & Smits (1986)	2.89	80 000- 40 000	CTA	Scales estimated from spectra of (ρu)'
Bestion 1982 Debieve 1983	2.3	4200 - 2900	CCA	Spectra of u' (fluctuation diagram technique)
Bestion et al 1983	1.8	5000- 3500	CCA	Spectra of u' (fluctuation diagram technique)
Audiffren 1993 Audiffren, Debieve 1995	2.2	6300- 3800	CCA	Spectra of u' (fluctuation diagram technique)
McGinley et al 1994	11	12 400- 1115 6500-633	CTA	Spectra of (ρu)'

Table 4: Sources for spectral data. Table from Dussauge & Smits (1995).

In the CCA data, two different generations of anemometers were used, where the compensation of the wire was performed in completely different ways. With such sets of independent measurements, it is believed that firm conclusions can be drawn from the results.

The characteristics of the boundary layers considered in the analysis of spectra are given in Table 4. As noted in the Introduction, Re_θ and $R_{\delta2}$ are Reynolds numbers based on momentum thickness. Re_θ is defined in the usual way ($R_\theta = \rho_e U_e \theta / \mu_e$), whereas $R_{\delta2} = \rho_e U_e \theta / \mu_w$.

The results on the integral scale Λ are given in figure 64. The outer-layer scaling was used, since most of the data

were obtained outside the inner layer. Plotting the data in inner-layer variables does not alter the conclusions. The data points from Smits & Dussauge (1989) were deduced from autocorrelations in a way which may underestimate the integral scale, due to a lack of experimental points for large time delays. The results in figure 64 were obtained by defining the boundary-layer thickness from the profiles of total pressure. This was recommended by Fernholz & Finley (1980) since the usual definition based on the velocity is probably not appropriate at high Mach numbers because variations of velocity near the edge of the layer are weak whereas the temperature or Mach number still vary significantly. Choosing a boundary-layer thickness based on $0.99U_e$ would make some difference in the magnitude of Λ/δ at Mach 3: in this experiment, the integral scale would be a little closer to its subsonic value. It would also significantly increase Λ/δ for the hypersonic experiment by McGinley *et al.* (1994), but in this case, the mean profiles indicate that the traditional choice based on $0.99U_e$ would be rather unphysical. In any case, a first result appears very clearly: the subsonic data indicate that in the external layer, Λ is about 0.5δ in subsonic flows, but is only about half that value in supersonic layers. The hypersonic data of McGinley *et al.* (1994) indicate a very low value, about 0.2δ, for $R_{\delta2} = 1,115$, but larger values at the lower Reynolds number. In this case, the spectra at low frequency reveal peaks and bumps which precludes an accurate estimate of the integral scale. The uncertainty on Λ has been evaluated and is indicated in figure 64 by error bars. In fact, the lower limit of the error bar overlaps the other high speed data. This could be due to the remnants of transition, as speculated formerly. In the data by Spina & Smits, the point at at $y/\delta = 0.1$ has an integral scale nearly equal to the subsonic value. This is due to the significant slope in the spectrum, observed at low frequency, where the spectra of u' and $(\rho u)'$ are
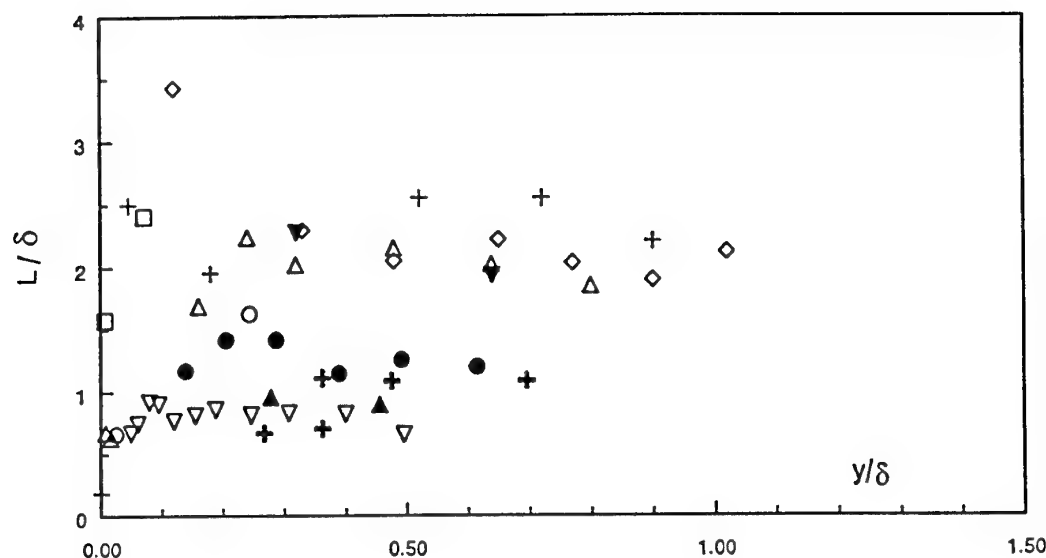
Figure 65: Production scales in turbulent boundary layers. Symbols as in figure 64. Figure from Dussauge & Smits (1995).

perhaps not proportional, as discussed above. In spite of this trend, the integral scales at Mach 2.9 in the middle of the layer are significantly below the subsonic results. Note that Demetriades & Martindale (1983) in a boundary layer on a flat plate at Mach 3 report measuring an integral scale of 0.28δ, also considerably smaller than that found in subsonic flows. Within the experimental accuracy the results are independent of Reynolds number.

The production scales L are given in figure 65. The Reynolds numbers in the subsonic and supersonic cases cover comparable ranges, except perhaps for the hypersonic data. It is clear that the production range is shifted to higher frequencies in supersonic flows. It should be emphasized that the limited spatial resolution of the wires probably precludes any accurate determination of the $-5/3$ law in the supersonic data, and it tends to shift the maximum of $fE(f)$ to lower frequencies, and therefore if such systematic errors are significant the values measured in high-speed flows are probably overestimated, reinforcing the notion that the scales are reduced with increasing Mach number.

It appears that the production scale L follows the same trends as Λ, and $L \approx 2\Lambda$. That is, L is about 2δ for low speed boundary layers, and about δ in high speed boundary layers. Note that the measurements of Morkovin & Phinney, quoted in Morkovin (1962) and not shown here, suggested the same trend for the production scales. Again, plotting these data in inner layer variables does not change the differences between the subsonic and supersonic data. The only discrepancy is found in the Mach 11 boundary layer, but several reasons can be found for this departure. First, the boundary layer is probably not fully turbulent, at least at the lower Reynolds number. Second, it is not clear that the velocity and mass flux spectra are proportional to each other at this Mach number. Third, the conclusions drawn from the power law analysis are probably not valid if strong compressibility

effects are present. Fourth, the change in the shape of the spectra may indicate a modification of the turbulence structure. In hypersonic boundary layers, most of the mass flux occurs near the external edge of the layer, and the mean mass flux profiles have an inflexion point. This suggests that the external layer can behave more like a mixing layer than like a classical boundary layer. Such free shear flows are known for containing turbulent structure of large spatial extent, with production scales several layer thicknesses in size. This would be consistent with the surprisingly high level of energy observed at low frequencies in the present Mach 11 experiments.

So it seems that the apparent size of the energetic eddies in the longitudinal direction, deduced from u' or $(\rho u)'$ measurements in zero pressure gradient boundary layers, decreases with increasing Mach number, whatever the experimental method. This trend can also be illustrated by using another representation. If we assume that the friction Mach number can be used to characterize compressibility in turbulent boundary layers is the friction Mach number M_τ. Since $M_\tau^2 = C_f M_e^2/2$, this parameter depends on Mach and Reynolds number. The average value of L/δ in the outer layer is shown as a function of M_τ in figure 66. The results obtained for $M_e = 2$ by Bestion, Debiève, Dussauge and Audiffren have practically the same values of M_τ and L/δ, and the results obtained by Smits et al. , although at $M_e = 2.89$, have a comparable value of M_τ. All these results agree on the average value of L/δ in supersonic flows. The hypersonic results by McGinley et al. have a value of M_τ only a little larger than 0.1, but they indicate a further decrease in the production scale.

This change in typical frequencies or time scales can be attributed either to variations in the convection velocity or variations in the spatial scales. Measurements of convection velocity by Spina & Smits (1987) in a high Reynolds number boundary layer at Mach 2.9 showed that
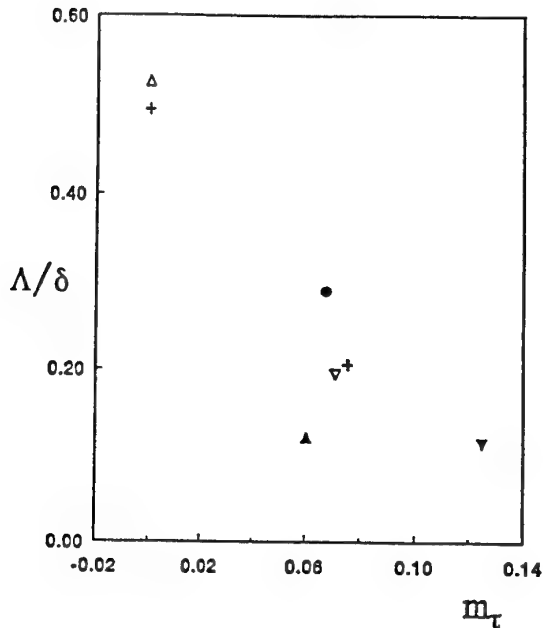
Figure 66: Evolution of the integral scale as a function of the friction Mach number. Symbols as in figure 65. Figure from Dussauge & Smits (1995).

this quantity is not very sensitive to compressibility. This implies that smaller space scales are found in supersonic flows. In contrast, the transverse scales related to turbulent diffusion remain unchanged, while the longitudinal scales determined from u' decrease. Now Spina & Smits (1987) showed that the direction of the maximum space-time correlation in their boundary layer at Mach 2.9 is steeper than at low speeds (see figures 46 and 67). If the boundary layer is thought of as a forest of hairpin vortices, it can be imagined that the cross-section of the vortices is unchanged, but their inclination is changed. In fact, Uddin (1994) suggested that at high Reynolds numbers, the cross-section of the vortices reduces. This purely geometric explanation is not sufficient to explain all the evolution observed seen in figure 66 since it would not be consistent either with the rather high values of v' measured in the same boundary layer.

It is expected that the observed modifications in the flow structure and scales are due to compressibility. Therefore, a possible interpretation can be found in the changes in the potential field induced in the external flow by the boundary layer, and in the generation of acoustic noise by supersonic boundary layers. Can they create smaller scales, and modify the orientation of the lines of maximum correlations? The variation of the angle has been interpreted in the previous paragraph as a change in the direction of vortical structures. In fact, the two-point measurements by Spina & Smits did not use conditional statistics, and therefore did not discriminate between the vortical and potential contributions in the intermittent zone. In supersonic flows, the induced pressure field can depend on local condition (the pressure perturbation induced by a large scale structure, for instance), but also by the noise radiated by Mach waves (see for example,

Laufer, 1961). These waves can have low levels of $(\rho u)'$, but they are generally more conservative than ordinary turbulence, and could modify the space-time correlations for large separation distances. The formation of these Mach waves necessitates the velocity difference between the sources and the external flow to be supersonic. In a boundary-layer, this condition is always fulfilled, but at moderate supersonic Mach numbers the part of the layer able to radiate Mach waves is very thin and generally confined to the viscous sublayer or the logarithmic zone. In this case, the behaviour will be Reynolds and Mach number dependent. The orientation of the Mach waves will depend on this Mach number difference. For example, transonic perturbations would be very steep, and would contribute to make the maximum space-time correlation locus more vertical. Another element, as noted by Laufer (1961), is an increase of the radiated field near Mach 3, which could be interpreted as follows. If the convection velocity of the large eddies in the external layer is typically $0.8U_e$, as at low speeds, the velocity difference with respect to the external flow is $0.2U_e$. Now, it may be expected that these large eddies will start forming eddy shocklets when this relative Mach number is larger than, say, 0.6. This corresponds to an external Mach number of 3, and this criterion would be independent of the Reynolds number since the convection velocity of the large structures appears to be independent of Reynolds number. The measurements taken at a Mach number of 2.9 would then be at the onset of a new regime, and represent the first manifestation, in boundary layers, of compressible turbulence phenomena as observed in mixing layers. Of course, the previous interpretation is very approximate, because it depends critically on the value of the instantaneous convection velocities which are not known very accurately, so that the value of the Mach number for which such effects are important remains poorly determined. Such an interpretation, although speculative in many respects, is tempting because it can explain changes in the structure of u', as long as the radiated noise does not affect significantly the shear stress. To conclude, the spectral data show that there are modifications to the motions which contribute to the energy scales but not to the turbulent transport. This implies that the primary action of compressibility is to alter inactive motions. As these motions are related to the irrotational part of the fluctuations and to the pressure fluctuations induced by the layer, this explanation may be correct, but a full assessment would require a more complete knowledge of the two-point correlations, and of conditional statistics of turbulence in these flows.

4.9 Boundary-Layer Structure

The eddy-structure and internal dynamics of compressible turbulent boundary layers play an important role in many aerospace engineering applications. These include turbulent mixing for high-speed propulsion systems, tripping of hypersonic laminar boundary layers (for inlet efficiency), acoustic noise generation and propagation from high-speed engines, surface heat-transfer on high-speed vehicles, performance optimization for low-observable configurations, and unsteadiness in shock/turbulent boundary layer interactions. The following review was adapted from
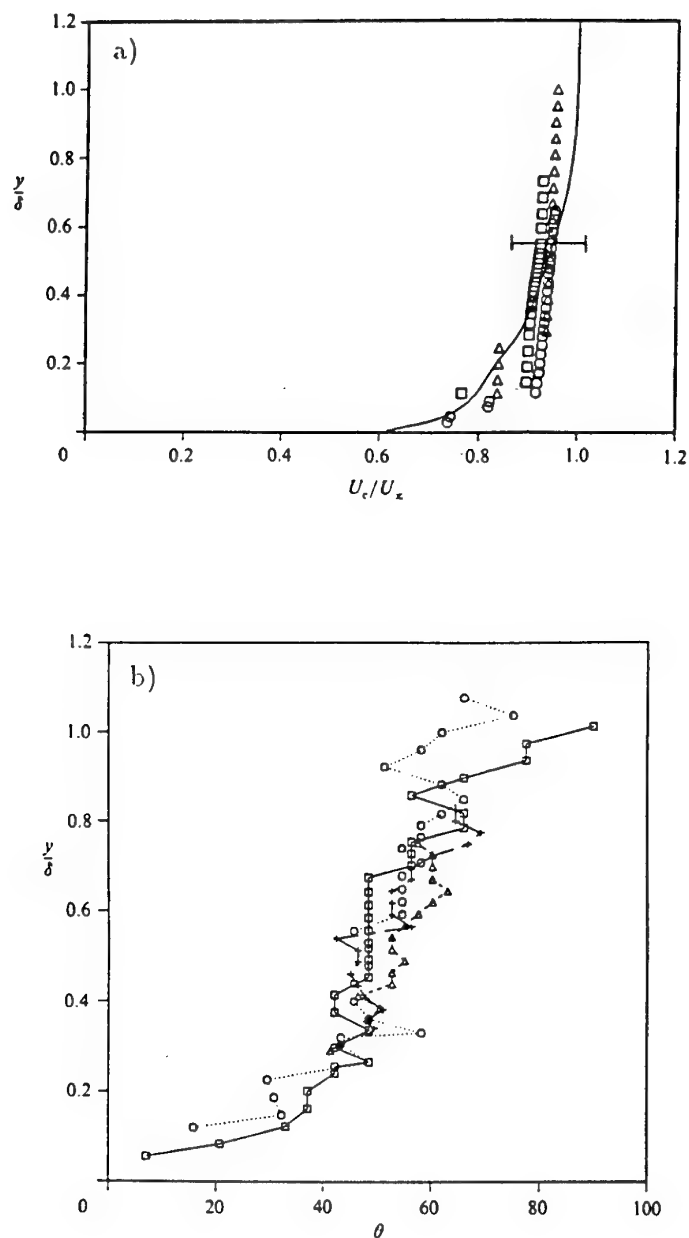
Figure 67: Characteristics of the large scale structure, as measured by Spina *et al.* (1991a), in a turbulent boundary layer at $Re_\theta = 81,000$ and $M = 2.9$. a) Broadband convection velocity based on measurements with three different streamwise probe separations. $\xi_x/\delta = 0.11$ □ ; 0.16 ○; 0.18 △. b) Broadband structure angle based on different wall-normal probe separations. $\xi_y/\delta = 0.09$ ———————□; 0.21 ·················○, 0.30 ————————△; 0.40 ——————— -+. Figure from Spina *et al.* (1991a).

the paper by Spina *et al.* , where further details may be found.

The current state of knowledge concerning compressible boundary layer structure is limited to large-scale motions in the outer-region, and is derived largely from recent studies by Spina *et al.* (1991a), Spina *et al.* (1991b), Smits *et al.* (1989), Spina & Smits (1987), Fernando & Smits (1990), Donovan *et al.* (1994), and Robinson (1986) of flat-plate layers with free-stream Mach numbers of approximately 3.0. These studies were preceded by a pioneering investigation by Owen & Horstman (1972), who made extensive two-point cross-correlation measurements with hot-wires in a Mach 7.2 boundary layer. Most of the results available in the literature were obtained using hot-wire anemometry (with its attendant limitations), with some degree of corroboration by high-speed flow visualization techniques (Cogne *et al.* , 1993, Smith & Smits, 1988).

For moderate Mach numbers, the outer region of the boundary layer (beyond the logarithmic region) is dominated by the entrainment process rather than by turbulence production. Thus the available studies of supersonic turbulent boundary layer structure are primarily relevant to the processes by which the boundary layer grows. In contrast, for subsonic turbulent boundary layers, most of the attention has focused upon the near-wall turbulence production processes. In addition, while most structure measurements in supersonic flow have been conducted at very high Reynolds number, the majority of studies in subsonic flow has been at quite low Reynolds number. These mismatches in emphases between subsonic and supersonic investigations sometimes make comparisons inconclusive, at least for isolating effects of compressibility on turbulence physics. To avoid the additional uncertainties due to measurement difficulties, it seems best to study quantities which are largely independent of calibration and measurement errors, such as the intermittency, ratios of Reynolds stresses, space-time correlations and structure angles.

The intermittency is one measure of the wallward extent of the entrainment process. The intermittency profile is often estimated with measurements of u' flatness. The measured flatness profile displays an apparent Mach-number dependence (see figure 37), wherein the onset of intermittency (corresponding to the rise in flatness factor) occurs nearer the boundary-layer edge as the Mach number increases. Since the cone of influence of a flow disturbance is inversely proportional to Mach number, the intermittent zone could become thinner as the Mach number increases. This interpretation is not fully supported by high-speed flow visualizations, however, so the data remain provocative. For example, double-pulsed Rayleigh-scattering flow visualization by Cogne *et al.* (1993) show deep potential incursions into the turbulent eddies of a Mach 3 boundary layer (figure 44) in patterns that are strikingly similar to visualizations of low-speed boundary layers.

For both incompressible low Reynolds number boundary layers, and compressible high Reynolds number boundary layers, the most identifiable feature of the outer-region is a downstream-sloping shear-layer interface between upstream high-speed fluid and downstream low-speed fluid.

(Unfortunately, these structures have been labeled both "fronts" and "backs" in the literature.) These interfaces are three-dimensional shear layers which are believed to form the upstream side of the largest of the boundary-layer eddies, and remain coherent long enough to convect several boundary-layer thicknesses downstream. They are not inert, however, since Spina *et al.* (1991a) have shown that 40% of the outer-layer Reynolds shear stress can be found in the neighborhood of these sloping interfaces (causality is not implied.) The intense turbulence production processes near the wall in the Mach 3 layer have not been investigated, but incompressible experience suggests that the large-scale sloping interfaces are not closely affiliated with near-wall regions of high Reynolds shear stress.

Sloping interfaces are easily detected with dual hot-wires separated in y, using either traditional space-time correlations, or a variety of conditional sampling techniques. For Mach 3 turbulent boundary layers, the effect of compressibility on the large-scale outer structures has been found to be generally small, which may be expected since the fluctuating Mach number in the outer regions is unlikely to approach unity (figure 3). However, differences between subsonic and supersonic large-scale motions have been observed, and some of these results were mentioned in earlier sections. The main results can be summarized as follows.

The average "structure angle" at which delta-scale interfaces lean downstream in a Mach 3 turbulent boundary layer ranges from 45° to 60° (standard deviation ≈ 20°) across most of the boundary layer, with a decrease near the wall and an increase near the boundary layer edge. The measured value of the structure angle is strongly dependent on measurement technique, although one method in current favor employs two hot-wires, separated by a fixed distance in y of 0.1 to 0.3δ, with both traversed across the layer. Structure angles measured using this technique in subsonic, low-Reynolds-number turbulent boundary layers are somewhat lower than those for Mach 3, high-Reynolds-number layers (see figures 46 and 67). As indicated in Section 3.4, it seems likely that increasing Reynolds number decreases the structure angle, while increasing Mach number increases the structure angle.

Hot-wire and flow visualizations show that the sloping delta-scale structures convect downstream at approximately 90% of the freestream velocity (slightly greater than for similar structures in low Reynolds number, incompressible turbulent boundary layers), and persist for at least 4 boundary-layer thicknesses (and probably much farther) downstream (Spina *et al.* , 1991b).

Outer-region space-time correlations suggest that the average spanwise extent of the largest eddies in the Mach 3 turbulent boundary layer is similar to that of subsonic turbulent boundary layers: approximately $1/2\delta$ in the outer layer, decreasing near the wall. (Although mean and instantaneous results for the sloping interface structure are in good agreement, the average cross-correlations used to deduce spanwise extent probably suffer from 'jitter' averaging, and the instantaneous extents may be larger.) The average streamwise scales of the largest eddies in the high Reynolds number, Mach 3 turbulent boundary layer are about two to three times those of low Reynolds number,
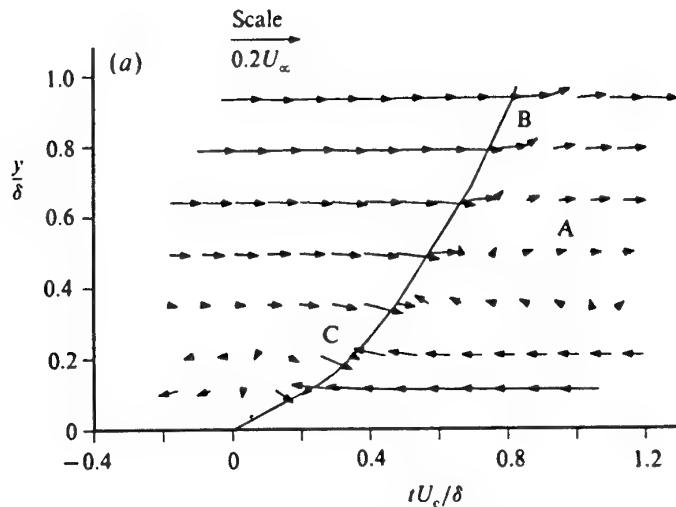
Figure 68: Ensemble-averaged view of the large-scale motions in a Mach 2.9 boundary layer. Figure from Spina *et al.* (1991a).

subsonic turbulent boundary layers (see figures 49, 50, 51 and 52). This seems to be the most significant structural difference between the two flows yet found, and as indicated earlier Reynolds number and compressibility appear to be important. Increasing Reynolds number will increase the streamwise scales, whereas increasing Mach number will decrease them. Otherwise, the structural model for the large-scale motions in a supersonic is very similar to that derived from studies of subsonic flows, as cam be seen by comparing Figures 42 and 68.

Since the influence of compressibility on the large-scale turbulent boundary layer motions seems to be subtle, explanations for the observed differences between low- and high-speed boundary layer structure are mostly speculative. Density-gradient effects are known to play a significant role in turbulent shear layers, but these effects are most likely to influence the near-wall region of the wall-layer, out of reach of standard measurement techniques. Parallels have also been drawn between the 45-degree slope of the interfacial structures in supersonic boundary layers and that of the hairpin-vortex structure observed in incompressible boundary layers. Insufficient evidence exists to support either side of this comparison, however. More conclusive results concerning compressibility effects on large-scale structure require higher Mach number investigations.

For boundary layers with freestream Mach numbers above 5, the near-wall region is more likely to show significant departures from known incompressible structure. The viscous sublayer for hypersonic boundary layers is likely to be much more quiescent than for incompressible flows (although pressure fluctuations will be imposed from above), and may not display the familar streaky structure. Since the mass-flux near the wall is very low for high Mach numbers, the buffer region may not be the dominant region for turbulence production, as in subsonic boundary layers (note that hypersonic laminar boundary layers undergo transition by disturbances spreading inward from the outer layer). Further investigation will depend on the

development and application of non-intrusive measurement techniques to the near-wall regions of hypersonic boundary layers.

Finally, we note that the rate of decay of the large scale motions, as measured by the rate at which the peak in the space-time correlation decays with distance, appears to decrease significantly with Mach number. For example, the distance over which the peak decreased to half its original level differs by an order of magnitude in the experiments by Favre *et al.* (1957), Favre *et al.* (1958) at Mach 0.04 and Owen & Horstman (1972) at Mach 7 when scaled by δ. A better scaling for the rate of decay may be the time scale of the energy-containing eddies, Λ/u'. Λ and u' both decrease with Mach number, so that their ratio seems to remain approximately constant. This result may in turn suggest that the decrease in the streamwise length scales with Mach number simply reflects the fact that the time scale of the large eddies remains constant as the absolute fluctuation level decreases. The more complex scaling arguments presented by Smith & Smits (1991) to explain the experimental observations may therefore not be necessary.

5 Summary

This AGARDograph has provided a lengthy, but certainly not exhaustive, review of the literature on turbulent boundary-layer structure. The emphasis has been on Reynolds-number effects and Mach-number effects. A major drawback of the current knowledge of these effects is that the data have been collected from many different flows, using different data acquisition and analysis procedures. These differences have resulted in large variations among the published results. Nevertheless, some definite conclusions can be made.

From the review of the subsonic flows, it is clear that the classic arguments on inner- and outer-layer similarity hold extremely well over a very large range of Reynolds

numbers (approximately $350 \leq Re_\theta \leq 210,000$), and the overlap region is well established over the same range (see Fernholz & Finley, 1995). There still exist certain issues, such as the Reynolds number dependence of the constants in the log-law, and the evidence for power-law similarity arguments, which cannot be answered on the basis of the existing data, primarily because of the difficulty of measuring accurately the friction at the wall. The wake parameter becomes constant for $Re_\theta > 5,000$, and although there have been some previous indications that it may decrease at very high Reynolds numbers, we believe there is enough uncertainty in the data to invalidate any strong conclusions regarding the asymptotic behavior.

In contrast to the mean-flow behavior, the scaling of the turbulent stresses does not necessarily follow the inner/outer scaling arguments. For example, as found previously by Sreenivasan (1989) and Gad-el-Hak & Bandyopadhyay (1994), the Reynolds number can have a significant effect on the level of the maximum turbulence stresses, and the location of that maximum in the boundary layer. In other respects, the scaling arguments put forward by Perry and his co-workers (see, for example, Perry & Li, 1990) indicate how the stresses may scale in the overlap region, and the experimental evidence tends to support their conclusions. It is clear, however, that an overlap region for the turbulent stresses appears only at a much higher Reynolds number than the Reynolds number at which an overlap region appears in the mean velocity profile.

The evolution of the organized motions in the boundary layer also depends on Reynolds number. In particular, the streamwise scaling of the outer-layer structure is rather sensitive, where the scale increases with Reynolds number. This was confirmed by Smith (1994) by direct measurements of the space-time correlation, and by Dussauge & Smits (1995) from measurements of the spectra. In contrast, the spanwise scaling appears to be insensitive to Reynolds number, so that on average the structures become more elongated in the streamwise direction with increasing Reynolds number. The average inclination of the outer-layer structures also decreases, which may be related to the increase in the streamwise aspect ratio. It also appears that the spanwise scaling of the sublayer streaks is fixed at a mean value of about $100\nu/u_\tau$ over a very wide Reynolds-number range.

From the review of supersonic flows with moderate Mach number, it appears that the direct effects of compressibility on wall turbulence are rather small: the most notable differences between subsonic and supersonic boundary layers may be attributed to the variation in fluid properties across the layer. Under the assumption that the length scales are not affected by compressibility, the mean velocity profile can be transformed into an "equivalent" incompressible profile, and the agreement with the incompressible scaling appears to hold over very wide Reynolds number and Mach number ranges. Furthermore, the turbulent stresses in the outer region scale on the wall stress, as first suggested by Morkovin (1962), as far as we can tell from the available data. This result is not surprising in some ways since the fluctuating Mach number ($M' = M - \overline{M}$) for moderately supersonic flows is considerably less than one, as illustrated in figure 3. However, a more detailed inspection of the turbulence

properties reveals certain characteristics that cannot be collapsed by a simple density scaling. For example, there are suggestions that the intermittency profile is fuller than the corresponding subsonic profile, and the shear correlation coefficient R_{uv} decreases with distance from the wall instead of remaining approximately constant. There are other results, however, which indicate that R_{uv} follows the incompressible trend, and there is the possibility that the differences may be caused by a Reynolds-number rather than a Mach-number dependence. Unfortunately the data base is very sparse, and considerable effort needs to be spent before these issues can be laid to rest. With respect to the streamwise and spanwise length scales of the large-scale motions, and their average inclination to the wall, there exists strong evidence to indicate the effect of Mach number. The streamwise length scales are reduced significantly by increasing Mach number, and the angle of inclination is increased, although in coming to these conclusions we have implicitly assumed that Mach and Reynolds number effects are independent. It is necessary to make this assumption since the data do not overlap to any significant extent, and we are forced to compare experiments in supersonic flow with the results obtained in subsonic flow, usually at a different Reynolds number. In fact, the actual Reynolds number to be used in such a comparison is controversial, since the temperature varies significantly across the layer, and there is usually a major difference between the values of Re_θ and $R_{\delta 2}$. Finally, there is an order-of-magnitude decrease in the rate of decay of the large-scale motions as the Mach number increases from low-subsonic to high supersonic values (Smits *et al.*, 1989). Even if we account for the change in time scale of the energy-containing eddies Λ/u', we see that the lateral correlations are almost unaffected by changes in Mach and Reynolds number.

How can we explain these differences? Part of the answer may lie in understanding the role of Reynolds number more clearly, but understanding the effects of fluid-property variations may be more important. In that respect, a direct numerical simulation of a strongly heated, incompressible turbulent boundary layer in the absence of buoyancy effects would be particularly valuable. Experimentally, we urgently need detailed turbulence data at higher Mach numbers. We are seeing subtle differences at supersonic speeds that may signal the onset of direct compressibility effects such as the increased importance of pressure fluctuations and pressure-velocity correlations. These effects will become more obvious at hypersonic Mach numbers, and such studies would contribute to our understanding of the supersonic behavior.

While few specifics are known, the turbulence physics become more complex as the Mach number increases beyond about five. For example, the Strong Reynolds Analogy and Morkovin's hypothesis are staples of boundary-layer analyses at moderate Mach number. However, an upper-Mach-number limit must exist on the applicability of these simplifying assumptions, if only because there is a limit on the magnitude of temperature fluctuations. Indeed, the change in magnitude of the fluctuating Mach number distribution as the flow enters the hypersonic range (see figure 3) points to the possibility of a dramatic alteration of turbulence dynamics due to compressibility effects around Mach 5 (in comparison, the Mach num-

ber of the fluctuations, $u'_{rms}/\bar{a}$ is less than 0.3 even for the Mach 7.2 and 9.4 flows). Unlike the distribution of $u'_{rms}/\bar{a}$, the fluctuating Mach number develops a peak near the middle of the boundary layer where both the velocity and temperature fluctuations are important. This behavior, when considered together with the large gradients in density and viscosity near the wall, also leads to the conclusion that there may be substantial differences in turbulence dynamics at high Mach number.

At the same time, the near-wall gradients in density and viscosity are strongly dependent on heat transfer, and therefore the thickness of the sublayer will depend on Mach number, Reynolds number, and wall temperature. This leads to the issue of how the viscous instability of the sublayer changes when fluid properties vary with distance from the wall (see Morkovin, 1992). Since the local Reynolds number increases away from an adiabatic wall faster in supersonic flow than in incompressible flow, we would expect the flow to become less stable as we move away from the wall at a rate that is faster than in an incompressible flow at the same friction velocity. At the same time, the increasing Mach number is known to be a stabilizing influence in laminar-to-turbulent transition, where the most unstable disturbance changes from being two-dimensional to being three-dimensional as the Mach number increases. What is then the proper basis of comparison between compressible and incompressible boundary layers in the near-wall region? Is it simply a matter of defining an "effective" Reynolds number? We can only hope that further results will become available to help shed light on these unanswered questions.

Acknowledgements

References

Alfredsson, P.H., Johansson, A.V., Haritonidis, J.H. & Eckelmann, H. 1988. The fluctuating wall shear stress and the velocity field in the viscous sublayer. *Physics of Fluids*, **31**, 1026–1033.

Allen, J.M. 1977. Reevaluation of compressible flow Preston tube calibrations. *NASA TM X-3488*.

Alving, A.E. & Smits, A.J. 1990a. Correlation measurements and structure angles in a turbulent boundary layer recovering from convex curvature. *In:* Kline, S.J. & Afgan, N.H. (eds), *Near-Wall Turbulence*. Hemisphere.

Alving, A.E., Smits, A.J. & Watmuff, J.H. 1990b. Turbulent boundary layer relaxation from convex curvature. *Journal of Fluid Mechanics*, **211**, 529–556.

Andreopoulos, J., Durst, F., Zarić, Z. & Jovanovic, J. 1984. Influence of Reynolds number on characteristics of turbulent wall boundary layers. *Experiments in Fluids*, **2**, 7–16.

Antonia, R.A., Subramanian, C.S., Rajagopalan, S. & Chambers, A.J. 1982. Reynolds number dependence of the large structure in a slightly heated turbulent boundary layer. *In:* Zarić, Z.P. (ed), *Structure of Turbulence in Heat and Mass Transfer*. Hemisphere.

Antonia, R.A., Bisset, D.K. & Browne, L.W.B. 1990a. Effect of Reynolds number on the topology of the organized motion in a turbulent boundary layer. *Journal of Fluid Mechanics*, **213**, 267–286.

Antonia, R.A., Browne, L.W.B. & Bisset, D.K. 1990b. Effect of Reynolds number on the organized motion in a turbulent boundary layer. *In:* Kline, S.J. & Afgan, N.H. (eds), *Near Wall Turbulence*. Hemisphere.

Audiffren, N. 1993. *Turbulence d'une couche limite soumise à une variation de densité due à une onde de choc ou à un chauffage pariétal*. Thèse d'Université, Université d'Aix-Marseille II.

Beckwith, I.E. 1970. Recent advances in research on compressible turbulent boundary layers. *NASA SP-228, 355–416*.

Bertram, M.H. & Neal, L. 1965. Recent experiments in hypersonic turbulent boundary layers. *NASA TM X-56335*.

Bestion, D. 1982. *Méthodes anémométriques par fil chaud: Application à l'étude d'interactions turbulence-gradient de pression élevé en couches limites à vitesse supersonique*. Thèse de Docteur-Ingénieur, Université d'Aix-Marseille II.

Bestion, D., Debième, J.F. & Dussauge, J.P. 1983. Two rapid distortions in supersonic flows: Turbulence/shock wave and turbulence/expansion. *In:* Dumas, R. & Fulachier, L. (eds), *Structure of Complex Turbulent Shear Flow*. Springer Verlag.

Bisset, D.K. & Antonia, R.A. 1991. Mean velocity and Reynolds shear stress in a turbulent boundary layer at low Reynolds numbers. *Aeronautical Quarterly*, **95**, 244–247.

Blackwelder, R.F. & Haritonidis, J.H. 1983. Scaling of the bursting frequency in turbulent boundary layers. *Journal of Fluid Mechanics*, **132**, 87.

Blackwelder, R.F. & Kaplan, R.E. 1976. On the wall structure of the turbulent boundary layer. *Journal of Fluid Mechanics*, **76**, 89.

Blackwelder, R.F. & Kovasznay, L.S.G. 1972. Time scales and correlations in a turbulent boundary layer. *The Physics of Fluids*, **15**, 1545–1554.

Bogard, D.G. & Tiederman, W.G. 1986. Burst detection with single-point velocity measurements. *Journal of Fluid Mechanics*, **162**, 389–414.

Bogard, D.G. & Tiederman, W.G. 1987. Characteristics of ejections in turbulent channel flow. *Journal of Fluid Mechanics*, **179**, 1–20.

Bradshaw, P. 1967. "Inactive" motion and pressure fluctuations in turbulent boundary layers. *Journal of Fluid Mechanics*, **30**, 241–258.

Bradshaw, P. 1977. Compressible turbulent shear layers. *Annual Review of Fluid Mechanics*, **9**, 33–54.

Bradshaw, P. 1994. Turbulence: The chief outstanding difficulty of our subject. *Experiments in Fluids*, **16**, 203–216.

Bradshaw, P. & Unsworth, K. 1974. Comment on "Evaluation of Preston tube calibration equations in supersonic flow". *AIAA Journal*, **12**, 1293–1296.

Brasseur, J.G. 1991. Comments on the Kolmogorov hypothesis of isotropy in the small scales. *AIAA Paper 91-0230*.

Brederode, V. de & Bradshaw, P. 1974. A note on the empirical constants appearing in the logarithmic law for turbulent wall flows. *Report 74-03, Imperial College of Science and Technology, Department of Aeronautics*.

Brodkey, R.S., Wallace, J.M. & Eckelmann, H. 1974. Some properties of truncated turbulence signals in bounded shear flows. *Journal of Fluid Mechanics*, **63**.

Brown, G.L. & Thomas, A.S.W. 1977. Large structure in a turbulent boundary layer. *The Physics of Fluids*, **20**, S243–S252.

Browne, L.W.B., Antonia, R.A. & Shah, D.A. 1988. Selection of wires and wire spacing for X-wires. *Experiments in Fluids*, **6**, 286–288.

Bruns, J., Dengel, P. & Fernholz, H.H. 1992. Mean flow and turbulence measurements in an incompressible two-dimensional turbulent boundary layer. Part I: Data. *Institutsbericht Nr. 02/92, Hermann-Föttinger-Institut für Thermo- und Fluiddynamik, Technische Universität Berlin*.

Bushnell, D.M., Johnson, C.B., Harvey, W.D. & Feller, W.V. 1969. Comparison of prediction methods and studies of relaxation in hypersonic turbulent nozzle-wall boundary layers. *NASA TN D-5433*.

Bushnell, D.M., Cary, Jr., A.M. & Harris, J.E. 1976. Calculation methods for compressible turbulent boundary layers. State of the art. *NASA SP-422*.

Cantwell, B.J. 1981. Organized motion in turbulent flow. *Annual Review of Fluid Mechanics*, **13**, 457–515.

Carvin, C., Debiève, J.F. & Smits, A.J. 1988. The near-wall temperature profile of turbulent boundary layers. *AIAA Paper 88-0136*.

Cebeci, T. & Smith, A.M.O. 1974. *Analysis of Turbulent Boundary Layers*. Academic Press.

Chen, C.-H.P. & Blackwelder, R.F. 1978. Large-scale motion in a turbulent boundary layer: A study using temperature contamination. *Journal of Fluid Mechanics*, **89**.

Clauser, F.H. 1954. Turbulent boundary layers in adverse pressure gradients. *Journal of the Aeronautical Sciences*, **21**, 91–108.

Cogne, S., Forkey, J., Miles, R.B. & Smits, A.J. 1993. The evolution of large-scale structures in a supersonic turbulent boundary layer. *In:* Stock, D.E., Smits, A.J. & Sheriff, S.A. (eds), *Proc. of the Symposium on Transitional and Turbulent Compressible Flows*. ASME Fluids Engineering Division.

Coles, D. 1953. Measurements in the boundary layer on a smooth flat plate in supersonic flow. *J.P.L. CalTech. Reports 20-69, 20-70, 20-71*.

Coles, D. 1956. The law of the wake in the turbulent boundary layer. *Journal of Fluid Mechanics*, **1**, 191–226.

Coles, D. 1962. The turbulent boundary layer in a compressible fluid. *Report R-403-PR, The Rand Corporation, Santa Monica, California*.

Coles, D. 1987. Coherent structures in turbulent boundary layers. *Pages 93–113 of:* Meier, H.U. & Bradshaw, P. (eds), *Perspectives in Turbulence Studies*. Springer-Verlag.

Corcos, G.M. 1963. The structure of the turbulent pressure field in boundary-layer flows. *Journal of Fluid Mechanics*, **18**, 353–378.

Corino, E.R. & Brodkey, R.S. 1969. A visual investigation of the wall region in turbulent flow. *Journal of Fluid Mechanics*, **37**, 1–30.

Corrsin, S. & Kistler, A.L. 1955. Free-stream boundaries of turbulent flows. *NACA Report 1244*.

Debiève, J.F. 1982. Turbulent behaviour through a shock-wave. Turbulent macroscale evolution. *Arch. Mech., Warszawa*, **34**, 581–592.

Debiève, J.F. 1983. *Étude d'une interaction turbulence/onde de choc*. Thèse de Doctorat d'État, Université d'Aix-Marseille II.

Demetriades, A. & Martindale, W.R. 1983. Determination of one dimensional spectra in high speed boundary layers. *The Physics of Fluids*, **26**, 397–403.

Dhawan, S. & Narasimha, R. 1958. Some properties of boundary layer flow during the transition from laminar to turbulent motion. *Journal of Fluid Mechanics*, **3**, 418.

Djenidi, L. & Antonia, R.A. 1993. LDA measurements in low Reynolds number turbulent boundary layers. *Experiments in Fluids*, **14**, 280–283.

Donovan, J.F., Spina, E.F. & Smits, A.J. 1994. The structure of a supersonic turbulent boundary layer subjected to concave surface curvature. *Journal of Fluid Mechanics*, **259**, 1–24.

Duncan, W.J., Thom, A.S. & Young, A.D. 1970. *Mechanics of Fluids*. 2 edn. Edward Arnold.

Dussauge, J.P. 1981. *Évolution de transferts turbulents dans une détente rapide, en écoulement supersonique*. Thèse de Doctorat d'État, Université d'Aix Marseille.

Dussauge, J.P. & Gaviglio, J. 1987. The rapid expansion of a supersonic turbulent flow: Role of bulk dilatation. *Journal of Fluid Mechanics*, **174**, 81–112.

Dussauge, J.P. & Smits, A.J. 1995. Characteristic scales for energetic eddies in turbulent supersonic boundary layers. *In: Proceedings of the Tenth Symposium on Turbulent Shear Flows*. Pennsylvania State University.

Dutton, R.A. 1955. *Experimental studies of the turbulent boundary layer on a flat plate with and without distributed suction*. Ph.D. Thesis, University of Cambridge.

Eléna, M. & Gaviglio, J. 1993. La couche limite turbulente compressible: Méthodes D'étude et Résultats, synthèse. *La Recherche Aérospatiale*, 1–21.

Eléna, M. & Lacharme, J.P. 1988. Experimental study of a supersonic turbulent boundary layer using a laser Doppler anemometer. *Journal Mécanique Théorique et Appliquée*, **7**, 175–190.

Erm, L.P. 1988. *Low-Reynolds-number turbulent boundary layers*. Ph.D. Thesis, University of Melbourne.

Erm, L.P. & Joubert, P.N. 1991. Low-Reynolds-number turbulent boundary layers. *Journal of Fluid Mechanics*, **230**, 1–44.

Erm, L.P., Smits, A.J. & Joubert, P.N. 1985. Low Reynolds number turbulent boundary layers on a smooth flat surface in a zero pressure gradient. *In: Proceedings of the Fifth Symposium on Turbulent Shear Flows.* Cornell University.

Erm, L.P., Joubert, P.N. & Spalart, P.R. 1994. *Low-Reynolds-number turbulent boundary layers: experimental data compared with numerical simulations.* Unpublished report.

Ewing, D., Hussein, H.J. & George, W.K. 1995. Spatial resolution of parallel hot-wire probes for derivative measurements. *Experimental Thermal and Fluid Science,* **11**, 155–173.

Falco, R.E. 1977. Coherent motions in the outer region of turbulent boundary layers. *The Physics of Fluids,* **20**, S124–S132.

Falco, R.E. 1991. A coherent structure model of the turbulent boundary layer and its ability to predict Reynolds number dependence. *Pages 103–129 of:* Walker, J.D.A. (ed), *Turbulent Flow Structure Near Walls.* The Royal Society. First published in *Phil. Trans. R. Soc. London A.* 336.

Favre, A. 1965. Equations des gaz turbulents compressibles. *Journal de Mécanique,* 4, 361–421.

Favre, A., Gaviglio, J. & Dumas, R. 1967. Structure of space-time correlations in a boundary layer. *The Physics of Fluids,* **10**, S138–S145.

Favre, A.J., Gaviglio, J.J. & Dumas, R.J. 1957. Space-time double correlations and spectra in a turbulent boundary layer. *Journal of Fluid Mechanics,* **2**, 313–342.

Favre, A.J., Gaviglio, J.J. & Dumas, R.J. 1958. Further space-time correlations of velocity in a turbulent boundary layer. *Journal of Fluid Mechanics,* **3**, 344–356.

Feller, W.V. 1973. Effects of upstream wall temperatures on hypersonic tunnel wall boundary-layer profile measurements. *AIAA Journal,* **11**, 556–558.

Fernando, E.M. & Smits, A.J. 1990. A supersonic turbulent boundary layer in an adverse pressure gradient. *Journal of Fluid Mechanics,* **211**, 285–307.

Fernholz, H.H. 1969. Geschwindigkeitsprofile, Temperaturprofile und halbempirische Gesetze in kompressiblen turbulenten Grenzschichten bei konstantem Druck. *Ing. Archiv,* **38**, 311–328.

Fernholz, H.H. 1971. Ein halbempirisches Gesetz für die Wandreibung in kompressiblen turbulenten Grenzschichten bei isothermer und adiabater Wand. *ZAMM,* **51**, T148–T149.

Fernholz, H.H. & Finley, P.J. 1976. A critical compilation of compressible turbulent boundary layer data. *AGARDograph 223.*

Fernholz, H.H. & Finley, P.J. 1980. A critical commentary on mean flow data for two-dimensional compressible turbulent boundary layers. *AGARDograph 253.*

Fernholz, H.H. & Finley, P.J. 1981. A further compilation of compressible turbulent boundary layer data with a survey of turbulence data. *AGARDograph 263.*

Fernholz, H.H. & Finley, P.J. 1996. Incompressible zero-pressure-gradient turbulent boundary layers: An assessment of the data. *Progress in Aerospace Science,* **32**.

Fernholz, H.H., Smits, A.J., Dussauge, J.P. & Finley, P.J. 1989. A survey of measurements and measuring techniques in rapidly distorted compressible turbulent boundary layers. *AGARDograph 315.*

Fernholz, H.H., Krause, E., Nockemann, N. & Schober, M. 1995. Comparative measurements in the canonical boundary layer at $Re_{\delta_2} \leq 6x10^4$ on the wall of the German-Dutch windtunnel. *The Physics of Fluids,* **7**, 1275–1281.

Fiedler, H. & Head, M.R. 1966. Intermittency measurements in the turbulent boundary layer. *Journal of Fluid Mechanics,* **25**.

Finley, P.J. 1994. The Preston tube in adiabatic compressible flow. *Report 94-02, Imperial College of Science and Technology, Department of Aeronautics.*

Frenkiel, F.N. 1954. Effects of wire length in turbulence investigations with a hot-wire anemometer. *The Aeronautical Quarterly,* **5**.

Fulachier, L. 1972. *Contribution à l'étude des analogies des champs dynamiques et thermiques dans une couche limite turbulente. Effet de l'aspiration.* Thèse de Doctorat ès Sciences Physiques, Université de Provence, Aix-Marseille.

Gad-el-Hak, M. & Bandyopadhyay, P. 1994. Reynolds number effects in wall-bounded flows. *Applied Mechanics Reviews,* **47**.

Gaviglio, J. 1987. Reynolds analogies and experimental study of heat transfer in the supersonic boundary layer. *International Journal of Heat and Mass Transfer,* **30**, 911–926.

George, W.K. & Castillo, L. 1993. Boundary layers with pressure gradient: Another look at the equilibrium boundary layer. *In:* So, R.M.C., Speziale, C.G. & Launder, B.E. (eds), *Near-Wall Turbulent Flows.* Elsevier Science Publishers B. V.

George, W.K., Knecht, P. & Castillo, L. 1992. The zero-pressure gradient turbulent boundary layer revisited. *In: Proceedings of the Thirteenth Biennial Symposium on Turbulence.*

Grant, H.L. 1958. The large eddies of turbulent motion. *Journal of Fluid Mechanics,* **4**.

Grant, H.L., Stewart, R.W. & Moilliet, A. 1962. Turbulence spectra from a tidal channel. *Journal of Fluid Mechanics,* **12**, 241–268.

Head, M.R. & Bandyopadhyay, P.R. 1981. New aspects of turbulent boundary-layer structure. *Journal of Fluid Mechanics,* **107**, 297–338.

Hinze, J.O. 1975. *Turbulence.* 2 edn. McGraw-Hill.

Hopkins, E.J. & Keener, E.R. 1966. Study of surface Pitots for measuring turbulent skin friction at supersonic Mach numbers — Adiabatic wall. *NASA TN D-3478.*

Hopkins, E.J. & Keener, E.R. 1972. Pressure-gradient effects on hypersonic turbulent skin-friction and boundary-layer profiles. *AIAA Journal,* **10**, 1141–1142.

Hopkins, E.J., Keener, E.R., Polek, T.E. & Dwyer, H.A. 1972. Hypersonic turbulent skin-friction and boundary-layer profiles on nonadiabatic flat plates. *AIAA Journal,* **10**, 40–48.

Horstman, C.C. & Owen, F.K. 1972. Turbulent properties of a compressible boundary layer. *AIAA Journal,* **10**, 1418–1424.

Howarth, L. (ed). 1953. *Modern Developments in Fluid Dynamics, High Speed Flow.* Oxford Clarendon Press.

H.P., Bakewell, Jr. & Lumley, J.L. 1967. Viscous sublayer and adjacent wall region in turbulent pipe flow. *The Physics of Fluids*, **10**.

Huffman, G.D. & Bradshaw, P. 1972. A note on von Kármán's constant in low Reynolds number turbulent flows. *Journal of Fluid Mechanics*, **53**, 45–60.

Hussain, A.K.M.F. 1983. Coherent structures — Reality and myth. *The Physics of Fluids*, **26**, 2816–2850.

Johansson, A.V. & Alfredsson, P.H. 1983. Effects of imperfect spatial resolution on measurements of wall-bounded turbulent shear flows. *Journal of Fluid Mechanics*, **137**, 409–421.

Johnson, D.A. 1989. Laser Doppler anemometry. *Chapter 6, AGARDograph 315*.

Johnson, D.A. & Rose, W.C. 1975. Laser velocimeter and hot-wire anemometer comparison in a supersonic boundary layer. *AIAA Journal*, **13**, 512–515.

Karlsson, R.I. & Johansson, T.G. 1988. LDV measurements of higher order moments of velocity fluctuations in a turbulent boundary layer. *In: Laser Anemometry in Fluid Mechanics*. Instituto Superior Técnico, Lisbon. No. 1096.

Kemp, J.H. & Owen, F.K. 1972. Nozzle wall boundary layers at Mach numbers 20 to 47. *AIAA Journal*, **10**, 872–879.

Kim, H.T., Kline, S.J. & Reynolds, W.C. 1971. The production of turbulence near a smooth wall in a turbulent boundary layer. *Journal of Fluid Mechanics*, **50**, 133–160.

Kim, J. & Spalart, P.R. 1987. Scaling of the bursting frequency in turbulent boundary layers at low Reynolds numbers. *Physics of Fluids*, **30**.

Kim, K.S., Lee, Y. & Settles, G.S. 1991. Laser interferometry/Preston tube skin-friction comparison in a shock/boundary layer interaction. *AIAA Journal*, **29**, 1007–1009.

Kistler, A.L. 1959. Fluctuation measurements in a supersonic turbulent boundary layer. *Physics of Fluids*, **2**, 290–296.

Klebanoff, P.S. 1955. Characteristics of turbulence in a boundary layer with zero pressure gradient. *NACA Report 1247*.

Klewicki, J.C. & Falco, R.E. 1990. On accurately measuring statistics associated with small-scale structure in turbulent boundary layers using hot-wire probes. *Journal of Fluid Mechanics*, **219**, 119–142.

Kline, S.J., Reynolds, W.C., Schraub, F.A. & Runstadler, P.W. 1967. The structure of turbulent boundary layers. *Journal of Fluid Mechanics*, **30**, 741–773.

Kolmogorov, A.N. 1961. The local structure of turbulence in incompressible viscous fluid for very large Reynolds numbers. *In:* Friedlander, S.K. & Topper, L. (eds), *Turbulence: Classic Papers on Statistical Theory*. Interscience.

Konrad, W. 1993. *A three-dimensional supersonic turbulent boundary layer generated by an isentropic compression*. Ph.D. Thesis, Princeton University, Princeton, NJ.

Kovasznay, L.S.G., Kibbens, V. & Blackwelder, R.F. 1970. Large-scale motion in the intermittent region of a turbulent boundary layer. *Journal of Fluid Mechanics*, **41**, 283–325.

Kussoy, M.I., Horstman, C.C. & Acharya, M. 1978. An experimental documentation of pressure gradient and Reynolds number effects on compressible turbulent boundary layers. *NASA TM 78488*.

Laderman, A.J. & Demetriades, A. 1974. Mean and fluctuating flow measurements in the hypersonic boundary layer over a cooled wall. *Journal of Fluid Mechanics*, **63**, 121–144.

Laufer, J. 1961. Aerodynamic noise in supersonic wind tunnels. *Journal of the Aerospace Sciences*, **28**, 685–692.

Lele, S.K. 1994. Compressibility effects on turbulence. *Annual Review of Fluid Mechanics*, **26**, 211–254.

Lewis, J.E., Gran, R.L. & Kubota, T. 1972. An experiment on the adiabatic compressible turbulent boundary layer in adverse and favourable pressure gradients. *Journal of Fluid Mechanics*, **51**, 657–672.

Li, J.D. 1989. *The turbulence structure of wall shear flow*. Ph.D. Thesis, University of Melbourne.

Li, J.D. & Perry, A.E. 1989. Shear stress profiles in zero-pressure-gradient turbulent boundary layers. *In: Proceedings of the Tenth Australasian Fluid Mechanics Conference*.

Libby, P.A. & Visich, M. 1959. The law of the wake in compressible turbulent boundary layers. *Journal of the Aeronautical Sciences*, **26**, 541–542.

Ligrani, P.M. & Bradshaw, P. 1987. Spatial resolution and measurement of turbulence in the viscous sublayer using subminiature hot-wire probes. *Experiments in Fluids*, **5**, 407–417.

Liu, Z.-C., Adrian, R.J. & Hanratty, T.J. 1992. Structure of turbulent channel flow: Reynolds number effects. *In: Bulletin of the American Physical Society, 37 (8)*. APS. Paper AA3.

Logan, P. 1987. *Studies of supersonic turbulence and hot wire response using laser-induced fluorescence*. Ph.D. Thesis, Stanford University. 154 pp.

Lu, S.S. & Willmarth, W.W. 1973. Measurements of the structure of the Reynolds stress in a turbulent boundary layer. *Journal of Fluid Mechanics*, **60**, 481–511.

Luchik, T.S. & Tiederman, W.G. 1987. Timescale and structure of ejections and bursts in turbulent channel flows. *Journal of Fluid Mechanics*, **174**, 529–552.

Mabey, D.G., Meier, H.U. & Sawyer, W.G. 1974. Experimental and theoretical studies of the boundary layer on a flat plate at Mach numbers from 2.5 to 4.5. *RAE TR 74127*.

MacAulay, P. & Gartshore, I.P. 1991. A tentative model of outer-region structure in a turbulent boundary-layer developing on a smooth-wall. *In:* Keffer, J.F., Shah, R.K. & Ganić, E.N. (eds), *Experimental Heat Transfer, Fluid Mechanics, and Thermodynamics 1991*. Elsevier Science.

Maise, G. & McDonald, H. 1968. Mixing length and kinematic eddy viscosity in a compressible boundary layer. *AIAA Journal*, **6**, 73–80.

Mathews, D.C., Childs, M.E. & Paynter, G.C. 1970. Use of Coles' universal wake function for compressible turbulent boundary layers. *Journal of Aircraft*, **7**, 137–140.

McGinley, C.B., Spina, E.F. & Sheplak, M. 1994. Turbulence measurements in a Mach 11 helium boundary layer. *AIAA Paper 94-2364*.

Meier, H.U. & Rotta, J.C. 1971. Temperature distributions in supersonic turbulent boundary layers. *AIAA*

Journal, **9**, 2149–2156.

Mikulla, V. & Horstman, C.C. 1975. Turbulence stress measurements in a non-adiabatic hypersonic boundary layer. *AIAA Journal*, **13**, 1607–1613.

Miles, R.B. & Nosenchuck, D.M. 1989. Three-dimensional quantitative flow diagnostics. *Pages 33–107 of:* Gad-el-Hak, M. (ed), *Lecture Notes in Engineering, Advances in Fluid Mechanics Measurements*, vol. 45. Springer-Verlag.

Millikan, C.B.A. 1938. A critical discussion of turbulent flows in channels and circular tubes. *Pages 386–392 of: Proceedings of the Fifth International Congress of Applied Mechanics.*

Moin, P. & Spalart, P.R. 1987. Contributions of numerical simulation data base to the physics, modeling, and measurement of turbulence. *NASA TM 100022.*

Morkovin, M.V. 1962. Effects of compressibility on turbulent flows. *Pages 367–380 of:* Favre, A.J. (ed), *Mécanique de la Turbulence.* CNRS.

Morkovin, M.V. 1992. Mach number effects on free and wall turbulent structures in light of instability flow interactions. *Pages 269–284 of:* Gatski, T.B., Sarkar, S. & Speziale, C.G. (eds), *Studies in Turbulence.* Springer Verlag.

Morkovin, M.V. & Phinney, R.E. 1958. Extended applications of hot wire anemometry to high-speed turbulent boundary layers. *Johns Hopkins University, Baltimore, MD, Report AFOSR TN-58-469.*

Morrison, J.F., Subramanian, C.S. & Bradshaw, P. 1992. Bursts and the law of the wall in turbulent boundary layers. *Journal of Fluid Mechanics*, **241**, 75–108.

Murlis, J., Tsai, H.M. & Bradshaw, P. 1982. The structure of turbulent boundary layers at low Reynolds numbers. *Journal of Fluid Mechanics*, **122**, 13–56.

Naguib, A.M. & Wark, C.E. 1992. An investigation of wall-layer dynamics using a combined temporal filtering and correlation technique. *Journal of Fluid Mechanics*, **243**.

Nakayama, A. & Westphal, R.V. 1986. The effects of sensor length and spacing on X-wire measurements in a boundary layer. *NASA TM 88352.*

Narasimha, R. & Kailas, S.V. 1987. Energy events in the atmospheric boundary layer. *In:* Meier, H.U. & P.Bradshaw (eds), *Perspectives in Turbulence Studies.* Springer-Verlag.

Nikuradse, J. 1932. Gesetzmäßigkeit der turbulenten Stromüng in glatten Rohren. *Forsch. Arb. Ing.-Wes. No. 356.* English translation NACA TT F-10, 359.

Nikuradse, J. 1933. Stromüngsgesetze in rauhen Rohren. *Forsch. Arb. Ing.-Wes. No. 361.*

Nockemann, M., Abstiens, R., Schober, M., Bruns, J. & Eckert, D. 1994. Vermessung der Wandgrenzschicht im Deutsch-Niederländischen Windkanal bei hohen Reynolds-zahlen. *Institutsreport DNW 1994, Aerodynamisches Institut RWTH Aachen.*

Owen, F.K. 1990. Turbulence and shear stress measurements in hypersonic flow. *AIAA Paper 90-1394.*

Owen, F.K. & Horstman, C.C. 1972. On the structure of hypersonic turbulent boundary layers. *Journal of Fluid Mechanics*, **53**, 611–636.

Owen, F.K., Horstman, C.C. & Kussoy, M.I. 1975. Mean and fluctuating flow measurements of a fully-developed, non-adiabatic, hypersonic boundary layer. *Journal of Fluid Mechanics*, **70**, 393–413.

Pao, Y.-H. 1965. Structure of turbulent velocity and scalar fields at large wavenumbers. *The Physics of Fluids*, **8**, 1063.

Park, S.-R. & Wallace, J.M. 1993. The Influence of Instantaneous Velocity Gradients on Turbulence Properties Measured with Multi-Sensor Hot-Wire Probes. *Experiments in Fluids*, **16**, 17–26.

Patel, V.C. 1965. Calibration of the Preston tube and limitations on its use in pressure gradients. *Journal of Fluid Mechanics*, **23**, 185–208.

Perry, A.E. & Abell, C.J. 1975. Scaling laws for pipe-flow turbulence. *Journal of Fluid Mechanics*, **67**, 257–271.

Perry, A.E. & Abell, C.J. 1977. Asymptotic similarity of turbulence structures in smooth- and rough-walled pipes. *Journal of Fluid Mechanics*, **79**, 785–799.

Perry, A.E. & Chong, M.S. 1982. On the mechanism of wall turbulence. *Journal of Fluid Mechanics*, **119**, 173–219.

Perry, A.E. & Li, J.D. 1990. Experimental support for the attached-eddy hypothesis in zero-pressure-gradient turbulent boundary layers. *Journal of Fluid Mechanics*, **218**, 405–438.

Perry, A.E., Smits, A.J. & Chong, M.S. 1979. The effects of certain low frequency phenomena on the calibration of hot wires. *Journal of Fluid Mechanics*, **90**, 415–431.

Perry, A.E., Lim, K.L. & Henbest, S.M. 1985. A spectral analysis of smooth flat-plate boundary layers. *In: Proceedings of the Fifth Symposium on Turbulent Shear Flows.* Cornell University.

Perry, A.E., Henbest, S. & Chong, M.S. 1986. A theoretical and experimental study of wall turbulence. *Journal of Fluid Mechanics*, **165**, 163–199.

Perry, A.E., Li, J.D. & Marušić, I. 1991. Towards a closure scheme for turbulent boundary layers using the attached eddy hypothesis. *In:* Walker, J.D.A. (ed), *Turbulent Flow Structure Near Walls.* The Royal Society. First published in *Phil. Trans. R. Soc. London A.* 336, 1991.

Perry, A.E., Uddin, A.K.M. & Marušić, I. 1992. An experimental and computational study on the orientation of attached eddies in turbulent boundary layers. *In: Proceedings of the Eleventh Australasian Fluid Mechanics Conference.*

Petrie, H.L., Fontaine, A.A., Sommer, S.T. & Brungart, T.A. 1990. Large flat plate turbulent boundary layer evaluation. *TM 89-207, Pennsylvania State University Applied Research Laboratory.*

Prandtl, L. 1933. Recent results of turbulence research. *Zeitschrift des Vereines Deutscher Ingenieure*, **77**. English translation NACA TM 720 (1933).

Praskovsky, A. 1993. The sweeping decorrelation hypothesis and energy-inertial scale interaction in high Reynolds number flows. *Journal of Fluid Mechanics*, **248**, 493–511.

Preston, J.H. 1958. The minimum Reynolds number for a turbulent boundary layer and the selection of a transition device. *Journal of Fluid Mechanics*, **3**, 373–384.

Purtell, L.P., Klebanoff, P.S. & Buckley, F.T. 1981. Turbulent boundary layer at low Reynolds number. *Physics of Fluids*, **24**, 802–811.

Rao, K.N., Narasimha, R. & Narayanan, M.A. 1971. The

bursting phenomenon in a turbulent boundary layer. *Journal of Fluid Mechanics*, **48**, 339–352.

Roach, P.E. & Brierley, D.H. 1989. The influence of a turbulent freestream on zero pressure gradient transitional boundary layer developement including the condition test cases T3A and T3B. *In:* O. Pironneau, et al. (ed), *Numerical Simulation of Unsteady Flows and Transition to Turbulence.* Cambridge University Press, 1992.

Robinson, S.K. 1983. Hot-wire and laser Doppler anemometer measurements in a supersonic boundary layer. *AIAA Paper 83-1723.*

Robinson, S.K. 1986. Space-time correlation measurements in a compressible turbulent boundary layer. *AIAA Paper 86-1130.*

Robinson, S.K. 1991a. Coherent motions in the turbulent boundary layer. *Annual Review of Fluid Mechanics*, **23**, 601–639.

Robinson, S.K. 1991b. The kinematics of turbulent boundary layer structure. *NASA TM 103859.*

Rose, W.C. & Johnson, D.A. 1975. Turbulence in a shock-wave boundary-layer interaction. *AIAA Journal*, **13**, 884–889.

Rotta, J.C. 1950. Über die Theorie der turbulenten Grenzschichten. *Mitteilung Max·Planck Institut für Strömungs Forschung, No. 1.* English translation NACA TM 1344.

Rotta, J.C. 1962. Turbulent boundary layers in incompressible flow. *Pages 5–219 of:* Küchemann, D. (ed), *Progress in Aeronautical Science*, vol. 2. Pergamon Press.

Rubesin, M.W. & Rose, W.C. 1973. The turbulent mean-flow, Reynolds-stress, and heat-flux equations in mass- averaged dependent variables. *NASA TM X-62248.*

Runstadler, P.W., Kline, S.J. & Reynolds, W.C. 1963. An experimental investigation of flow structure of the turbulent boundary layer. *Mechanical Engineering Department, Stanford University Report MD-8.*

Saddoughi, S.G. & Veeravalli, S.V. 1994. Local isotropy in turbulent boundary layers at high Reynolds numbers. *Journal of Fluid Mechanics*, **268**, 333–372.

Sandborn, V.A. 1974. A review of turbulence measurements in compressible flow. *NASA TR X-62337.*

Schlichting, H. 1979. *Boundary-Layer Theory.* 7th edn. McGraw-Hill.

Schubauer, G.B. & Tchen, C.M. 1959. Turbulent flow. *Pages 75–195 of:* Lin, C.C. (ed), *Turbulent Flows and Heat Transfer.* High-Speed Aerodynamics and Jet Propulsion, vol. V. Princeton University Press.

Settles, G.S. & Dodson, L.J. 1991. Hypersonic shock-boundary layer interaction database. *NASA CR 177577.*

Shah, D.A. & Antonia, R.A. 1989. Scaling of the bursting period in turbulent boundary layer and duct flows. *Physics of Fluids A*, **1**, 318–325.

Simpson, R.L. 1970. Characteristics of turbulent boundary layers at low Reynolds numbers with and without transpiration. *Journal of Fluid Mechanics*, **42**.

Smith, C.R. & Metzler, S.P. 1983. The characteristics of low-speed streaks in the near-wall region of a turbulent boundary layer. *Journal of Fluid Mechanics*, **129**, 27–54.

Smith, D.R. & Smits, A.J. 1993a. The simultaneous measurement of velocity and temperature fluctuations in the boundary layer of a supersonic flow. *Experimental Thermal and Fluid Science*, **7**, 221–229.

Smith, D.R., Fernando, E.M., Donovan, J.F. & Smits, A.J. 1992. Conventional skin friction measurement techniques for strongly perturbed supersonic turbulent boundary layers. *European Journal of Mechanics, B/Fluids*, **11**, 719–740.

Smith, M.W. & Smits, A.J. 1988. Cinematic visualization of coherent density structures in a supersonic turbulent boundary layer. *AIAA Paper 88-0500.*

Smith, R.W. 1994. *Effect of Reynolds number on the structure of turbulent boundary layers.* Ph.D. Thesis, Princeton University.

Smith, R.W. & Smits, A.J. 1991. Effect of Reynolds number on the large structure of turbulent boundary layers. *AIAA Paper 91-0526.*

Smits, A.J. & Dussauge, J.-P. 1989. Hot-wire anemometry in supersonic flow. *Chapter 5, AGARDograph 315.*

Smits, A.J. & Muck, K.-C. 1984. Constant-temperature hot-wire anemometer practice in supersonic flows. Part 2: The inclined wire. *Experiments in Fluids*, **2**, 33–41.

Smits, A.J., Matheson, N. & Joubert, P.N. 1983b. Low-Reynolds-number turbulent boundary layers in zero and favorable pressure gradients. *Journal of Ship Research*, **27**, 147–157.

Smits, A.J., Spina, E.F., Alving, A.E., Smith., R.W., Fernando, E.M. & Donovan, J.F. 1989. A comparison of the turbulence structure of subsonic and supersonic boundary layers. *Physics of Fluids A*, **1**, 1865–1875.

Spalart, P.R. 1988. Direct simulation of a turbulent boundary layer up to $R_\theta = 1410$. *Journal of Fluid Mechanics*, **187**, 61–98.

Spalding, D.B. 1961. A single formula for the law of the wall. *Transactions of the ASME, Series E: Journal of Applied Mechanics*, **28**, 455–458.

Spina, E.F. 1988. *Organized structures in a supersonic turbulent boundary layer.* Ph.D. Thesis, Princeton University.

Spina, E.F. & Smits, A.J. 1987. Organized structures in a compressible turbulent boundary layer. *Journal of Fluid Mechanics*, **182**, 85–109.

Spina, E.F., Donovan, J.F. & Smits, A.J. 1991a. On the structure of high-Reynolds-number supersonic turbulent boundary layers. *Journal of Fluid Mechanics*, **222**, 293–327.

Spina, E.F., Donovan, J.F. & Smits, A.J. 1991b. Convection velocity in supersonic turbulent boundary layers. *Physics of Fluids A*, **3**, 3124–3126.

Spina, E.F., Smits, A.J. & Robinson, S.K. 1994. The physics of supersonic turbulent boundary layers. *Annual Review of Fluid Mechanics*, **26**, 287–319.

Sreenivasan, K.R. 1988. A unified view of the origin and morphology of the turbulent boundary-layer structure. *In:* Liepmann, H. & Narasimha, R. (eds), *Turbulence Management and Relaminarization.* Springer Verlag Berlin.

Sreenivasan, K.R. 1989. The turbulent boundary layer. *Pages 159–210 of:* Gad-el-Hak, M. (ed), *Frontiers in Experimental Fluid Mechanics.* Springer-Verlag.

Stalmach, C.J. 1958. Experimental investigation of the surface impact probe method of measuring local skin friction at supersonic speed. *Univ. of Texas Report*

DRL-410, CF 2675.

Sternberg, J. 1967. On the interpretation of space-time correlation measurements in shear flow. *The Physics of Fluids*, **10**, S146–S152.

Sun, C.C. & Childs, M.E. 1973. A modified wall-wake velocity profile for turbulent compressible boundary layers. *Journal of Aircraft*, **10**, 381–383.

Sun, C.C. & Childs, M.E. 1976. A wall-wake velocity profile for compressible non-adiabatic flows. *AIAA Journal*, **14**, 820–822.

Tennekes, H. & Lumley, J.L. 1972. *A First Course in Turbulence.* MIT Press.

Theodorsen, T. 1955. The structure of turbulence. *In:* Görtler, H. & Tollmien, W. (eds), *50 Jahre Grenzschichtforschung.* Friedr. Vieweg and Sohn.

Tinh, N. van. 1982. A study of the intermittent phases in the wall region of a turbulent flow. *In:* Zarić, Z.P. (ed), *Structure of Turbulence in Heat and Mass Transfer.* Hemisphere.

Townsend, A.A. 1961. Equilibrium layers and wall turbulence. *Journal of Fluid Mechanics*, **11**.

Townsend, A.A. 1976. *The Structure of Turbulent Shear Flow.* 2 edn. Cambridge University Press.

Tritton, D.J. 1967. Some new correlation measurements in a turbulent boundary layer. *Journal of Fluid Mechanics*, **28**.

Tu, B.-J. & Willmarth, W.W. 1966. An experimental study of the structure of turbulence near the wall through correlation measurements in a thick turbulent boundary layer. *University of Michigan ORA 02920-3-T.*

Uberoi, M.S. & Kovasznay, L.S.G. 1953. On mapping and measurement of random fields. *Quarterly of Applied Mathematics*, **10**.

Uddin, A.K.M. 1994. *The structure of a turbulent boundary layer.* Ph.D. Thesis, University of Melbourne.

Ueda, H. & Hinze, J.O. 1975. Fine-structure turbulence in the wall region of a turbulent boundary layer. *Journal of Fluid Mechanics,* **67**, 125–143.

van Driest, E.R. 1951. Turbulent boundary layer in compressible fluids. *Journal of the Aeronautical Sciences,* **18**, 145–160.

van Driest, E.R. 1956. On turbulent flow near a wall. *Journal of the Aeronautical Sciences,* **23**, 1007–1011 and 1036.

Van Dyke, M. 1982. *An Album of Fluid Motion.* Parabolic Press.

von Kármán, T. 1930. Mechanische Ähnlichkeit und Turbulenz. *Nachrichten der Akademie der Wissenschaften Göttingen, Math. Phys. Klasse,* **58**. *Proc. 3rd Int. Congr. Appl. Mech.,* Stockholm, Pt. I, 1930, p. 85; English trans. NACA TM 611 (1931).

Wallace, J.E. 1969. Hypersonic turbulent boundary-layer measurements using an electron beam. *AIAA Journal,* **7**, 757–759.

Wallace, J.M., Eckelmann, H. & Brodkey, R.S. 1972. The wall region in turbulent shear flow. *Journal of Fluid Mechanics,* **54**, 39–48.

Walz, A. 1966. *Strömungs- und Temperaturgrenzschichten.* Braun Verlag, Karlsruhe. English translation *Boundary Layers of Flow and Temperature,* MIT Press, 1969.

Wark, C.E., Naguib, A.M. & Robinson, S.K. 1991. Scaling of spanwise length scales in a turbulent boundary layer. *AIAA Paper 91-0235.*

Watson, R.D. 1977. Wall cooling effects on hypersonic transitional/turbulent boundary layers at high Reynolds numbers. *AIAA Journal,* **15**, 1455–1461.

Watson, R.D. 1978. Characteristics of Mach 10 transitional and turbulent boundary layers. *NASA TP-1243.*

Watson, R.D., Harris, J.E. & Anders, J.B. 1973. Measurements in a transitional/ turbulent Mach 10 boundary layer at high Reynolds number. *AIAA Paper 73-165.*

Westphal, R.V. 1990. Near-wall measurement errors for hot-wire probes with finite spatial resolution. *In:* Stock, D.E., Sheriff, S.A. & Smits, A.J. (eds), *The Heuristics of Thermal Anemometry, FED-Vol. 97.* ASME Fluids Engineering Division.

White, B.R. 1981. Low-Reynolds-number turbulent boundary layers. *ASME Fluids Engineering Transactions,* **103**, 624–630.

Willmarth, W.W. 1975. Structure of turbulence in boundary layers. *Advances in Applied Mechanics,* **15**, 159–254.

Willmarth, W.W. & Sharma, L.K. 1984. Study of turbulent structure with hot wires smaller than the viscous length. *Journal of Fluid Mechanics,* **142**, 121–149.

Winter, K.G. & Gaudet, L. 1973. Turbulent boundary-layer studies at high Reynolds numbers and Mach numbers between 0.2 and 2.8. *ARC Reports and Memoranda No. 3712.*

Wyngaard, J.C. 1968. Measurement of small-scale turbulence structure with hot wires. *Journal of Scientific Instruments: Journal of Physics E,* **1** **(Series 2)**, 1105–1108.

Wyngaard, J.C. 1969. Spatial resolution of the vorticity meter and other hot-wire arrays. *Journal of Scientific Instruments: Journal of Physics E,* **2** **(Series 2)**, 983–987.

Yanta, W.J. & Crapo, B.J. 1976. Applications of the laser Doppler velocimeter to measure subsonic and supersonic flows. *AGARD CP No. 193.*

Yeung, P.K., Brasseur, J.G. & Bell, D.M. 1993. Evolution of passive scalar sources in a numerically simulated boundary layer. *In:* So, R.M.C., Speziale, C.G. & Launder, B.E. (eds), *Near-Wall Turbulent Flows.* Elsevier.

Young, A.D. 1951. The equations of motion and energy and the velocity profile of a turbulent boundary layer in a compressible fluid. *Report No. 42, College of Aeronautics, Cranfield.*

REPORT DOCUMENTATION PAGE

1. Recipient's Reference	2. Originator's Reference	3. Further Reference	4. Security Classification of Document
	AGARD-AG-335	ISBN 92-836-1040-7	UNCLASSIFIED/ UNLIMITED

5. Originator   Advisory Group for Aerospace Research and Development
North Atlantic Treaty Organization
7 rue Ancelle, 92200 Neuilly-sur-Seine, France

6. Title
Turbulent Boundary Layers in Subsonic and Supersonic Flow

7. Presented at/sponsored by

8. Author(s)/Editor(s)	9. Date
Multiple	July 1996

10. Author's/Editor's Address	11. Pages
Multiple	80

12. Distribution Statement   There are no restrictions on the distribution of this document. Information about the availability of this and other AGARD unclassified publications is given on the back cover.

13. Keywords/Descriptors

Turbulent boundary layer	Supersonic flow
Experimentation	Mach number
Reynolds number	Research projects
Subsonic flow	

14. Abstract

Current research on the structure of zero pressure gradient, flat plate turbulent boundary layers is reviewed. The behavior of boundary layers in subsonic and supersonic flow is discussed, with a particular emphasis on scaling laws with respect to Reynolds number and Mach number. For subsonic flows, it is shown that for the mean flow the classic arguments on inner and outer layer similarity hold extremely well over a large range of Reynolds numbers (approximately $350 \leq R_{e\cdot\theta} \geq 210,000$), and the overlap region is well established over the same region. In contrast, the Reynolds number can have a significant effect on the level of the maximum turbulence stresses, and the location of that maximum in the boundary layer. In particular, the streamwise scaling of the outer-layer is rather sensitive, where the scale increases with the Reynolds number. For supersonic flows with moderate Mach number, it appears that the direct effects of compressibility on wall turbulence are rather small: the most notable differences between subsonic and supersonic boundary layers may be attributed to the variation in fluid properties across the layer. However, certain characteristics cannot be collapsed by simple scaling. Among other observations, there exists strong evidence to indicate that the streamwise length scales are reduced significantly by increasing Mach number.

AGARD holds limited quantities of the publications that accompanied Lecture Series and Special Courses held in 1993 or later, and of AGARDographs and Working Group reports published from 1993 onward. For details, write or send a telefax to the address given above. *Please do not telephone.*

AGARD does not hold stocks of publications that accompanied earlier Lecture Series or Courses or of any other publications. Initial distribution of all AGARD publications is made to NATO nations through the National Distribution Centres listed below. Further copies are sometimes available from these centres (except in the United States). If you have a need to receive all AGARD publications, or just those relating to one or more specific AGARD Panels, they may be willing to include you (or your organisation) on their distribution list. AGARD publications may be purchased from the Sales Agencies listed below, in photocopy or microfiche form.

NATIONAL DISTRIBUTION CENTRES

BELGIUM
Coordonnateur AGARD — VSL
Etat-major de la Force aérienne
Quartier Reine Elisabeth
Rue d'Evere, 1140 Bruxelles

CANADA
Director Scientific Information Services
Dept of National Defence
Ottawa, Ontario K1A 0K2

DENMARK
Danish Defence Research Establishment
Ryvangs Allé 1
P.O. Box 2715
DK-2100 Copenhagen Ø

FRANCE
O.N.E.R.A. (Direction)
29 Avenue de la Division Leclerc
92322 Châtillon Cedex

GERMANY
Fachinformationszentrum Karlsruhe
D-76344 Eggenstein-Leopoldshafen 2

GREECE
Hellenic Air Force
Air War College
Scientific and Technical Library
Dekelia Air Force Base
Dekelia, Athens TGA 1010

ICELAND
Director of Aviation
c/o Flugrad
Reykjavik

ITALY
Aeronautica Militare
Ufficio del Delegato Nazionale all'AGARD
Aeroporto Pratica di Mare
00040 Pomezia (Roma)

LUXEMBOURG
See Belgium

NETHERLANDS
Netherlands Delegation to AGARD
National Aerospace Laboratory, NLR
P.O. Box 90502
1006 BM Amsterdam

NORWAY
Norwegian Defence Research Establishment
Attn: Biblioteket
P.O. Box 25
N-2007 Kjeller

PORTUGAL
Estado Maior da Força Aérea
SDFA - Centro de Documentação
Alfragide
2700 Amadora

SPAIN
INTA (AGARD Publications)
Carretera de Torrejón a Ajalvir, Pk.4
28850 Torrejón de Ardoz - Madrid

TURKEY
Millî Savunma Başkanliği (MSB)
ARGE Dairesi Başkanliği (MSB)
06650 Bakanliklar-Ankara

UNITED KINGDOM
Defence Research Information Centre
Kentigern House
65 Brown Street
Glasgow G2 8EX

UNITED STATES
NASA Headquarters
Code JOB-1
Washington, D.C. 20546

The United States National Distribution Centre does NOT hold stocks of AGARD publications.
Applications for copies should be made direct to the NASA Center for AeroSpace Information (CASI) at the address below.
Change of address requests should also go to CASI.

SALES AGENCIES

NASA Center for
   AeroSpace Information (CASI)
800 Elkridge Landing Road
Linthicum Heights, MD 21090-2934
United States

ESA/Information Retrieval Service
European Space Agency
10, rue Mario Nikis
75015 Paris
France

The British Library
Document Supply Centre
Boston Spa, Wetherby
West Yorkshire LS23 7BQ
United Kingdom

Requests for microfiches or photocopies of AGARD documents (including requests to CASI) should include the word 'AGARD' and the AGARD serial number (for example AGARD-AG-315). Collateral information such as title and publication date is desirable. Note that AGARD Reports and Advisory Reports should be specified as AGARD-R-nnn and AGARD-AR-nnn, respectively. Full bibliographical references and abstracts of AGARD publications are given in the following journals:

Scientific and Technical Aerospace Reports (STAR)
published by NASA Scientific and Technical
Information Division
NASA Headquarters (JTT)
Washington D.C. 20546
United States

Government Reports Announcements and Index (GRA&I)
published by the National Technical Information Service
Springfield
Virginia 22161
United States
(also available online in the NTIS Bibliographic
Database or on CD-ROM)